

1988

198 AFS

DOT HS- 805 500

CONTACT LOADS — AN EXPERIMENTAL STUDY

Volume III

**A.J. King
A.J. Padgaonkar
K.W. Krieger**

**Biomechanics Research Center
Wayne State University
Detroit, MI 48202**

**Contract No. DOT-HS-146-3-711
Contract Amt. \$224,020**



**PRINTED AUGUST 1980
FINAL REPORT**

This document is available to the U S. public through the
National Technical Information Service,
Springfield, Virginia 22161

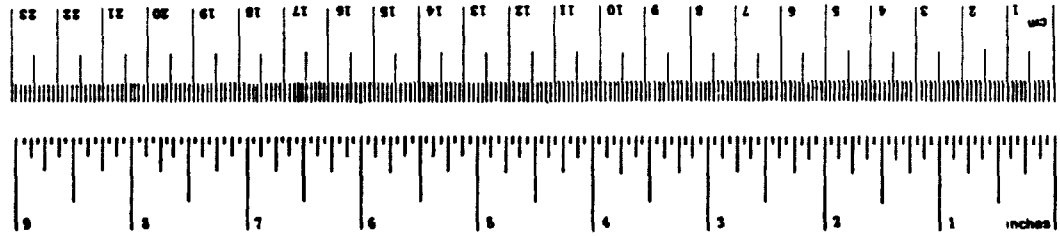
Prepared For
**U.S. DEPARTMENT OF TRANSPORTATION
National Highway Traffic Safety Administration
Washington, D.C. 20590**

This document is disseminated under the sponsorship of the Department of Transportation in the interest of information exchange. The United States Government assumes no liability for its contents or use thereof.

1 Report No DOT-HS-805 500		2 Government Accession No		3 Recipient's Catalog No	
4 Title and Subtitle Contact Loads - An Experimental Study Vol. III				5 Report Date Oct. 20, 1976	
				6 Performing Organization Code	
7 Author(s) A. I. King, A. J. Padgaonkar & K. W. Krieger				8 Performing Organization Report No	
9 Performing Organization Name and Address Biomechanics Research Center Wayne State University Detroit, MI 48202				10 Work Unit No (TRAIS)	
				11 Contract or Grant No DOT-HS-146-3-711	
12 Sponsoring Agency Name and Address National Highway Traffic Safety Administration U. S. Dept. of Transportation Washington, D.C. 20590				13 Type of Report and Period Covered Final Report July, 1973 - Dec., 1975	
				14 Sponsoring Agency Code	
15 Supplementary Notes					
16 Abstract The objectives of this study were to obtain detailed kinematics of the crash victim during a simulated pedestrian-vehicle collision and to compare these data with the output of a computer simulation using the three-dimensional model developed by Calspan Corp. A total of 10 dummy and 6 cadaver impacts were carried out experimentally. As many as 53 accelerometers were used in a single test. A reliable method for measuring angular acceleration of rigid bodies was developed. Pre and post-run measurements are also described, including anthropometry, joint properties, static and dynamic force-deflection characteristics and mass moments of inertia of body segments. The Calspan model was used to validate single segment impacts, the drop test carried out by a previous investigator and the full-scale tests made with extensively instrumented surrogates. In general, there was good correlation for both displacement and acceleration. The contact model should be improved for better correlation.					
17 Key Words Pedestrian Impact, Mathematical Modelling, Model Validation			18. Distribution Statement Unlimited. Available through the National Technical Information Service, Springfield, VA 22151		
19 Security Classif (of this report) Unclassified		20. Security Classif (of this page) Unclassified		21. No of Pages 147	22. Price

METRIC CONVERSION FACTORS

Approximate Conversions to Metric Measures			Approximate Conversions from Metric Measures		
Symbol	When You Know	Multiply by	Symbol	When You Know	To Find
LENGTH					
in	inches	2.5	mm	millimeters	inches
ft	feet	30	cm	centimeters	inches
yd	yards	0.9	m	meters	feet
mi	miles	1.6	km	kilometers	yards
AREA					
in ²	square inches	6.5	cm ²	square centimeters	square inches
ft ²	square feet	0.09	m ²	square meters	square yards
yd ²	square yards	0.8	km ²	square kilometers	square miles
mi ²	square miles	2.6	ha	hectares	acres
MASS (weight)					
oz	ounces	28	g	grams	ounces
lb	pounds (2000 lb)	0.45	kg	kilograms	pounds
		0.9	t	tonnes (1000 kg)	short tons
VOLUME					
teaspoon	teaspoons	5	ml	milliliters	fluid ounces
tablespoon	tablespoons	15	l	liters	pints
fluid ounce	fluid ounces	30	m ³	cubic meters	quarts
cup	cup	0.24			gallons
pint	pints	0.47			cubic feet
quart	quarts	0.96			cubic yards
gallon	gallons	3.8			
cubic foot	cubic feet	0.03			
cubic yard	cubic yards	0.76			
TEMPERATURE (exact)					
°F	Fahrenheit temperature	5/9 (after subtracting 32)	°C	Celsius temperature	
°C	Celsius temperature	9/5 (then add 32)	°F	Fahrenheit temperature	



* 1 in = 2.54 (exactly). For other exact conversions, see data list tables, see NBS Mon. Publ. 286, Units of Length and Mass, Price 12.25. SO Catalog No. C13 10 286

VOLUME III

TABLE OF CONTENTS

	Page
LIST OF TABLES	
LIST OF FIGURES	
CHAPTER	
11. MODEL DESCRIPTION AND MODIFICATIONS	
11.1 Introduction	1
11.2 Input and Output Features	2
11.3 Limitations	3
11.4 C.P.U. Time	4
11.5 Modifications	5
12. BASES FOR VALIDATION	
12.1 Introduction	1
12.2 Linear Displacement	12
12.3 Angular Acceleration	12
12.4 Linear And Angular Velocity	17
12.5 Reference Frames	17
13. DATASET PREPARATION	
13.1 Introduction	19
13.2 Single Segment Impact	19
13.3 Vehicular-Pedestrian Impact Simulation At Wayne State University	19
13.4 Vehicular-Pedestrian Impact Simulation At The Texas Transportation Institute	42
13.5 Discussion of Integrator Input	45
14. MODEL VALIDATION FOR SINGLE SEGMENT IMPACT	
14.1 Introduction	49
14.2 Leg-Bumper Contact Simulation	49
14.3 Head-Hood Contact Simulation	49
14.4 Discussion	58

CHAPTER

15.	MODEL VALIDATION FOR ANTHROPOMORPHIC DUMMY IMPACTS	
15.1	Introduction	69
15.2	Vehicular-Dummy Impact Simulation of TTI Drop Tests	69
15.3	Vehicular-Dummy Impact Simulation of Wayne State University Runs	69
15.4	Discussion	94
16.	MODEL VALIDATION OF CADAVER IMPACTS	
16.1	Comparison of Body Segment Displacements	97
16.2	Contact History	97
16.3	Kinematic Analysis	97
17.	DISCUSSION OF MODEL RESULTS	
17.1	Comparison of Model Results For Different Types of Impacts	121
17.2	Frequency Content Analysis	121
18.	DISCUSSION AND CONCLUSIONS	
18.1	Introduction	133
18.2	Experimental Aspects of the Research Program	133
18.3	Comments on Model Validation	134
18.4	Conclusions	135
	References	137

VOLUME III

LIST OF TABLES

TABLE		Page
11.1	C.P.U. TIME FOR THE EXECUTION OF THE CAL3-D PROGRAM	6
12.1	GENERAL CONFIGURATION OF ACCELEROMETERS FOR RUN 5 D01 - D09	13
12.2	GENERAL CONFIGURATION OF ACCELEROMETERS FOR RUNS D10, C01 - C06	14
13.1	SUMMARY OF IMPACT EXPERIMENTS	20
13.2	SEGMENT DESCRIPTION OF DUMMY IMPACT	23
13.3	SEGMENT DESCRIPTION OF CADAVER IMPACT	24
13.4	JOINT DESCRIPTION FOR DUMMY IMPACTS	25
13.5	JOINT DESCRIPTION FOR CADAVER IMPACTS	26
13.6	EXPECTED CONTACTS FOR LATERAL IMPACT RUNS	30
13.7	EXPECTED CONTACTS FOR FRONTAL RUN D05 (Right Front End)	31
13.8	EXPECTED CONTACTS FOR PADDED BUMPER RUN C06	32
13.9	VEHICLE VELOCITY COMPARISON FROM MODEL AND EXPERIMENT	34
13.10	EXPECTED CONTACTS FOR TTI RUNS (Frontal-M1)	34
15.1	CONTACT HISTORY FOR RUN D10	81
15.2	CONTACT HISTORY FOR RUN D05	82
16.1	CONTACT HISTORY FOR RUN C06	98

LIST OF FIGURES

<u>Figure No.</u>		<u>Page</u>
12.1	Schematic of an Experimental Set-Up Simulating Leg-Bumper Contact	8
12.2	Camera Set-Up for Texas Transportation Institute Drop Test	9
12.3	Camera and Inertial Target Set-Up with Respect to Impact Site for Wayne State University Impact Tests	11
12.4	Definition of Yaw, Pitch, and Roll	16
12.5	Determination of Direction Cosines in 3-D Space from Two Orthogonal Planar Views	18
13.1	Schematic of an Experimental Set-Up Simulating Head-Hood Impact	21
13.2	Schematic of a Crash Victim	22
13.3	Schematic of Frontal Planes of the Impact Vehicle - a 1973 Chevrolet	28
13.4	Vehicle Front End Geometry for Run C06 (Padded Front End)	29
13.5	Fifth Wheel for the Measurement of Vehicle Velocity	33
13.6	Vehicle Deceleration Pulse from a Vehicle Mounted Accelerometer (Run D05)	35
13.7	Frequency Content of the Vehicle Deceleration Pulse (Run D05)	36
13.8	Photograph of Cadaver C05-Preimpact Left Lateral View	37
13.9	Photograph of Cadaver C05-Preimpact Right Lateral View	38
13.10	Photograph of Cadaver C05-Preimpact Frontal View	39
13.11	Photograph of Cadaver C05-Preimpact Dorsal View	40
13.12	Photograph of Cadaver C05-Preimpact Top View	41
13.13	Vehicle Mock-Up Used by Texas Transportation Institute	43
13.14	Definition of Euler Angles	47
14.1	Model Predictions of Angular Displacements for a Single Segment Impact (Leg-Bumper Drop Test)	50
14.2	Comparison of Model and Experimental Results for Angle Roll During Leg-Bumper Impact	51
14.3	Model Predictions of Segment Angular Acceleration Components During Leg-Bumper Impact	52
14.4	Comparison of X-Axis Angular Acceleration During Leg-Bumper Impact	53
14.5	Comparison of Y-Axis Linear Acceleration During Leg-Bumper Impact	54
14.6	Comparison of X-Axis Linear Displacement During Leg-Bumper Impact	55
14.7	Comparison of Z-Axis Linear Displacement During Leg-Bumper Impact	56
14.8	Comparison of X-Axis Linear Acceleration During Leg-Bumper Impact	57
14.9	Model Predictions of Angular Displacements and Comparison of Pitch-Angle for Head-Hood Drop Test	59
14.10	Model Predictions of Angular Accelerations for Head-Hood Impact	60
14.11	Comparison of Z-Axis Angular Acceleration During Head-Hood Impact	61
14.12	Model Predictions of Linear Accelerations During Head-Hood Impact	62
14.13	Comparison of Y-Axis Linear Acceleration During Head-Hood Impact	63

LIST OF FIGURES
(Continued)

<u>Figure No.</u>		<u>Page</u>
14.14	Comparison of X-Axis Linear Acceleration During Head-Hood Impact	64
14.15	Model Predictions of Linear Displacement During Head-Hood Impact	65
14.16	Comparison of Z-Axis Linear Displacement During Head-Hood Impact	66
14.17	Comparison of Y-Axis Linear Displacement During Head-Hood Impact	67
15.1(a)	Comparison of Whole Body Displacement for a Dummy Drop Test at 13.5 Km/h (M1) - Lateral View (0-200 ms) Mirror Image	70
15.1(b)	Comparison of Whole Body Displacement for a Dummy Drop Test at 13.5 Km/h (M1) Lateral View (300-500 ms) Mirror Image	71
15.2(a)	Comparison of Whole Body Displacement for a Dummy Drop Test at 13.5 Km/h (M1) - Frontal View (0-200 ms)	72
15.2(b)	Comparison of Whole Body Displacement for a Dummy Drop Test at 13.5 Km/h (M1) - Frontal View (300-500 ms)	73
15.3	Comparison of X-Axis Head Linear Acceleration for a Dummy Drop Test at 13.5 Km/h (M1)	74
15.4	Comparison of Z-Axis Upper Torso Linear Acceleration for a Dummy Drop Test at 13.5 Km/h (M1)	75
15.5(a)	Comparison of Whole Body Displacement for a Dummy (Lateral) Impact Test at 24.1 Km/h (D10) - Lateral View (0-200 ms)	76
15.5(b)	Comparison of Whole Body Displacement for a Dummy (Lateral) Impact Test at 24.1 Km/h (D10) - Lateral View (300-500 ms)	77
15.6(a)	Comparison of Whole Body Displacement for a Dummy (Frontal) Impact Test at 29.8 Km/h (D05) - Lateral View (100-200 ms)	79
15.6(b)	Comparison of Whole Body Displacement for a Dummy (Frontal) Impact Test at 29.8 Km/h (D05) - Lateral View (300-500 ms)	80
15.7	Comparison of Z-Axis Head Angular Acceleration for a Car-Dummy Impact at 24.1 Km/h (D10)	83
15.8	Comparison of Z-Axis Head Linear Acceleration for a Car-Dummy Impact at 24.1 Km/h (D10)	84
15.9	Comparison of X-Axis Head Linear Acceleration for a Car-Dummy Impact at 24.1 Km/h (D10)	85
15.10	Comparison of Y-Axis Head Linear Acceleration for a Car-Dummy Impact at 24.1 Km/h (D10)	86
15.11	Comparison of Resultant Head Linear Acceleration for a Car-Dummy Impact at 24.1 Km/h (D10)	87
15.12	Comparison of Y-Axis Lower Torso Angular Acceleration for a Car-Dummy Impact at 24.1 Km/h (D10)	88
15.13	Comparison of Z-Axis Lower Torso Linear Acceleration for a Car-Dummy Impact at 24.1 Km/h (D10)	89
15.14	Comparison of Resultant Lower Torso Linear Acceleration for a Car-Dummy Impact at 24.1 Km/h (D10)	90
15.15	Comparison of Y-Axis Left Upper Leg Linear Acceleration for a Car-Dummy Impact at 24.1 Km/h (D10)	91
15.16	Comparison of Y-Axis Left Lower Leg Linear Acceleration for a Car Dummy Impact at 24.1 Km/h (D10)	92

LIST OF FIGURES
(Continued)

<u>Figure No.</u>		<u>Page</u>
15.17	Model Predictions of Left Lower Leg Angular Accelerations for a Car-Dummy Impact at 24.1 Km/h (D10)	93
15.18	Comparison of X-Axis Head Linear Displacement for a Car-Dummy Impact at 39.4 Km/h (D09)	95
15.19	Comparison of Z-Axis Head Linear Displacement for a Car-Dummy Impact at 39.4 Km/h (D09)	96
16.1(a)	Comparison of Whole Body Displacement for a Cadaver (Lateral) Impact Test at 24.1 Km/h (C03) - Lateral View (0-200 ms)	100
16.1(b)	Comparison of Whole Body Displacement for a Cadaver (Lateral) Impact Test at 24.1 Km/h (C03) - Lateral View (300-500 ms)	101
16.2	Comparison of X-Axis Head Linear Acceleration for a Car-Cadaver Impact at 24.1 Km/h (C03)	102
16.3	Comparison of X-Axis Head Linear Acceleration for a Car-Cadaver Impact at 24.1 Km/h (C03)	103
16.4	Comparison of Z-Axis Lower Torso Angular Acceleration for a Car-Cadaver Impact at 24.1 Km/h (C03)	104
16.5	Comparison of Y-Axis Lower Torso Linear Acceleration for a Car-Cadaver Impact at 24.1 Km/h (C03)	105
16.6	Comparison of Y-Axis Left Upper Leg Linear Acceleration for a Car-Cadaver at 24.1 Km/h (C03)	106
16.7	Comparison of Y-Axis Left Lower Leg Linear Acceleration for a Car-Cadaver Impact at 24.1 Km/h (C03)	107
16.8	Model Prediction of Left Upper Leg Angular Accelerations for a Car-Cadaver Impact at 24.1 Km/h (C03)	108
16.9	Comparison of Y-Axis Head Angular Acceleration for a Car-Cadaver Impact at 37.3 Km/h (C06)	109
16.10	Comparison of X-Axis Head Linear Acceleration for a Car-Cadaver Impact at 37.3 Km/h (C06)	110
16.11	Comparison of Y-Axis Head Linear Acceleration for a Car-Cadaver Impact at 37.3 Km/h (C06)	111
16.12	Comparison of Y-Axis Lower Torso Linear Acceleration for a Car-Cadaver Impact at 37.3 Km/h (C06)	112
16.13	Comparison of Z-Axis Lower Torso Linear Acceleration for a Car-Cadaver Impact at 37.3 Km/h (C06)	113
16.14	Comparison of X-Axis Left Upper Leg Angular Acceleration for a Car-Cadaver Impact at 37.3 Km/h (C06)	114
16.15	Comparison of Y-Axis Left Lower Leg Linear Acceleration for a Car-Cadaver Impact at 37.3 Km/h (C06)	115
16.16	Comparison of X-Axis Head Linear Acceleration for a Car-Cadaver Impact at 32 Km/h (C05)	116
16.17	Comparison of Y-Axis Head Angular Acceleration for a Car-Cadaver Impact at 32 Km/h (C05)	117
16.18	Comparison of Z-Axis Lower Torso Linear Acceleration for a Car-Cadaver Impact at 32 Km/h (C05)	118
16.19	Comparison of X-Axis Left Lower Leg Linear Acceleration for a Car-Cadaver Impact at 32 Km/h (C05)	119
17.1	Comparison of Model Prediction X-Axis Head Angular Acceleration for Runs C03 (24.1 Km/h) and D10 (24.1 Km/h)	122

LIST OF FIGURES
(Continued)

<u>Figure No.</u>		<u>Page</u>
17.2	Comparison of Model Prediction Y-Axis Head Linear Acceleration for Runs C03 (24.1 Km/h) and D10 (24.1 Km/h)	123
17.3	Comparison of Model Prediction X-Axis Left Lower Leg Angular Acceleration for Runs D10 (24.1 Km/h) and C03 (24.1 Km/h)	124
17.4	Comparison of Model Prediction Y-Axis LLL Linear Acceleration for Runs D10 (24.1 Km/h) and C03 (24.1 Km/h)	125
17.5	Comparison of Model Prediction Y-Axis LLL Linear Acceleration for Runs C03 (24.1 Km/h) and C06 (24.1 Km/h)	126
17.6	Comparison of Model Prediction Z-Axis LLL Angular Acceleration for Runs C03 (24.1 Km/h) and C06 (24.1 Km/h)	127
17.7	Frequency Spectrum of Z-Axis Head Angular Acceleration for a Car-Dummy Impact at 24.1 Km/h (D10)	128
17.8	Comparison of Z-Axis Head Angular Acceleration (Filtered) for a Car-Dummy Impact at 24.1 Km/h (D10)	129
17.9	Frequency Spectrum of Z-Axis Head Angular Acceleration for a Car-Cadaver Impact at 24.1 Km/h (C03)	130
17.10	Comparison of Z-Axis Head Angular Acceleration (Filtered) for a Car-Cadaver Impact at 24.1 Km/h (C06)	131

MODEL DESCRIPTION AND MODIFICATIONS

11.1 Introduction

As mentioned in Volume 1, the experimental data acquired under this contract were primarily intended for the validation of a crash victim simulator (CVS) developed by Calspan Corporation. Volume 3 provides a description of the simulator, discusses the bases for validation and compares model output with experimental data obtained from several different impact conditions.

A detailed description of the Calspan CVS is given by Fleck et al. (1974). In the open literature, it has been summarized by Fleck (1975) and by Bartz (1972). A short discussion is presented here as background for this validation study.

The Calspan 3-D CVS is a digital computer program written in Fortran and requires a region size of about 500 K bytes for execution on IBM 360 or 370 series computers. The main program is attached to 66 subroutines, 8 double precision subfunctions, a blockdata and a clock rate function. The coding is in double precision. The original version of the Calspan model has been revised several times. Potential users are cautioned to ascertain the version number and release date before attempting to execute the program.

Because of the continual revisions, some of the difficulties will be listed for the simulation of pedestrian impact for the versions used. The first version, called Version II, was released in December, 1972 or early 1973. It was principally a vehicle occupant crash simulator and must be modified for pedestrian impact simulation. In subroutine INITIAL, card number INIT0440 should be changed from

```
12 VH (I,1) = XDOTO(I)    to
12 VH (I,1) = 0.000
```

or VH (I,1) can be set equal to any desired pre-impact velocity. In this case it is assigned to the 'pedestrian'. A ground plane attached to the vehicle must also be defined. Furthermore, this version does not provide the facility for specifying a minimum step size (HMIN) for the integrator. Therefore, execution may terminate prematurely if the initial step size is set too large.

Version III was first released in late 1973 but has undergone several revisions. The first version of Version III is a generalization of Version II. This program is capable of accommodating any number of segments and also has a dataset option for pedestrian crash simulation. However, it contained logical IF statements that were unacceptable to some IBM systems. An improved Version III was released in September, 1974. The difficulties and errors encountered in Version II were eliminated and the unit for vehicle speed was changed from mph to in./sec. Note that vehicle decelera-

tion is given in gravitational (g) units.

The final version of Version III released in late 1975 contained an improved integrator which can drastically reduce CPU time if the integration of the differential equations constitutes a large proportion of the computing effort. In the simulation of pedestrian impact there is a 50% reduction, whereas, that for a single segment was only about 20%.

11.2.1 Input and Output Features; Limitations

The current versions of the CVS are quite flexible and relatively free of restrictions. The number of segments, planes and contacts can be selected by the user. By suitably arranging the initial position of the crash victim and vehicle, the CVS can be used for the simulation of occupant impact or pedestrian-vehicle impact. This study calls for the use of the CVS as a pedestrian-vehicle impact simulator.

The card input is organized into logical sections and the input data are printed out in a very readable fashion in the output listing. The input is provided in the following order:

- (i) Restarting control.
- (ii) Choice of units of length, mass and time. These units determine the units of the variables listed in the output tabular data. It is important that the same units are used throughout the whole dataset. Relationship between the direction of gravity and the inertial reference frame is controlled by the magnitudes of the gravitational acceleration components along each inertial axis.
- (iii) Control of integrator. Variable or fixed step.
- (iv) Choice of output. If any diagnostic output is desired or if printer plots are required, they are specified here.
- (v) Variable number of segments and joints.
- (vi) Segment description. This includes segment mass, principal moments of inertia, semiaxes of contact ellipsoids and the location of the center of the ellipsoid with respect to center of gravity of the segment.
- (vii) Joint description. Type of joint, such as pinned or ball and socket joints, the location and orientation of the joint, and their spring and viscous characteristics.
- (viii) Integrator convergence tests on all variables.
- (ix) Flexible element data.
- (x) Vehicle description. Initial location and orientation, deceleration pulse, specification of contact planes, belts and bags such as geometry.

(xi) Provision for additional contact ellipsoids, and for body symmetry can also be made.

(xii) Contact Functions. Force-deflection characteristics, inertial spike data, energy absorption factor (R), permanent deflection factor (G), and the friction coefficient are specified here.

Each function can be expressed in one of three forms - as constants, in tabular form or as fifth degree polynomials. If desired it can be divided into two parts, such as a bilinear curve.

(xiii) Specification of possible contacts. Possible contact between planes and segments, between segments, and contacts of segments with restraint systems (seat belt or air bag) are specified in advance.

(xiv) Printer plot coordinate adjustments.

(xv) Initial conditions. The initial linear and angular position and velocity of a-1 segments are listed.

(xvi) Selection of output files. The desired output for linear kinematics is specified by denoting the points on body segments at which experimental data are available. For angular kinematics, desired body segments are quoted. Joint output data can also be selected.

11.2.2 Output Features

The printed output is well organized. At every "DT" time-step as specified in the input, a printer plot is produced. Positions of the joints and segment centers of gravity are shown. The program also produces tabular output of computed results, such as vehicle position and velocity, segment kinematics, joint forces and torques, external constraints and CPU time used. Diagnostic output is printed out on unit 6, while kinematic and kinetic information is available beginning with unit 21. The number of disk files created depends on the number of output options requested. The Michigan Terminal System (MTS) at Wayne State University permitted a maximum of 20 units, hence a special feature was added to accommodate units 21 to 75.

11.3 Limitations

The primary restriction is storage limitation. But this can be relaxed by increasing the allocated storage for such components. The present limitations are listed below.

Number of Segments	20
Number of Joints	21
Number of Contact Planes	20
Number of Belts	8
Number of Bags	5
Number of Contact ellipsoids (Segment ellipsoids included)	24
Number of Spring Dampers	20
Number of Contact Functions	50
Printer plot domain	0 < X < 61
	0 < Y < 61
	0 < Z < 121

The program is sufficiently flexible to simulate most of the impact situations. The difficulty frequently encountered is the simulation of a plane contacting more than five segments. This is overcome by defining a second plane identical to the first one. In addition to these programming limitations, there are additional circumstances which cause difficulty:

(i) Failure of the plane to sense contact occurs when it is small and the point of maximum penetration of the ellipsoid does not intersect the plane but intersects an extension of that plane. This problem can be solved by describing that plane as an ellipsoid attached to a vehicle and use the segment to segment contact option. For example, in the case of bumper-knee contact, the bumper is simulated by an ellipsoid.

(ii) No record is kept of the point of contact in the ellipsoid - ellipsoid contact routine which may fail for large penetrations (due to failure in subroutine INTERS). For example, when the penetration of an ellipsoid into another one exceeds the semi-axis of the latter, the subroutine assumes that the former had made its penetration from the opposite side. Thus, care must be exercised in describing the dimensions of ellipsoids which are used to replace planes or segments.

(iii) If the depth of penetration exceeds the specified upper limit of the force-deflection function, penetration continues with no further increase in resisting force. So care should be taken in assigning the upper limit of the contact function.

(iv) A severe weakness exists in the input scheme. This is due to the awkward "Chain System" of input for connectivity, wherein the subject's joint locations must be specified in terms of distances from the segment centers of gravity (c.g.). Moreover, the subject must be initially positioned by specifying the c.g. location of a single reference segment and the "Euler angles" between segments. Initial equilibrium is practically impossible to achieve in this manner. Sufficient simulation time prior to impact must be provided for the victim to attain equilibrium through several numerical integration steps. (See Progress Report, Boeing Computer Services, Inc. 1973).

(v) In some situations, such as large spring and viscous coefficients, a set of stiff equations are produced. The exponential integrator can integrate this system in most cases. If errors occur, they are probably associated with sub-routine VISPR, YPRDEG, and CFACTT. The minimum step size of the integrator should be reduced to overcome any difficulty (See Fleck et al. 1974, p. 248, Vol. 1).

(vi) It is also important to note that the input data set for angular position assumes the order of rotations to be roll, pitch and yaw, while that for model output is yaw, pitch and roll.

11.4 CPU Time

Restraint system subroutines for airbags and belts can only be eliminated by introduction of dummy subroutines which consist of their name, a return and an end statement. This saves compilation cost, but not execution cost.

Program execution time is roughly proportional to the number of segments, the number of constraints and the number of specified contacts. Version III released in September, 1974 was used for most of the work. Table 11.1 lists the CPU time required on an IBM 360/67 computer.

11.5 Modifications

To simulate impacting a surface with a single segment without joints, the following program modifications are required:*

In subroutine BINPUT card 550 is inserted before card 390 to read as follows:

C	card 380
NFLX = 0	card 550
IF (NJNT.EQ.0) GO TO 53	card 390

In subroutine FSMSOL, an additional statement is required after card 310:

MM = IABS (MX)	card 310
IF (MM.LE.0) GO TO 99	

These two changes will not affect normal execution of the program with the linked structure. If subroutine FSMSOL is not modified, the single segment should be provided with a 'null' joint, described by entering JNT(J) = 0 for that joint. All fictitious joint descriptions still must be provided, although they are not used during program execution.

* Calspan's latest version (12/75) has these changes.

TABLE 11.1

CPU TIME FOR THE EXECUTION OF THE CAL3-D PROGRAM

Dataset* #	Duration of Run - msec.	# of points for linear kinematics	# of segments for angular kinematics	# of plane- segment contacts	# of segment- segment contacts	CPU time sec.	Version 3 rel. date
1	250	3	3	16	0	1399	11/73
1	600	3	3	16	0	2225	11/73
2	600	3	3	13	0	2050	11/73
3	600	3	3	17	0	2456	11/73
1	350	3	3	16	0	1599	9/74
4	350	20	15	17	10	2340	9/74
5	600	16	12	10	14	4182	9/74
6	100	1	1	1	0	103	9/74
7	200	10	4	12	6	1283	9/74
7	200	10	4	12	6	675	12/75
8	500	10	4	28	14	2155	12/75

* Duplicate dataset # indicates that the same set is executed again.

CHAPTER 12

BASIS FOR VALIDATION

12.1 Introduction

A validated mathematical model is an effective, economical and versatile tool for studying the response of the system for a wide variety of input conditions. There are, however, no hard and fast rules defining the conditions that constitute a proper validation. For a gross motion simulator such as the CAL3-D model, initial validation should be based on body segment kinematics, which can become quite complex in a vehicle-pedestrian simulation. If reasonable kinematic correlation exists between predicted and measured results, some level of confidence can be placed in the computed forces and moments acting on the segments. Furthermore, linear acceleration measurement is often more practical than that of contact forces. Displacement data can be obtained from high-speed movie films. For a complete kinematic validation, both angular and linear kinematic parameters should be compared. The following discussion deals with the experimental aspects of making kinematic measurements.

12.2.1 Linear Displacement

In kinematics, linear displacement is the fundamental parameter. In a gross motion simulator, the displacement vector is an independent parameter. The model predicts the displacement-time history of different points on the body segments. To validate these computations, experimental techniques for determining the spatial position of these segments, as a function of time, must be developed. The most popular method is high-speed cinematography. Although cameras can only provide a planar view, two orthogonal views using two separate cameras define a three-dimensional motion. However, additional cameras are often required to cover a larger area, act as a back-up to the primary cameras, or record a close-up view of a critical aspect of the impact sequence.

There were basically three types of experiments in this study:

(i) Drop-tests for the validation of a single segment impact. A single segment was dropped onto a deformable surface. Figure 12.1 illustrates a schematic of the leg drop test set-up. The two cameras used were aligned along orthogonal directions to cover the X-Z and Y-Z plane relative to the inertial-fixed coordinate system. (With respect to the vehicle-fixed coordinate system, they covered the X-Z and X-Y plane for the leg drop tests and the X-Z and Y-Z plane for the head-hood impact).

(ii) Drop-tests conducted by the Texas Transportation Institute (TTI). A 95th percentile anthropomorphic male dummy (Sierra) was dropped onto a mock-up of the front end of a vehicle. Two cameras were placed on the floor, as shown in Figure 12.2, to cover the motion in the Y-Z and X-Z plane of the vehicle-fixed coordinate system. It was coincident with the inertial reference frame.

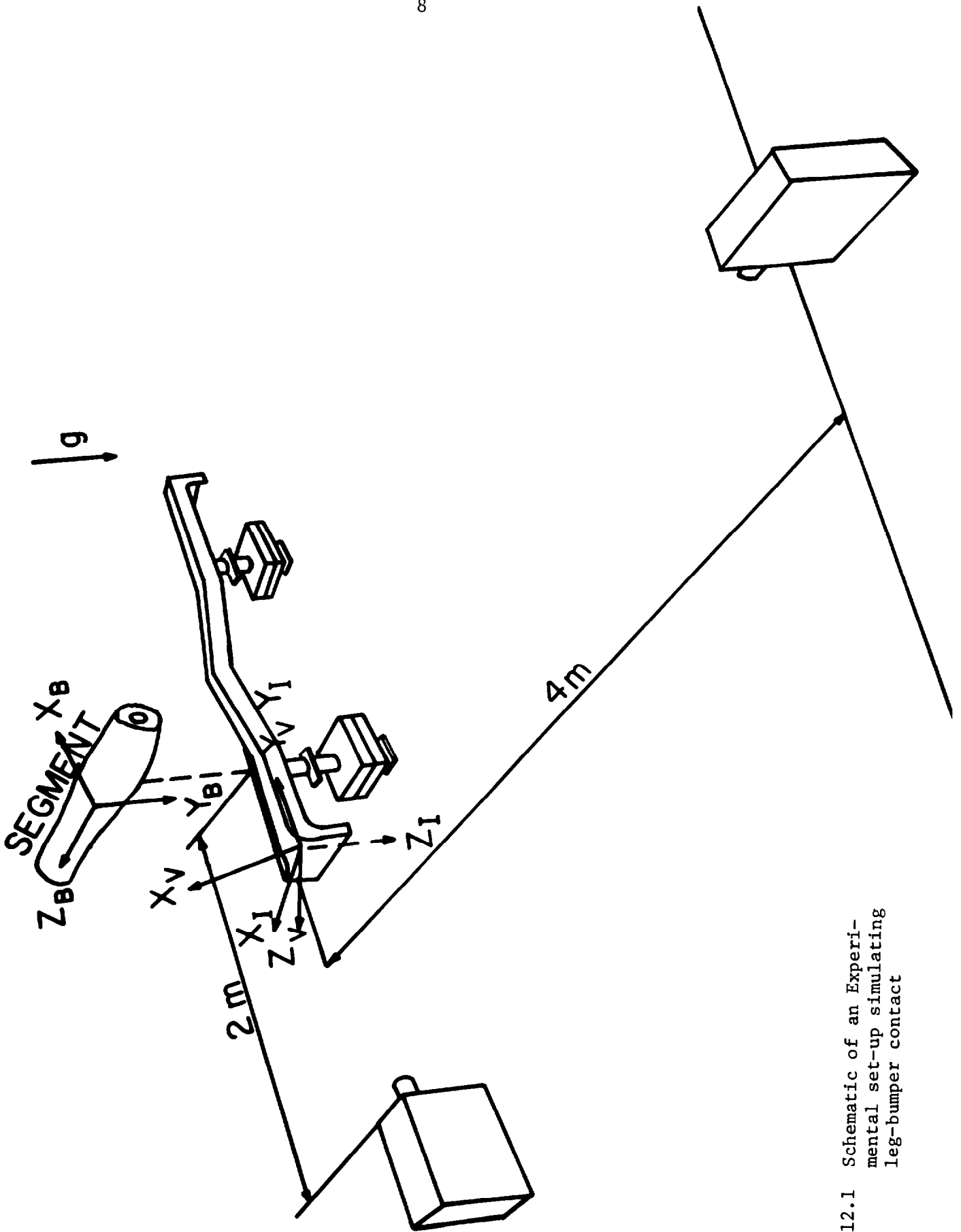


Figure 12.1 Schematic of an Experimental set-up simulating leg-bumper contact

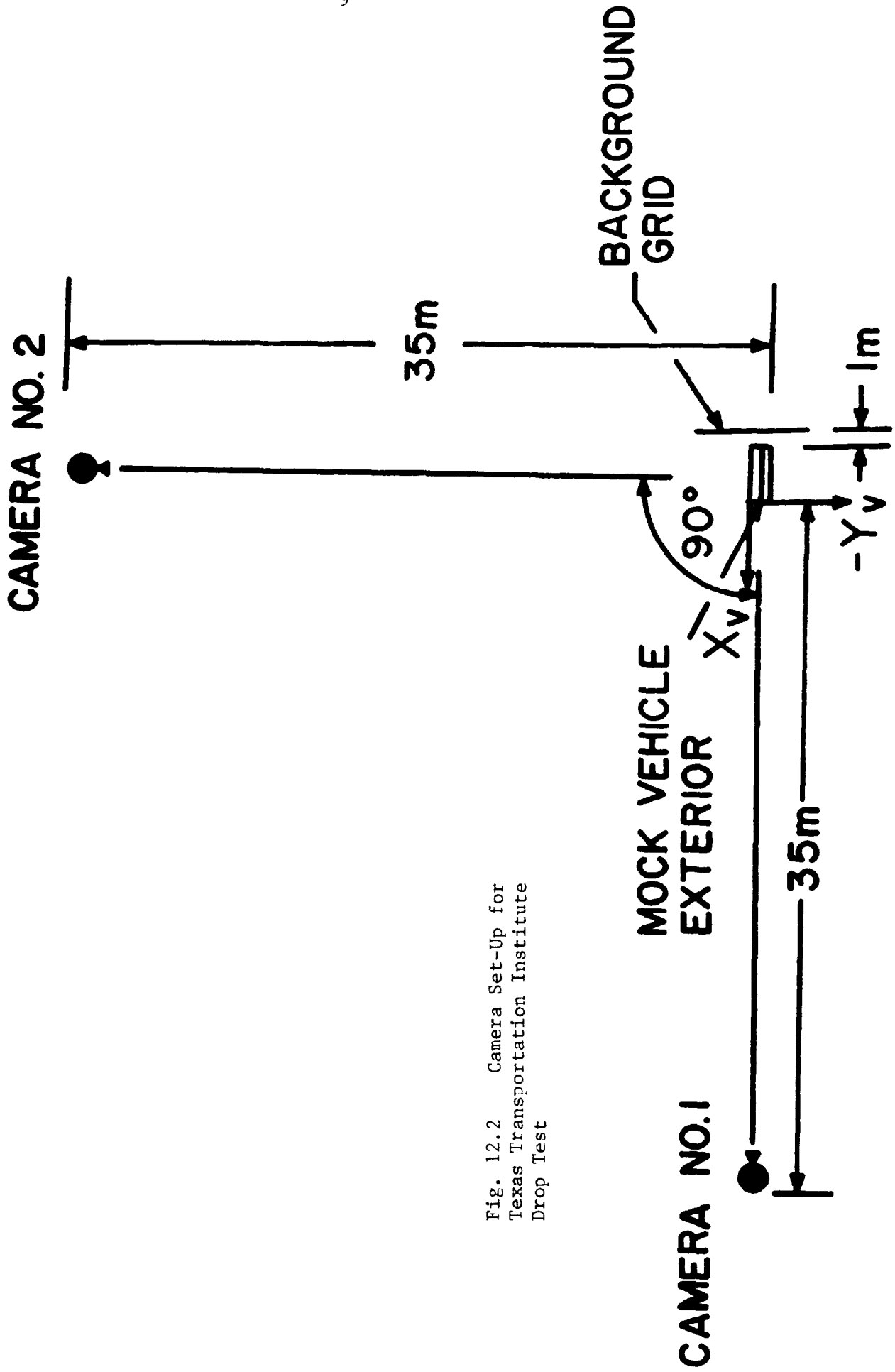


Fig. 12.2 Camera Set-Up for
Texas Transportation Institute
Drop Test

(iii) Vehicle-Pedestrian Impact Tests. A 1973 full-size Chevrolet was made to impact a pedestrian test subject. The same anthropomorphic dummy and several unembalmed cadavers were used as subjects. A set of seven cameras were used as subjects. A set of seven cameras were used to cover the impact event, as shown in Figure 12.3. They were identified by their locations as frontal, right lateral, top, left lateral 1 and 2, left lateral close-up (added for cadaver runs) and a vehicle-borne rear view camera. The lateral cameras record motion in the X-Z plane of the vehicle and the inertial-fixed coordinate system. Similarly, the frontal camera records motion in the Y-Z plane of the same coordinate systems.

A Vanguard motion-analyzer obtained displacement kinematic data. Its two cross-hairs can be adjusted to pin-point any desired target. The coordinate location of the point of intersection of the two cross-hairs is read out in arbitrary units of the screen coordinate system of the analyzer to an accuracy of four digits. The resolution is $\pm 0.1\%$. Reference laboratory targets of known dimensions were used to find the conversion factor between the arbitrary units and the physical dimensions. The following assumptions were made for film analysis:

(a) The lens is good enough to map a plane into a plane; This means that there is no lateral parallax. Nyquist's (1976) x-ray analysis is based on the same principle.

(b) Parallax due to depth of field can be corrected with the principle of similar triangles.

For lateral views, motion is executed at a fairly fixed distance from the film-plane. Therefore, motion in the X-Z (vehicle reference) plane can be described easily, based on these assumptions. However, difficulties arise during analysis of the frontal view because the subject-camera distance is not constant but is a function of time. Thus, the scale of conversion from the arbitrary units of the analyzer into physical units is variable; and it must be computed for each instant of time from the motion of the subject along the X-axis as measured from the lateral view. Thus, motion in the Y-Z (vehicle reference) plane can be obtained. The problem of change of scale does not arise in the case of drop tests, the TTI tests or the single segment impact tests.

Also, care should be exercised in determining time. Two principal concerns are:

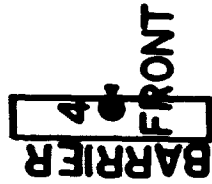
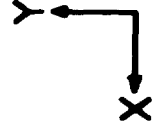
(I) Accurate initialization.

(II) Accurate determination of time interval between frames.

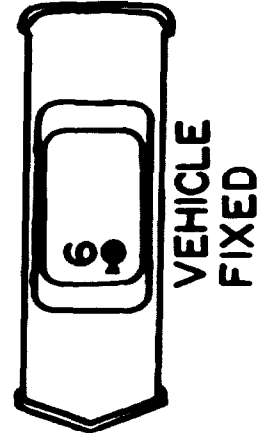
All film data were synchronized by short duration flash bulbs, visible to all cameras. Three separate flashes* were set off sequentially to record

* The second flash was added after the third dummy run (D03). The third flash was added after the fifth dummy run (D05).

1 ● RIGHT LATERAL



5 ● TOP ⊕ IMPACT LOCATION



7 ● CLOSE - UP VIEW

3 ● LEFT LATERAL (2) 2 ● LEFT LATERAL (1)

Fig. 12.3 Camera and Inertial Target Set-Up with Respect to Impact Site for Wayne State University Impact Tests

the instant of solenoid release of the supporting mechanism for the subject, that of actual release and that of bumper-knee contact. Thus, all films had the same instant of initialization. Although time interval between frames can be computed from the film speed of each camera, it is not always reliable. The interval is calculated more accurately from timing marks placed at 10 ms intervals on the film by a timing generator.

12.2.2 Linear Acceleration

Linear acceleration is another important kinematic parameter. It can be obtained by double differentiation of linear displacement with respect to time. However, numerical differentiation usually is not an accurate method. Furthermore, linear accelerometers are readily available. In this study, miniature accelerometers manufactured by Endevco (Model #2264-2000) were used. They were attached to every body segment in different configurations. In general, the aim was to measure the resultant acceleration of most of the body segments. Thus a set of triaxial accelerometers were installed along three orthogonal axes in the body-fixed coordinate system. Again the three types of experiments had three different arrangements.

(i) Single-Segment Drop Tests - A mount containing 9 accelerometers was attached to the segment. Detailed discussion on the use of this mount is given in the next chapter.

(ii) TTI Drop Tests - Triaxial acceleration was measured on the head, the upper torso and the lower torso.

(iii) Pedestrian-Vehicle Impact Experiments - The accelerometer configuration on dummy segments differed on cadaver segments. The dummy was first subjected to a series of 10 runs which were followed by 6 cadaveric runs. For dummy runs, the accelerometer configuration was designed to measure both angular and linear accelerations of every body segment. A six-accelerometer scheme* was used to determine both parameters on some of the segments, while on others, triaxial linear acceleration was measured and angular acceleration was to be computed from measured values for the adjoining segments. Also, on certain segments, there were redundant accelerometers to verify the computed results. Thus, for the first nine dummy runs (D01 through D09), the accelerometer configuration is shown in Table 12.1.

This arrangement was changed for all cadaver runs and the tenth dummy run (D10). The rearrangements eliminated difficulties encountered in measuring angular acceleration. The accelerometer configuration is shown in Table 12-2.

12.3.1 Angular Acceleration

Rotational motion of a rigid body is often conveniently defined by angular acceleration in view of the restrictive, non-commutative property of angular displacement. Angular acceleration is also one of the important criteria

* See Chapter 3 for details.

TABLE 12.1

GENERAL CONFIGURATION OF ACCELEROMETERS FOR RUNS D-01 - D-09

Segment	No. of Accelerometers
Head	6
Upper Torso	3
Central Torso	3
Lower Torso	6
Right Upper Leg	3
Right Lower Leg	1
Left Upper Leg	6
Left Lower Leg	2
Right Upper Arm	6
Right Lower Arm	2
Left Upper Arm	6
Left Lower Arm	2

TABLE 12.2

GENERAL CONFIGURATION OF ACCELEROMETERS FOR
RUNS D10, C01 - C06

Segment	No. of accelerometers	Remarks
Head	9	
Upper torso	4	triax on T1, X-dir. on sternum
Central Torso	0	
Lower Torso	9	
Right Upper Leg	3	triax
Right Lower Leg	1	in impact direction
Left Upper Leg	9	impacted leg
Left Lower Leg	9	impacted leg
Right Upper Arm	3	triax
Right Lower Arm	3	triax
Left Upper Arm	3	2 in X-dir., one in Y-dir.

for the assessment of head injury. However, three-dimensional angular accelerometers do not exist. Although angular velocity can be measured by means of rate gyroscopes, they are bulky and inconvenient where a large number of body segments are involved. A reliable method for measuring angular acceleration was developed, using miniature accelerometers. A detailed discussion of this problem is given in Chapter 3.

12.3.2 Angular Displacement

Angular displacement is the most important kinematic parameter for model validation. The linear and angular acceleration components of any segment are given along body-fixed axes, both mathematically and experimentally. Thus, if there is a mismatch in angular displacement, comparing experimental and analytical acceleration becomes rather meaningless. For a severe mismatch, validation should be based on the magnitude of the resultant accelerations.

As far as determining angular displacement is concerned, the standard approach is to express it in terms of direction cosines or Euler angles. An alternate approach is the use of quaternions. The CAL3-D Simulator output is in terms of direction cosines and it is therefore impractical to use quaternions for validation purposes. The determination of direction cosines for a 3-D-motion is a cumbersome process, because the angles observed on film are not true angles. Bortz (1971) proposed a method to compute angular displacement from gyroscopically measured angular velocities. This is a non-optical method which may not be directly applicable to angular displacement computations from measured accelerations. Moreover, to calculate displacements, predicted by the model, does not add new information to the validation process, since the procedure is only a check on integration. Therefore, the model results will be correlated with film data to obtain an independent comparison.

Although the use of high-speed movie film is cumbersome, it is still possible to estimate with reasonable accuracy the angular displacement of a rigid body. Suppose that the body undergoes a set of 3 finite rotations sequentially about the Z-, Y-, X-axes as shown in Figure 12.4, these angles are y (yaw), p (pitch), and r (roll). The initial X_I, Y_I, Z_I and final configuration (X_F, Y_F, Z_F) are related by a direction cosine matrix as follows:

$$\begin{bmatrix} X_F \\ Y_F \\ Z_F \end{bmatrix} = \begin{bmatrix} D_{11} & D_{12} & D_{13} \\ D_{21} & D_{22} & D_{23} \\ D_{31} & D_{32} & D_{33} \end{bmatrix} \begin{bmatrix} X_I \\ Y_I \\ Z_I \end{bmatrix} \quad (12.1)$$

where:

$$\begin{aligned} D_{11} &= \text{cosp} \cdot \text{cosy} \\ D_{12} &= \text{cosp} \cdot \text{siny} \\ D_{13} &= \text{sinp} \end{aligned}$$

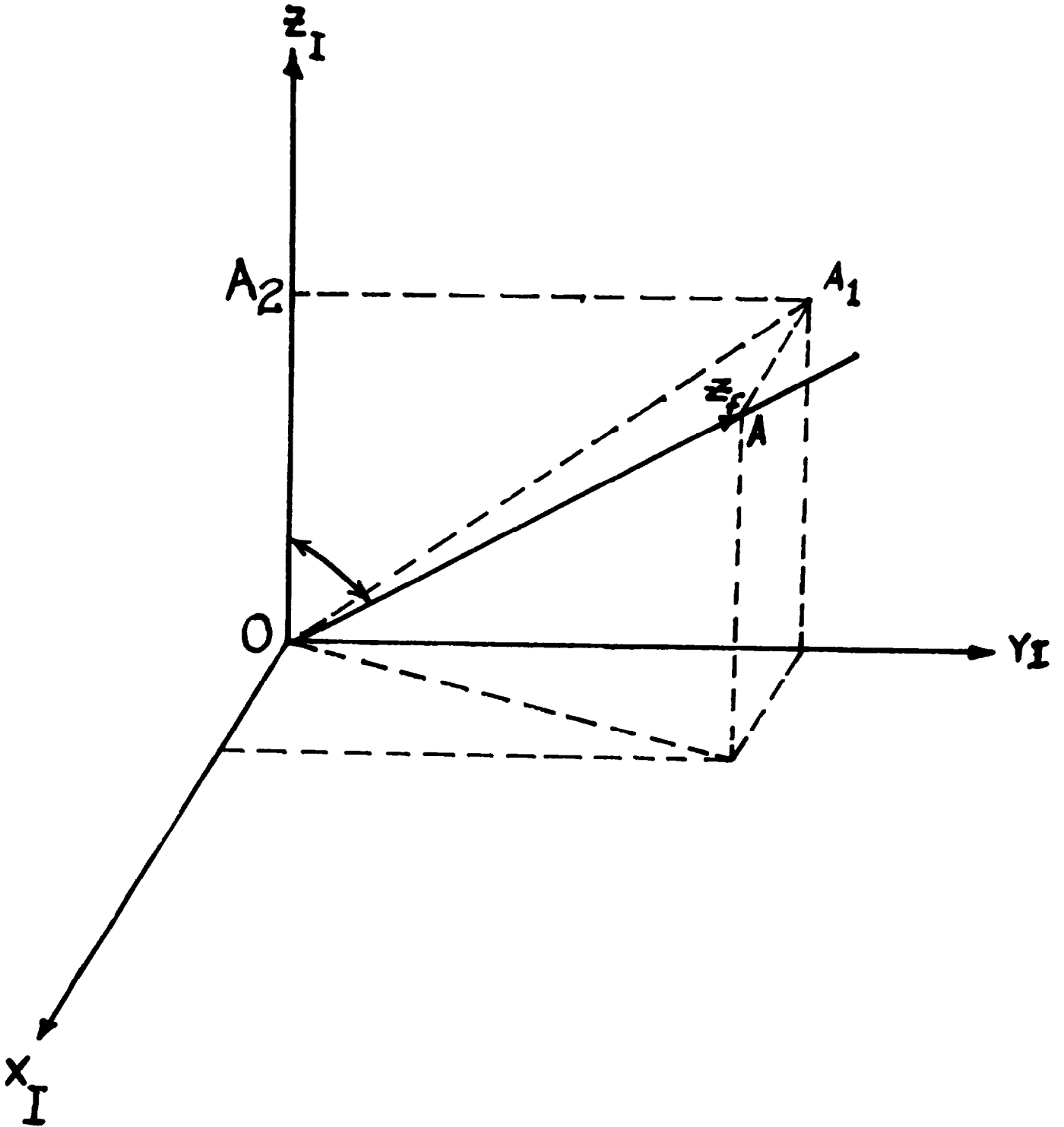


Figure 12.4 Definition of Yaw, Pitch and Roll

$$\begin{aligned}
D_{21} &= \sin r \cdot \sin p \cdot \cos y - \cos r \cdot \sin y \\
D_{22} &= \sin r \cdot \sin p \cdot \sin y + \cos r \cdot \cos y \\
D_{23} &= \sin r \cdot \cos p \\
D_{31} &= \cos r \cdot \sin p \cdot \cos y + \sin r \cdot \sin y \\
D_{32} &= \cos r \cdot \sin p \cdot \sin y - \sin r \cdot \cos y \\
D_{33} &= \cos r \cdot \cos p
\end{aligned}
\tag{12.2}$$

Thus:

$$\begin{aligned}
p &= -\arcsin (D_{13}) \\
y &= \arctan (D_{12}/D_{11}) \\
r &= \arctan (D_{23}/D_{33})
\end{aligned}
\tag{12.3}$$

The "Euler angles" can be determined if the five direction cosines given by Equation 12.3 can be measured from film. To determine D_{33} , for example, it can be seen from Figure 12.5 that:

$$D_{33} = \cos (\angle A_2OA)$$

From the film, any segment which has a length OA along the Z_F axis has a projected length OA_1 , in the $Z_I Y_I$ plane. The projected length of OA_1 , on the Z_I axis is OA_2 which can also be measured from the film. Since the actual length OA is known, D_{33} can be computed. Similarly, the other direction cosines can be found by this method. In case of singularities, different expressions formed from Equation 12.2 can be used to compute these angles (see Fleck, 1974).

12.4 Linear and Angular Velocity

Linear velocity is the time integral of linear acceleration or a time differentiation of linear displacement. In this validation procedure, both linear acceleration and linear displacement were considered. Linear velocity was not measured directly. Thus, little emphasis will be placed on linear velocity, for validation purposes.

Angular velocity is the time integral of angular acceleration. However, computations of angular acceleration in the model are dependent upon angular velocity. Thus there is little need to compare angular velocity, if a comparison of angular acceleration has been performed.

12.5 Reference Frames

Extreme care must be exercised when changing reference systems. For the CAL3-D model, accelerations are absolute, but their components are expressed in the direction of the body-fixed axes. Displacements are expressed with respect to a vehicle-fixed frame.

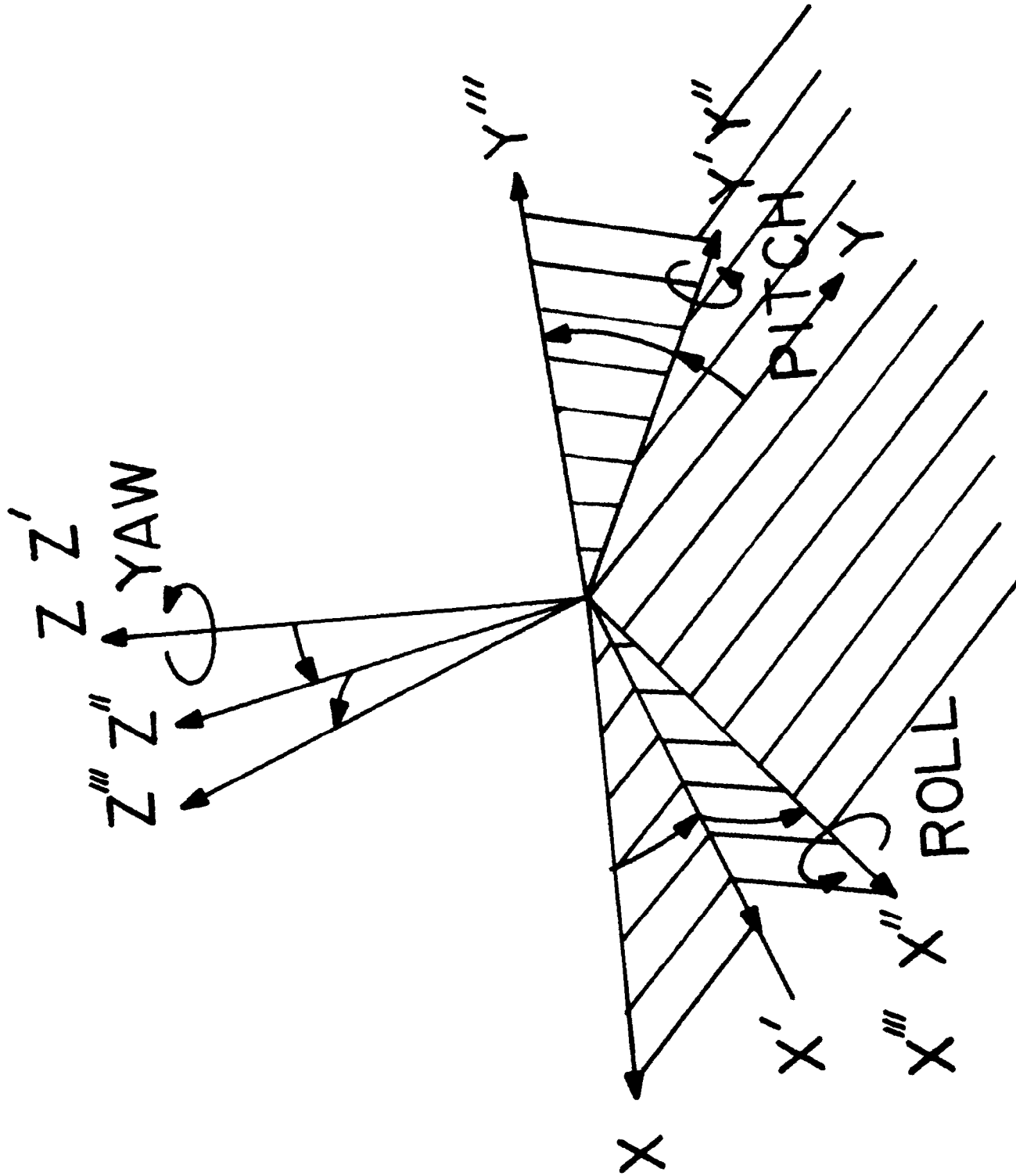


Figure 12.5 Determination of Direction Cosines in 3-D Space From Two Orthogonal Planar Views

CHAPTER 13

DATASET PREPARATION

13.1 Introduction

To execute the CAL3-D program, datasets were prepared in accordance with the input requirements delineated in Chapter 11. Basically, there were three different simulations, single segment impact with a deformable surface, vehicular impact with an anthropomorphic dummy and cadavers, and the drop tests carried out at TTI.

13.2 Single Segment Impact

This simulation involved contact between one surface and one body segment. Obviously, the number of joints was zero. Two types of contact were considered; impact of the lower leg against the bumper and head impact against the hood. Figure 12.1 illustrates the experimental set-up to acquire data for validation purposes. The lower leg of an anthropomorphic dummy is dropped onto a bumper, simulating vehicular impact. The coordinate axes for the vehicle are X_V , Y_V , and Z_V , and those for the inertial reference frame are X_I , Y_I , and Z_I . The body-fixed axes for body segments are X_B , Y_B , and Z_B . The instant of contact is identified on film by a flash. The simulation is started 25 msec (10 movie frames) before contact. The bumper is a small plane and is replaced by an ellipsoid in the computer simulation. Figure 13.1 illustrates a similar test set-up for head-hood impact.

13.3 Vehicular-Pedestrian Impact Simulation at Wayne State University

These runs involved the use of unembalmed cadavers and a 95th percentile male dummy (Sierra). The model was required to simulate impact of a 'pedestrian' subject with the front end of a 1973 Chevrolet. Table 13.1 summarizes the details of the experiments.

The crash-victim was divided into 15 segments with 14 joints for the dummy; 12 segments with 11 joints for the cadaver. Figure 13.2 shows a general outline of the crash-victim. Particulars describing dummy and cadaver segments are listed in Tables 13.2 and 13.3 respectively. Relevant information on joints is tabulated in Tables 13.4 and 13.5.

It is interesting to note from the high speed movies that the cadaver knee bends laterally during bumper contact. This observation shows that the knee cannot be considered as a pinned joint. Therefore, in cadaver impacts it is treated as a ball and socket joint. However, for the anthropomorphic dummy as shown in Figure 4.23, the metal rod in the leg bends but does not allow the knee to deflect laterally. In the model, it is simulated as a pinned joint for dummy impacts.

TABLE 13.1

SUMMARY OF IMPACT EXPERIMENTS

Run No.	Subject	Impact Speed km/h (mph)	Impact Mode	Bumper Contact from time of simulation Initiation (msec)	Simulation Duration (msec)
D03	95th percentile dummy	23.5 (14.6)	left lateral	**	500
D05	95th percentile dummy	29.8 (18.5)	frontal	100	500
D08	95th percentile dummy	22.2 (13.8)	left lateral	75	-
D09	95th percentile dummy	39.4 (24.5)	left lateral	50	600
D10	95th percentile dummy	24.1 (15.0)	left lateral	80	500
C02	female cadaver 3350	23.3 (14.5)	left lateral	110	-
C03	male cadaver 3352	24.1 (15.0)	left lateral	75	500
C05	female cadaver 3375	32.2 (20.0)	frontal	80	-
C06	male cadaver 3392	37.3 (23.2)	left lateral*	65	500
DYN16	Rt. lower leg (dummy)	23.5 (14.6)	right lateral	25	100
DYN34	Head (dummy)	23.2 (14.4)	right lateral	25	100
M1	95th percentile dummy	13.5 (8.4)	nose down	30	500

* Bumper was padded with 15 cm of urethane foam rubber. In these cases it was the respective plane of contact (not necessarily bumper)

** No bumper flash synchronization existed

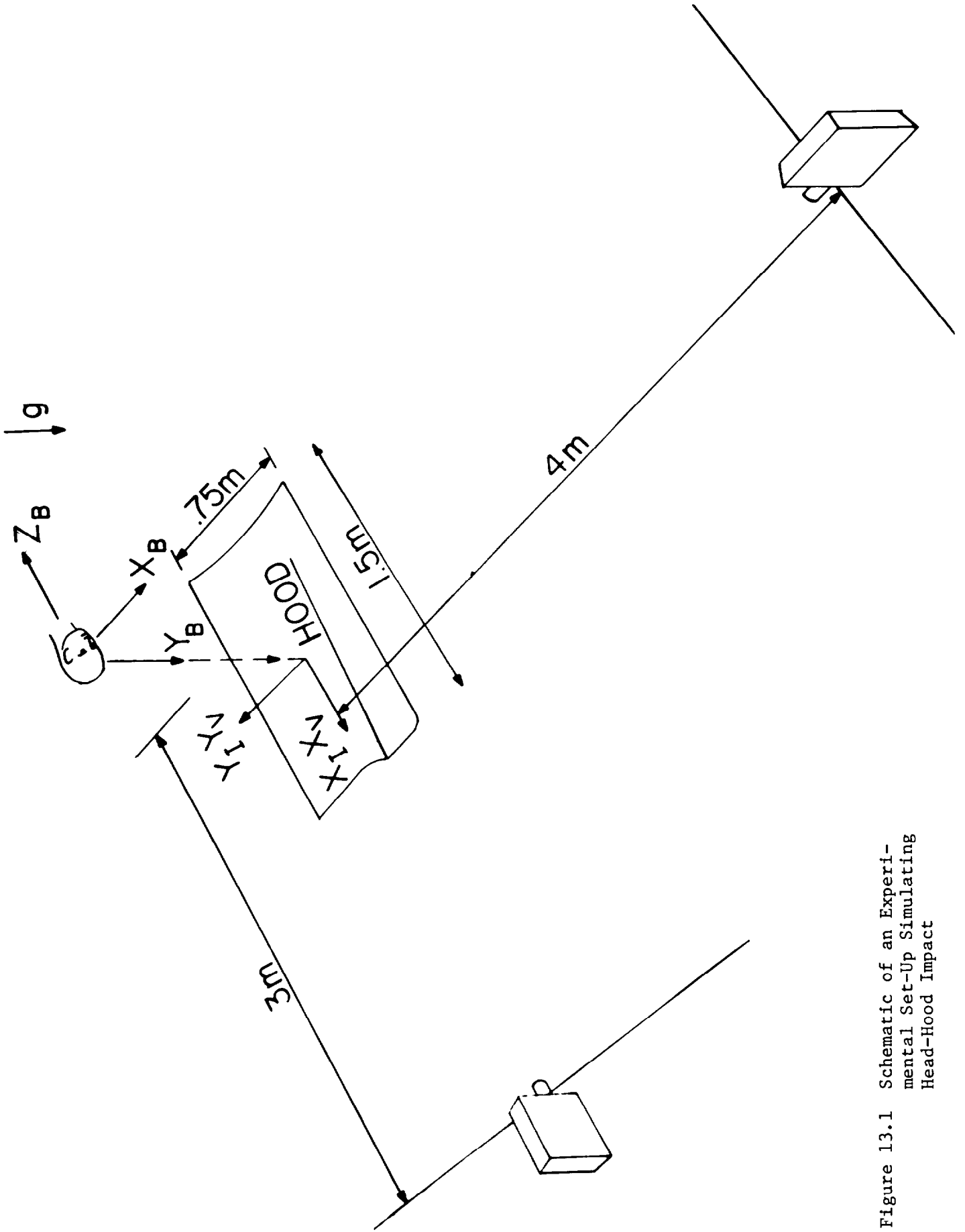


Figure 13.1 Schematic of an Experimental Set-Up Simulating Head-Hood Impact

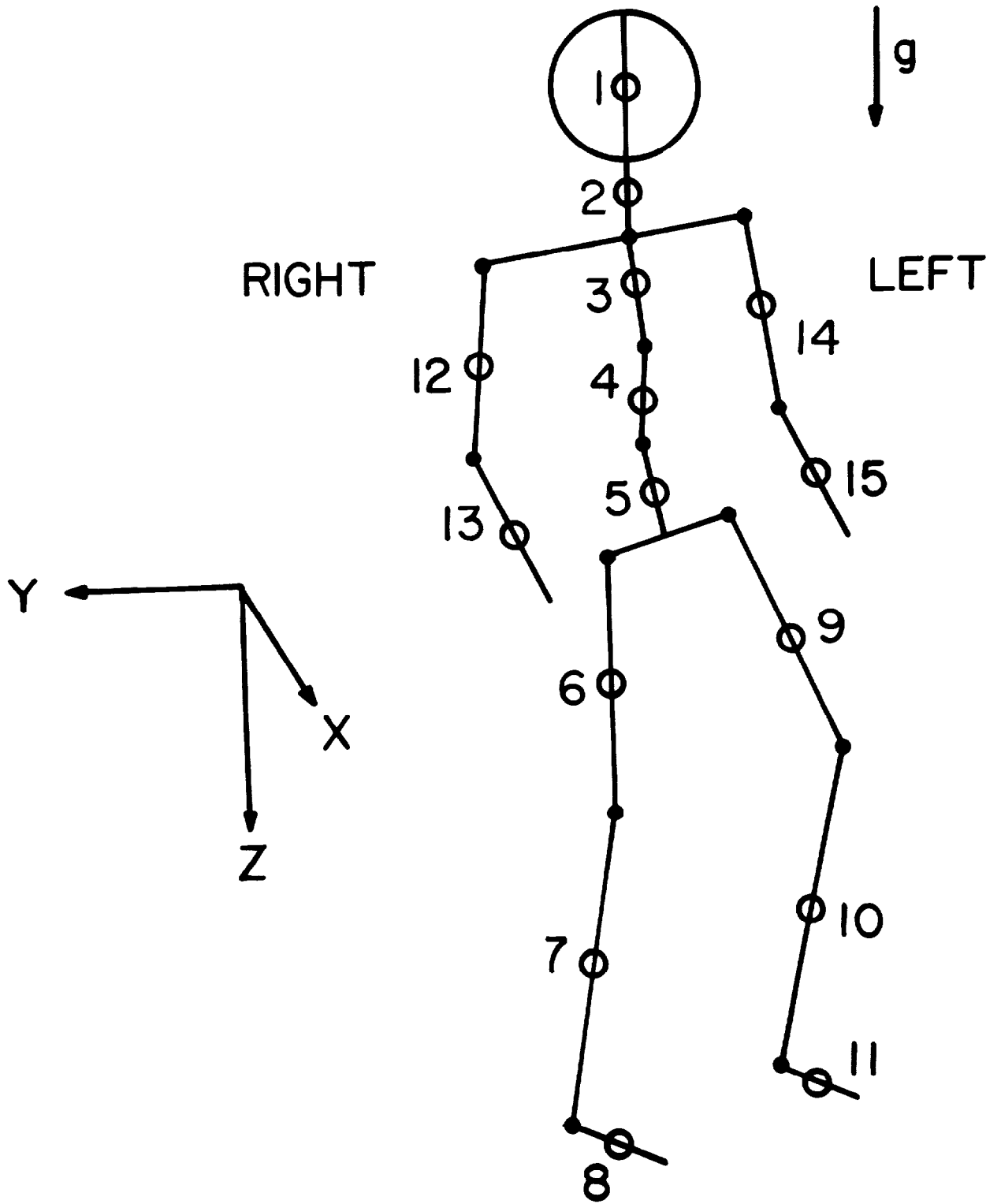


Figure 13.2 Schematic of a Crash Victim

TABLE 13.2

SEGMENT DESCRIPTION OF DUMMY IMPACTS

Segment	Number	Segment I.D.	Printer Plot Symbol*
Head	1	H	1
Neck	2	N	2
Upper Torso	3	UT	3
Central Torso	4	CT	4
Lower Torso	5	LT	5
Right Upper Leg	6	RUL	6
Right Lower Leg	7	RLL	7
Right Foot	8	RF	8
Left Upper Leg	9	LUL	9
Left Lower Leg	10	LLL	A
Left Foot	11	LF	B
Right Upper Arm	12	RUA	C
Right Lower Arm	13	RLA	D
Left Upper Arm	14	LUA	E
Left Lower Arm	15	LLA	F

* Even though number of segments was different for the dummy and cadaver runs and there was only one segment for the single segment impact the same printer plot symbol is used for each segment.

TABLE 13.3

SEGMENT DESCRIPTION OF CADAVER IMPACTS

Segment	Number	Segment I.D.	Printer Plot Symbol
Head and Neck	1	H-N	1
Upper Torso	2	UT	3
Central Torso	3	CT	4
Lower Torso	4	LT	5
Right Upper Leg	5	RUL	6
Right Lower Leg and Foot	6	RLLF	7
Left Upper Leg	7	LUL	9
Left Lower Leg and Foot	8	LLLF	A
Right Upper Arm	9	RUA	C
Right Lower Arm	10	RLA	D
Left Upper Arm	11	LUA	E
Left Lower Arm	12	LLA	F

TABLE 13.4

JOINT DESCRIPTION FOR DUMMY IMPACTS

Joint #	Joint I.D.	Joint* Type	Printer Plot Symbol	Adjoint Distal	Segment # (JNT(J))	Proximal
1	HP	0	M	1		2
2	NP	0	N	2		3
3	W	0	O	3		4
4	P	0	P	4		5
5	RH	0	Q	5		6
6	RK	1	R	6		7
7	RA	0	S	7		8
8	LH	0	T	5		9
9	LK	1	U	9		10
10	LA	0	V	10		11
11	RS	0	W	3		12
12	RE	1	X	12		13
13	LS	0	Y	3		14
14	LE	1	Z	14		15

* 0 means ball and socket
1 means pinned

Even though number of joints was different for the dummy and cadaver runs, the same printer plot symbol was used for each segment.

TABLE 13.5

JOINT DESCRIPTION FOR CADAVER IMPACTS

Joint #	Joint I.D.	Joint* Type	Printer Plot Symbol	Adjoint Segment # Distal	Segment # (JNT(J)) Proximal
1	NP	0	N	1	2
2	W	0	O	2	3
3	P	0	P	3	4
4	RH	0	Q	4	5
5	RK	0	R	5	6
6	LH	0	T	4	7
7	LK	0	U	7	8
8	RS	0	W	2	9
9	RE	1	X	9	10
10	LS	0	Y	2	11
11	LE	1	Z	11	12

* 0 means ball and socket
 1 means pinned

Anthropometric data were also acquired. An anthropometer was used for length measurements. The eccentricity of segment geometric centers with respect to their centers of gravity and segment weights were obtained using a center-of-gravity table and x-ray techniques. Mass moments of inertia were measured by a trifilar pendulum. Joint properties were acquired using a load cell and accelerometers. A detailed description of these measurement techniques is given in Volume 2.

The front end of the impacting vehicle was subdivided into 25 planes. They are shown in Figure 13.3, with the vehicle-fixed coordinate axes X_V , Y_V and Z_V . The inertial coordinates are identified as X_I , Y_I , and Z_I . For all runs except D05, the first 18 planes were sufficient for the simulation. For D05, planes 19 through 25 were used in place of the first few planes. Small planes such as 3,4,7,8,9,10, and 22 were replaced by ellipsoids attached to the vehicle. One run was made with a bumper and grille padded with 15 cm of polyurethane foam (Run C06). The shape of the front end is shown in Figure 13.4. Details concerning planes and expected contacts with body segments are given in Tables 13.6, 13.7 and 13.8. To synchronize film and analog data, an electronic flash was used as a reference. The flash occurred when the release solenoid was actuated. This time varied from 50 to 110 msec. before bumper contact and is listed for different runs in Table 13.1. As shown in Figure 13.5, a fifth wheel was attached to the vehicle. It indicated the velocity of the vehicle, which was differentiated numerically to obtain the deceleration pulse of the vehicle. Table 13.9 compares model and experimental vehicle kinematic data. Figure 13.6 illustrates the deceleration pulse and Figure 13.7 illustrates the frequency content of such a pulse, as measured by a vehicle-fixed triaxial accelerometer. These two figures indicate that since the deceleration pulse was useless as an input parameter an alternate approach is needed - numerical differentiation of the velocity pulse.

A typical set up for a lateral impact (Run C03) is illustrated in Figures 13.8, 13.9, 13.10, 13.11 and 13.12. Initial conditions are measured from these photographs. The rotation angles yaw, pitch and roll are shown in Figure 12.4. Using this order of rotation and the initial configuration shown in Figures 13.8 through 13.12, the initial conditions for the crash victim were found. The technique was described in Chapter 12. A computer program converted these rotations to the order of roll, pitch and yaw to suit input requirements of CAL3-D.

Location of accelerometers on body segments was determined using the technique described in Chapter 3. Angular acceleration could be computed for segments instrumented with 9 accelerometers and the acceleration output of the model was specified at accelerometer locations so comparisons could be made. Targets located on these accelerometers were used for linear displacement comparisons.

The five functions needed to compute contact forces are: force-deflection function, inertial spike, R-factor, G-factor and friction coefficient. These functions are briefly described below:

- (i) Force-deflection function: There are two basic types of contact

1973 CHEVROLET

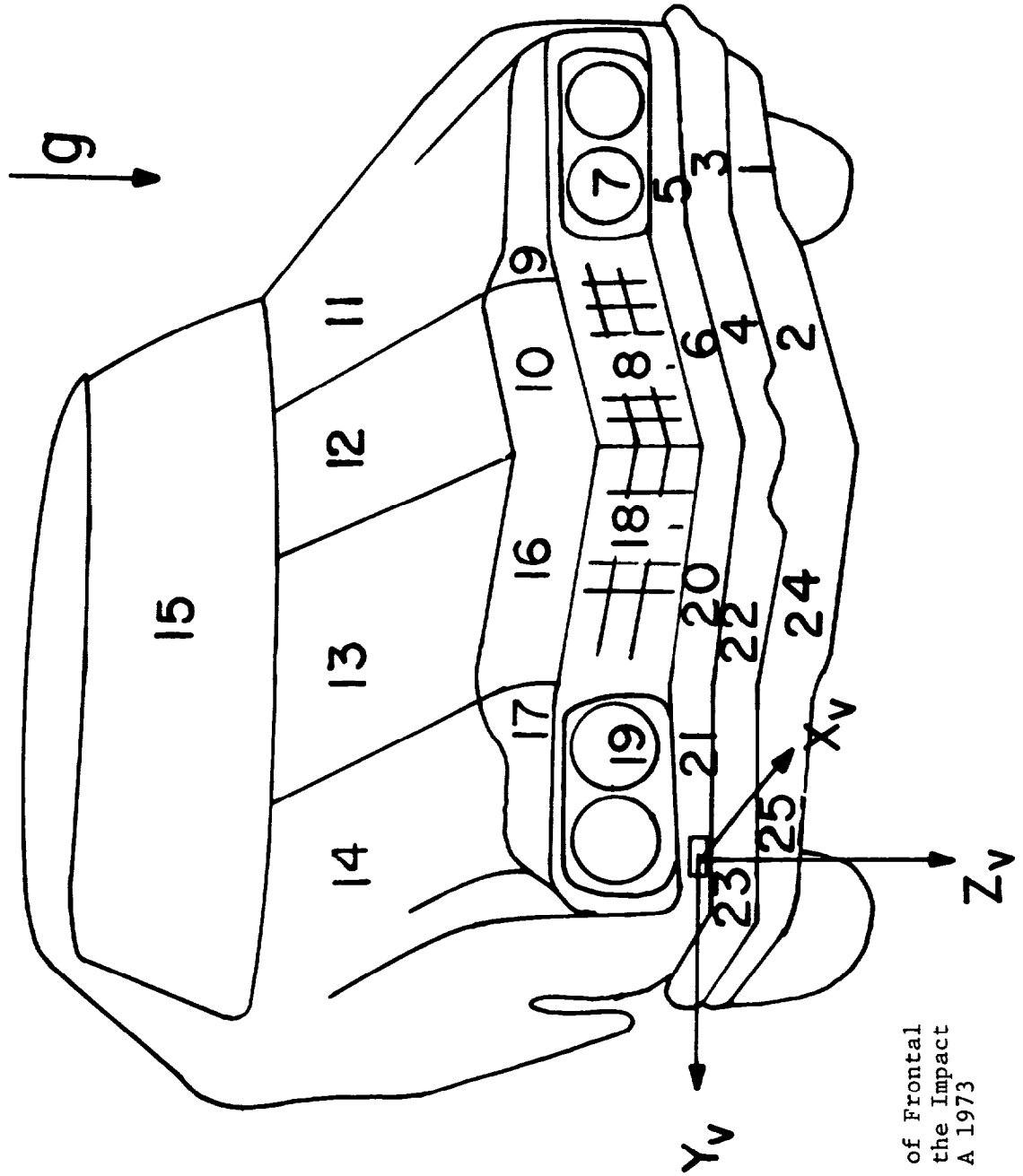


Figure 13.3 Schematic of Frontal
Planes of the Impact
Vehicle - A 1973
Chevrolet

Dimensions are
in C.M.

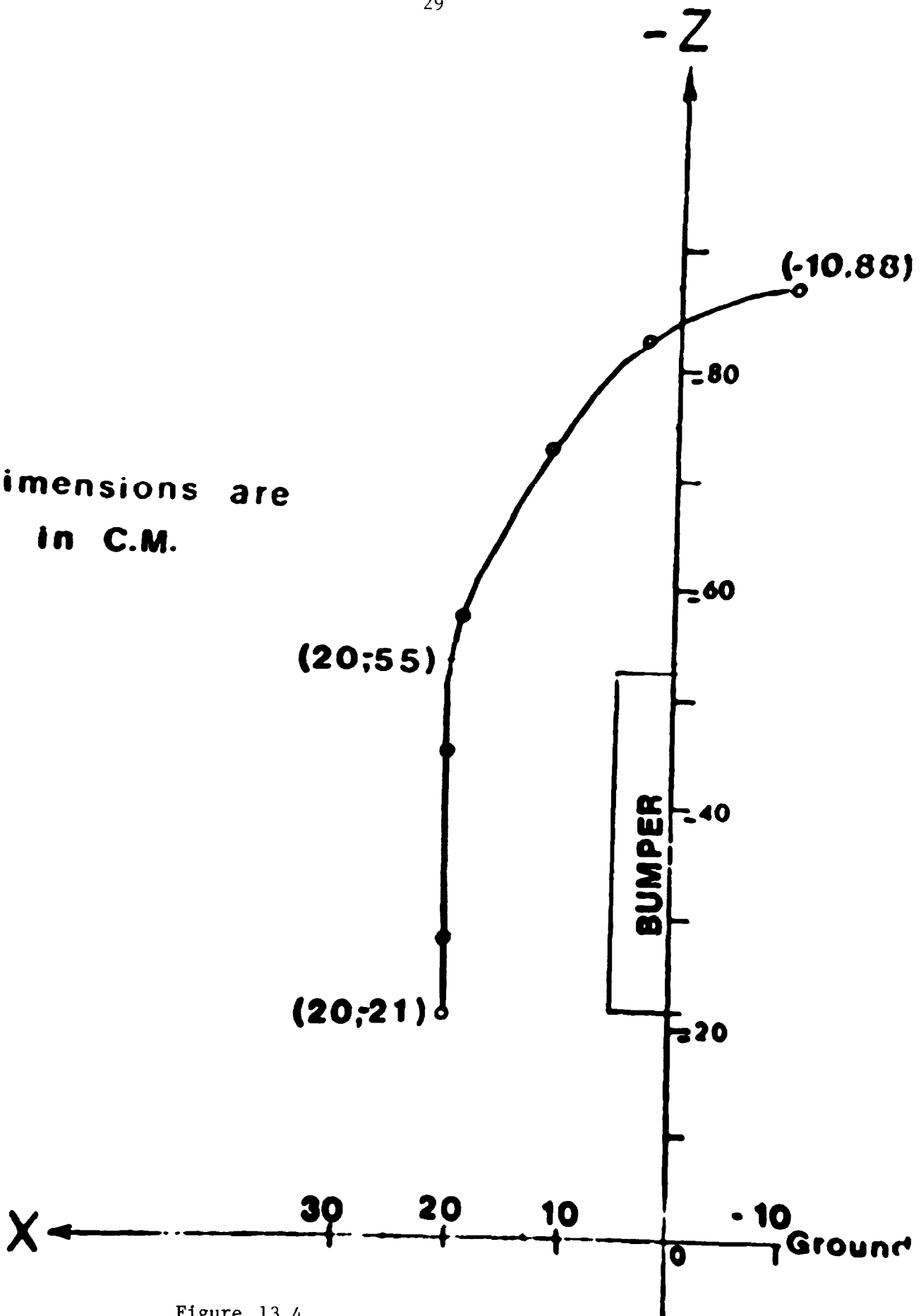


Figure 13.4
Vehicle Front End Geometry for Run
C06 (Padded Front End)

TABLE 13.6

EXPECTED CONTACTS FOR LATERAL IMPACT RUNS

D03, D08, D09, D10, C02, and C03

Segments	Planes	Segments Body	Plane
H	11, 12, 13		
N			
UT	11, 12, 13		
CT	11, 12, 13		
LT	11, 12, 13		
RUL	11, 12	LUL	4, 7, 8, 9, 10
RLL			3, 4
RF			
LUL	11, 12		4, 7, 8, 9, 10
LLL	2		3, 4
LF	Ground		
RUA	11, 12, 13		
RLA	11, 12, 13		
LUA	11, 12		
LLA	11, 12		

For definitions of segments refer to Tables 13.2 and 13.3.
 For definition of plane numbers, refer to Figure 13.3.

TABLE 13.7

EXPECTED CONTACTS FOR FRONTAL RUN

D05 (Right front end)

Segments	Planes	Vehicle Segments (planes)
H	13, 14	
N		
UT	13, 14	
CT	13, 14	
LT	13, 14	
RUL	13, 14	16, 17, 18, 19, 22
RLL	24, 25	22, 23
RF		
LUL	13, 14	16, 17, 18, 19, 22
LLL	24, 25	22, 23
LF	Ground	
RUA	13, 14	
RLA	13, 14	
LUA	13, 14	
LLA	13, 14	17

For definitions of plane numbers, refer to Figure 13.3.
 For definitions of segments refer to Tables 13.2 and 13.3.

TABLE 13.8

EXPECTED CONTACTS FOR PADDED BUMPER RUN C06

Segments	Planes	Body Segments
H-N	11, 12, 13	
UT	11, 12	
CT	11, 12	
LT	11, 12	
RUL	7, 8, 9, 10, 11, 12	LUL
RLL-F	1, 3, 2, 4, 7, 9, 8, 10	LLL-F
LUL	7, 9, 8, 10, 11, 12	
LLL-F	1, 3, 2, 4, 7, 9, 8, 10 Ground	
RUA	11, 12	
RLA	11, 12, 13	
LUA	11, 12	
LLA	7, 9, 8, 10, 11, 12	LT, LUL

These plane numbers relate to Figure 13.3. In actual dataset of Run C06, the plane numbers were different.

For definitions of segments refer to Tables 13.2 and 13.3.

For definitions of plane numbers, refer to Figure 13.3.

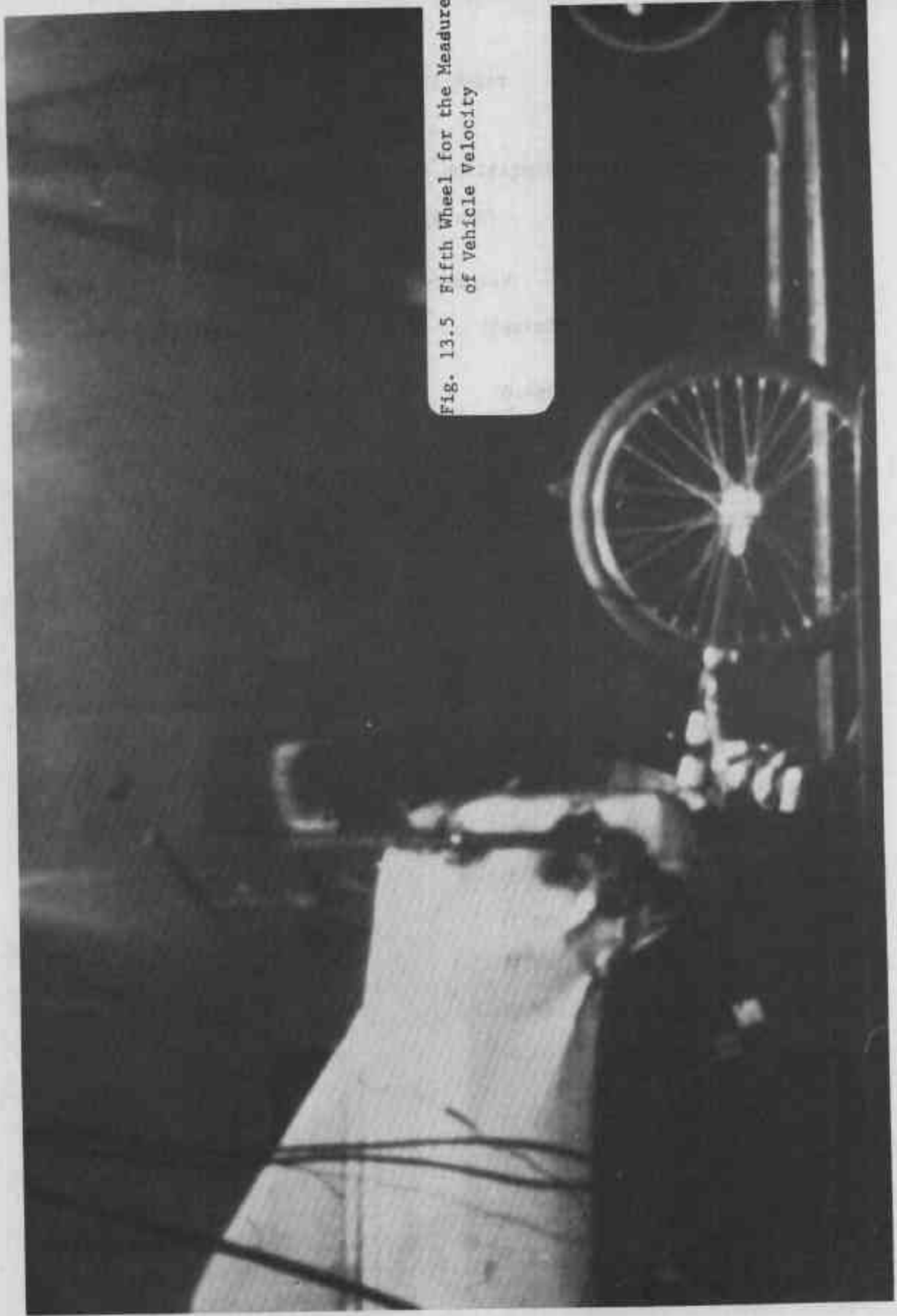


Fig. 13.5 Fifth Wheel for the Measurement of Vehicle Velocity

TABLE 13.9

VEHICLE VELOCITY COMPARISON FROM MODEL AND EXPERIMENT

(Run D10)

Time (ms)	Model Decel (g)	Velocity		Experiment	
		Model cm/sec	(in/sec)	cm/sec	(in/sec)
0	0.00	670.6	(264.0)	670.6	(264.0)
100	0.04	669.6	(263.6)	670.6	(264.0)
200	0.19	659.4	(259.6)	659.4	(259.6)
300	0.14	645.0	(253.9)	636.6	(250.6)
400	0.33	623.7	(246.6)	625.0	(246.1)
500	0.62	573.8	(225.9)	568.2	(223.7)
600	0.50	515.8	(203.1)	511.4	(201.3)
700	0.53	466.0	(183.5)	465.8	(183.4)
800	0.65	408.9	(161.0)	403.7	(158.9)
900	0.60	348.1	(137.0)	341.1	(134.3)
1000	0.57	291.1	(114.6)	284.3	(111.9)
1100	0.56	236.3	(93.0)	227.1	(89.4)
1200	0.61	179.5	(70.7)	170.3	(67.1)
1300	0.87	103.9	(40.9)	99.7	(39.2)
1400	0.78	19.9	(7.8)	11.2	(4.4)
1500	0.00	00.0	(0.0)	0.0	(0.0)

Stopping distance (at the end of 1500 ms)

As computed by model 607.3 cm (239.1 in.)

As measured during experiment 582.9 cm (229.5 in)

TRIA X

RUN NO.: DOT: D05

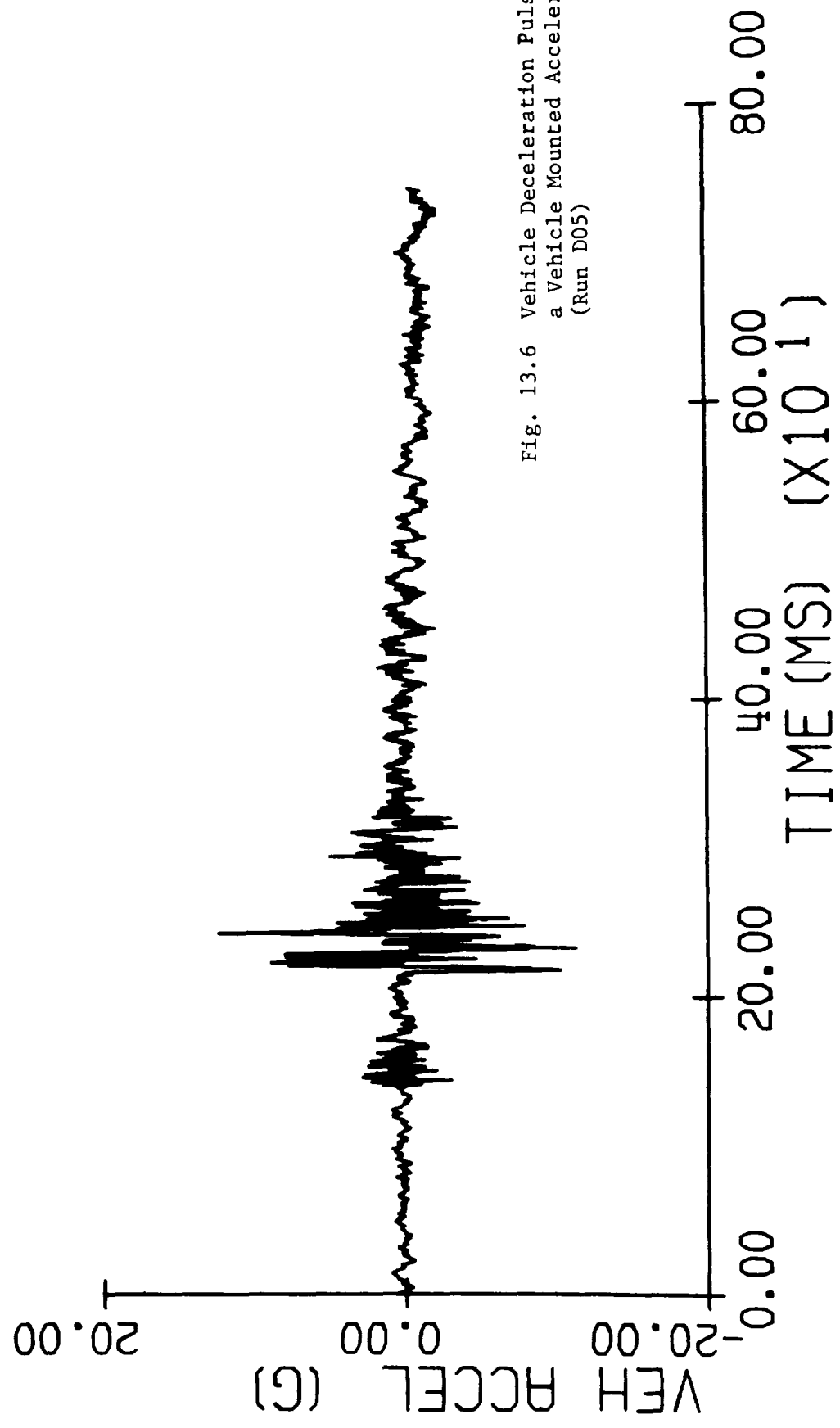


Fig. 13.6 Vehicle Deceleration Pulse from a Vehicle Mounted Accelerometer (Run D05)

TRIA X

RUN NO.: DOT: D05

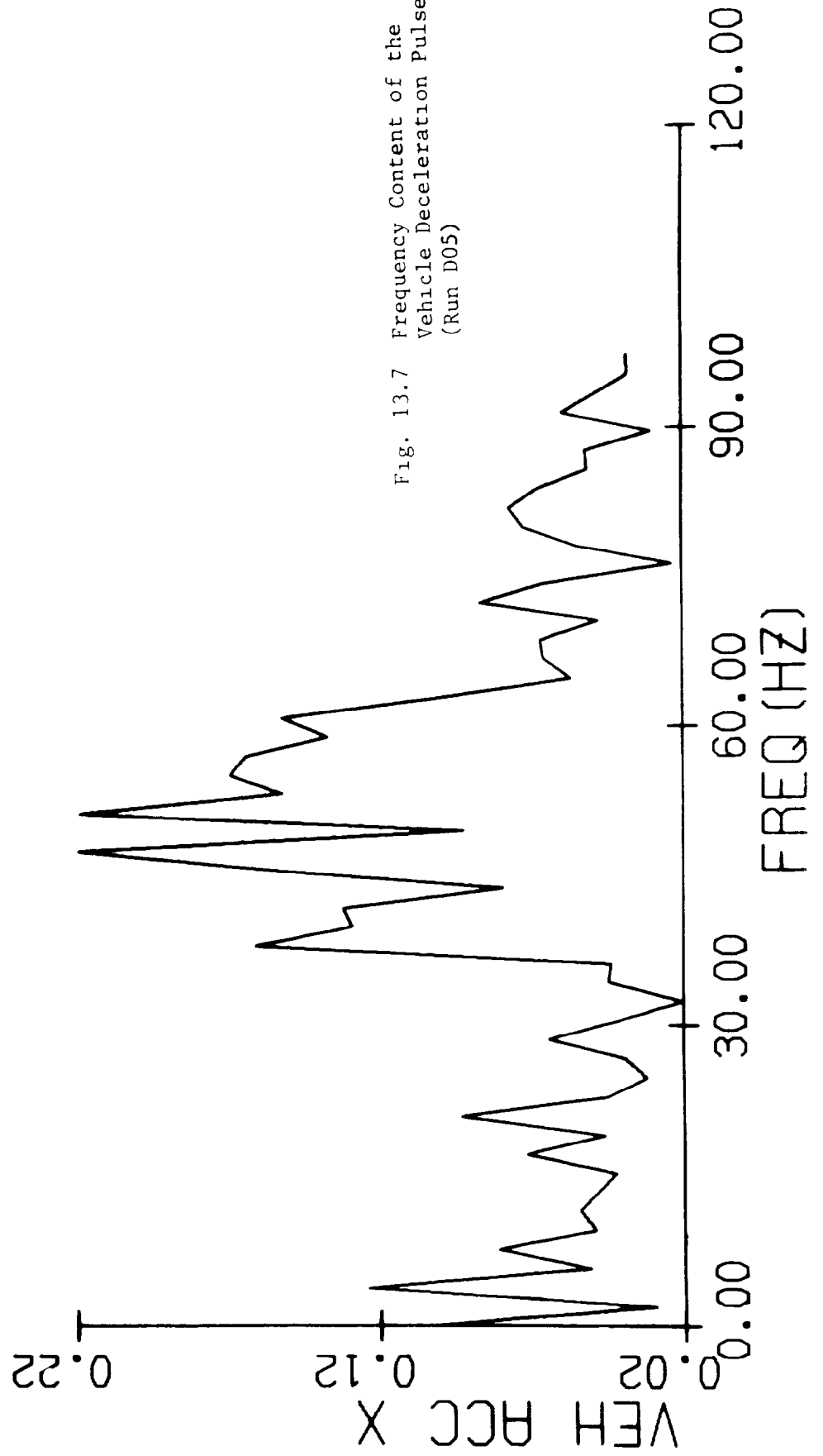


Fig. 13.7 Frequency Content of the Vehicle Deceleration Pulse (Run D05)

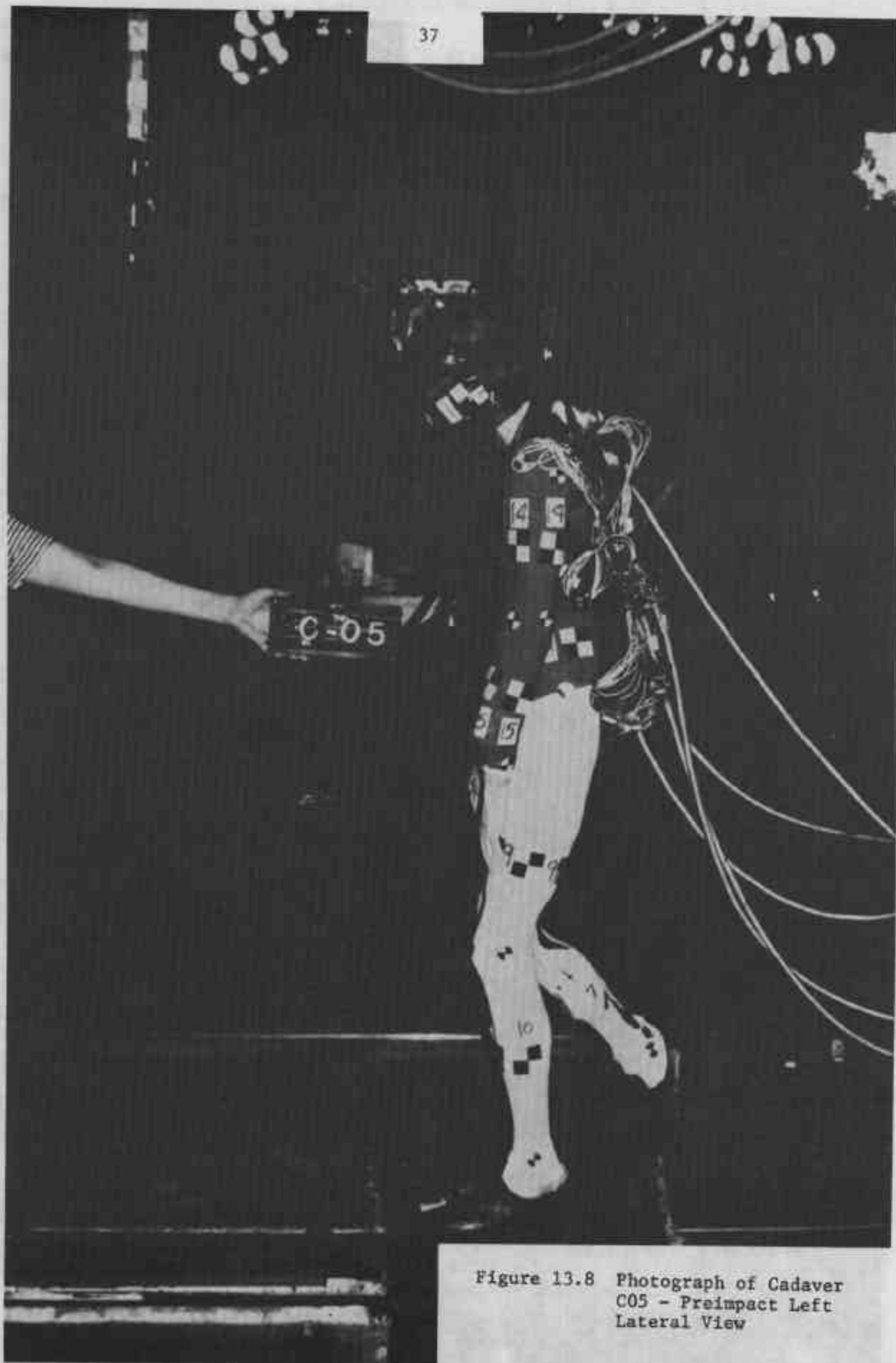


Figure 13.8 Photograph of Cadaver
C05 - Preimpact Left
Lateral View

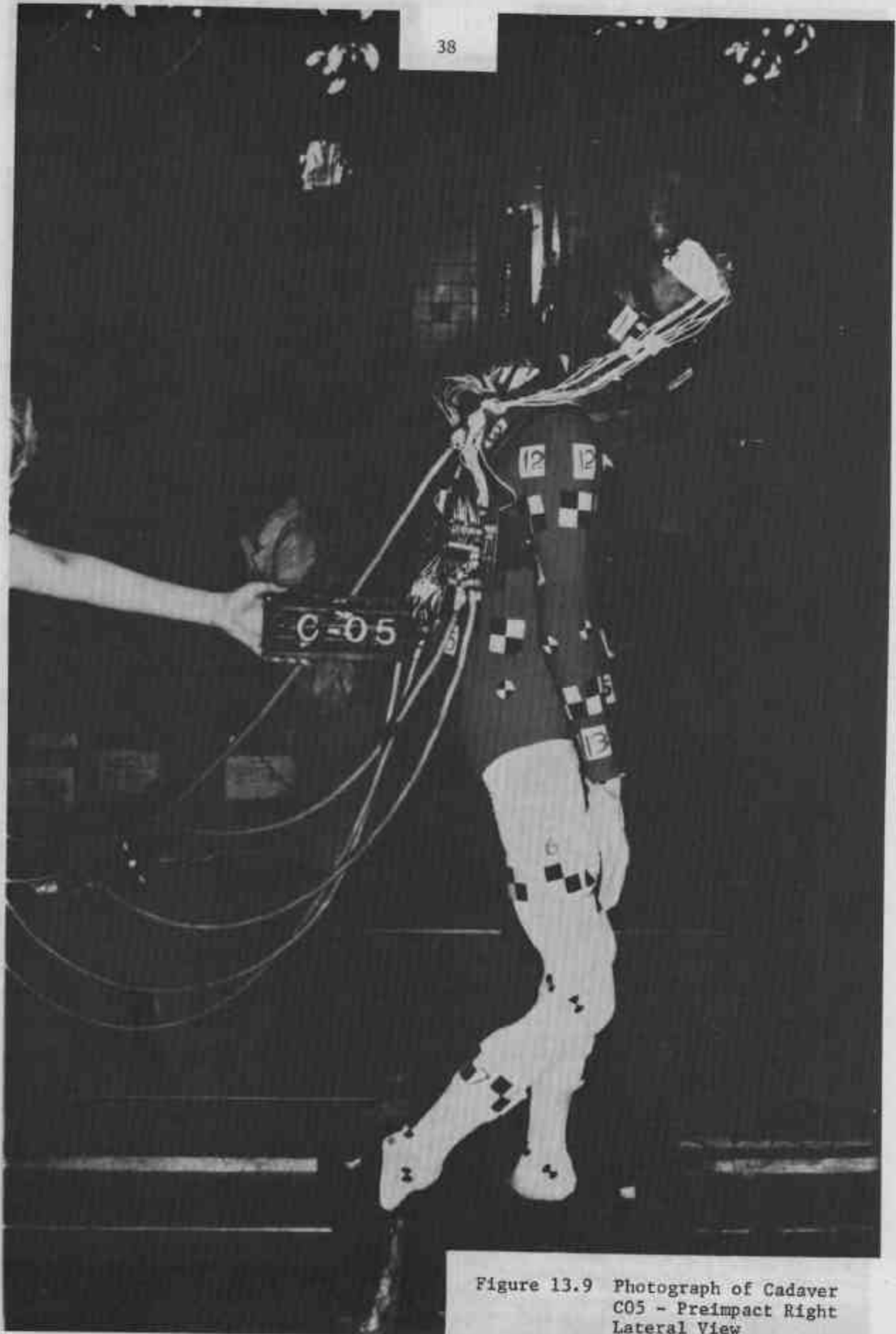


Figure 13.9 Photograph of Cadaver
C05 - Preimpact Right
Lateral View

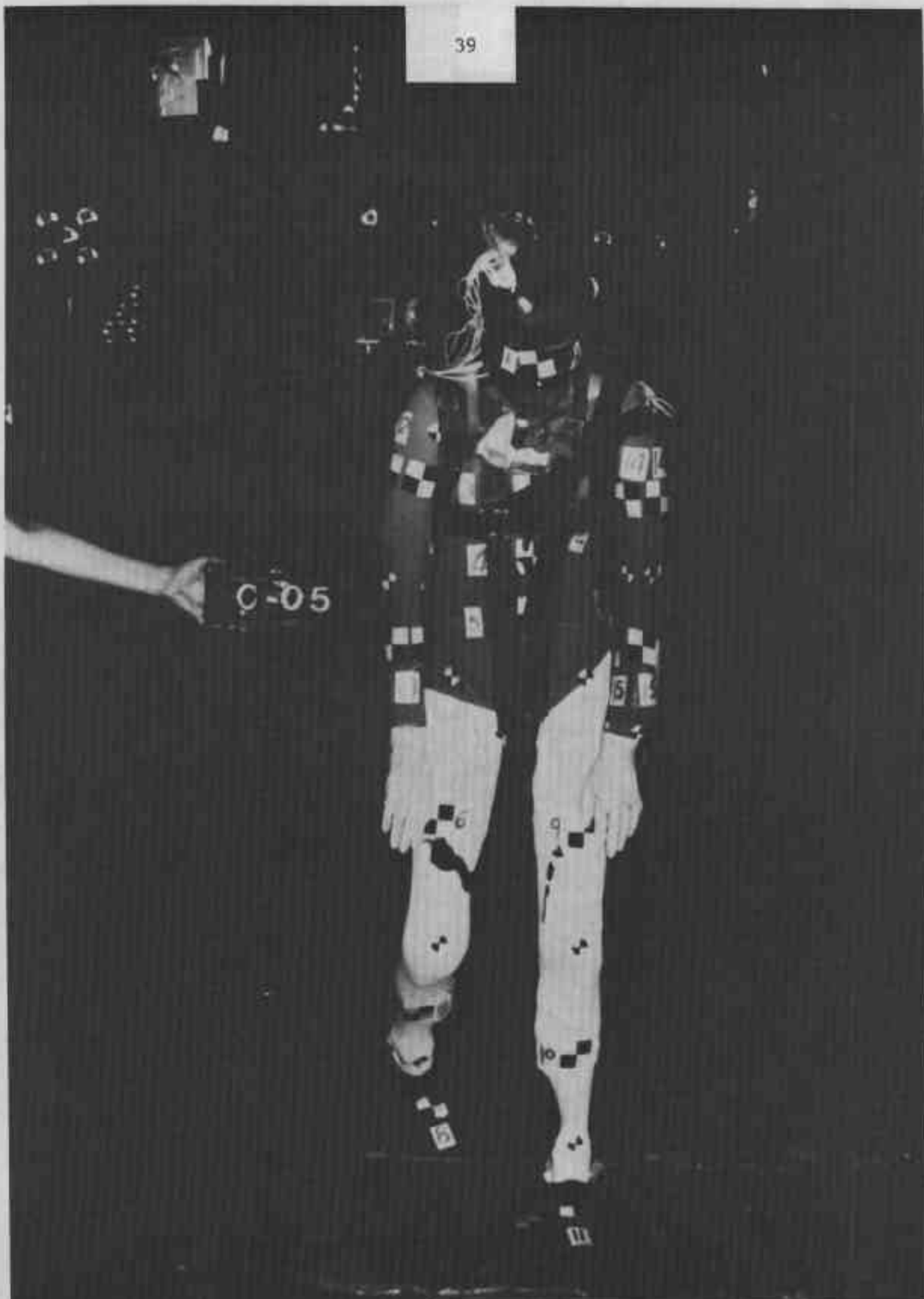


Figure 13.10 Photograph of Cadaver C05 - Preimpact Frontal View

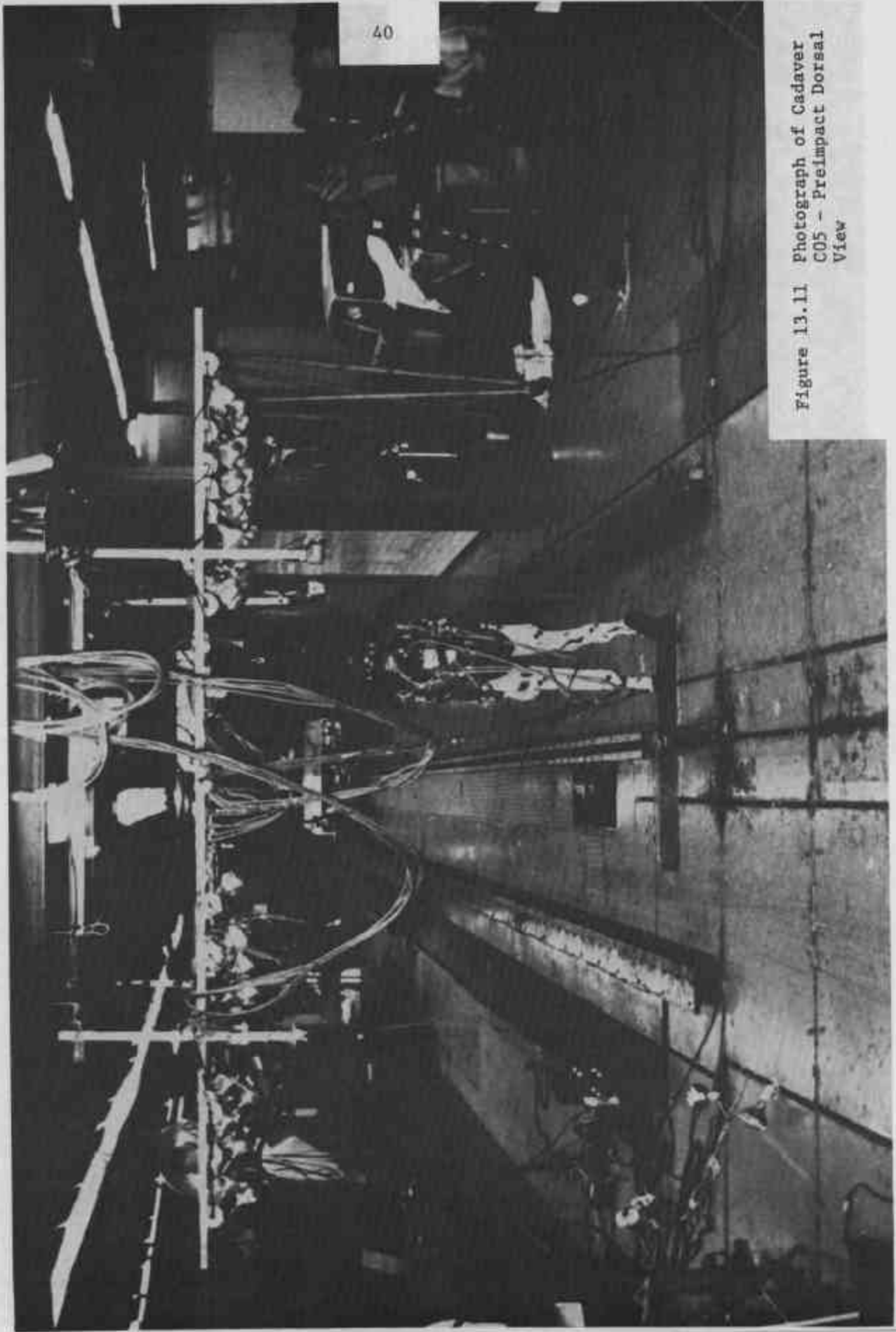


Figure 13.11 Photograph of Cadaver
C05 - PreImpact Dorsal
View

41



Figure 13.12 Photograph of Cadaver
C05 - Preimpact Top
View

during a pedestrian impact simulation, between a plane and a body segment, and segment-to-segment. For plane-to-segment contact, it is assumed that the plane is deformed by the rigid segment. This generates a contact force which is a function of the amount of penetration. For segment-to-segment contact, the contact force is computed by a different method. The semi-axes of the impacting ellipsoids are shrunk until they are tangential to each other. The force is a function of the change in semi-axis length. For both types of impact, either tabular data or a polynomial must be provided as a force-deflection function. As mentioned in Chapter 11, care must be taken to allow for a large deflection or penetration, if tearing of plane by a segment is not to be simulated. The user also has the option to specify the location of the resultant contact force. In this simulation the center of the ellipse formed by contacting surfaces was selected.

(ii) Inertial spike: Due to the velocity dependence of contact, an inertial spike is necessary to simulate dynamic contact. It is superimposed onto the static force-deflection curve described above.

(iii) R-factor: During unloading of a deformable member, energy is dissipated. This function is the ratio of area under the unloading curve to that under the loading curve. If the value of R is not a constant, it can be represented as a function of maximum deflection at which unloading began.

(iv) G-factor: This factor accounts for plastic deformation of the plane. It is the ratio of the permanent deflection to the maximum deflection. As in the case of the R-factor, it can be represented by a function of the maximum deflection.

(v) Friction coefficient: The coefficient of friction between the two contacting surfaces can be expressed in any one of the three forms of contact described above. It was found to be constant in magnitude for the contacting surfaces involved in the single segment tests. In the simulation, the constant values used ranged from 0.2 to 0.94.

Krieger (1976) made measurements to obtain values for these functions.

13.4 Vehicular-Pedestrian Impact Simulation at the Texas Transportation Institute

The Texas Transportation Institute (TTI) carried out a series of 9 dummy drop tests onto a mock-up of a vehicle front end simulating car-pedestrian impact. The mock-up is shown in Figure 13.13. Expected contacts, Table 13.10.

Data input for the Calspan model consisted of vehicular planes and anthropometric information for the dummy, including locations of accelerometers. All available information was obtained from Vol. IV of the Final Report from the Texas Transportation Institute (1973).

Joint properties were unavailable. A few measurements were made to verify the joint data provided by Calspan.

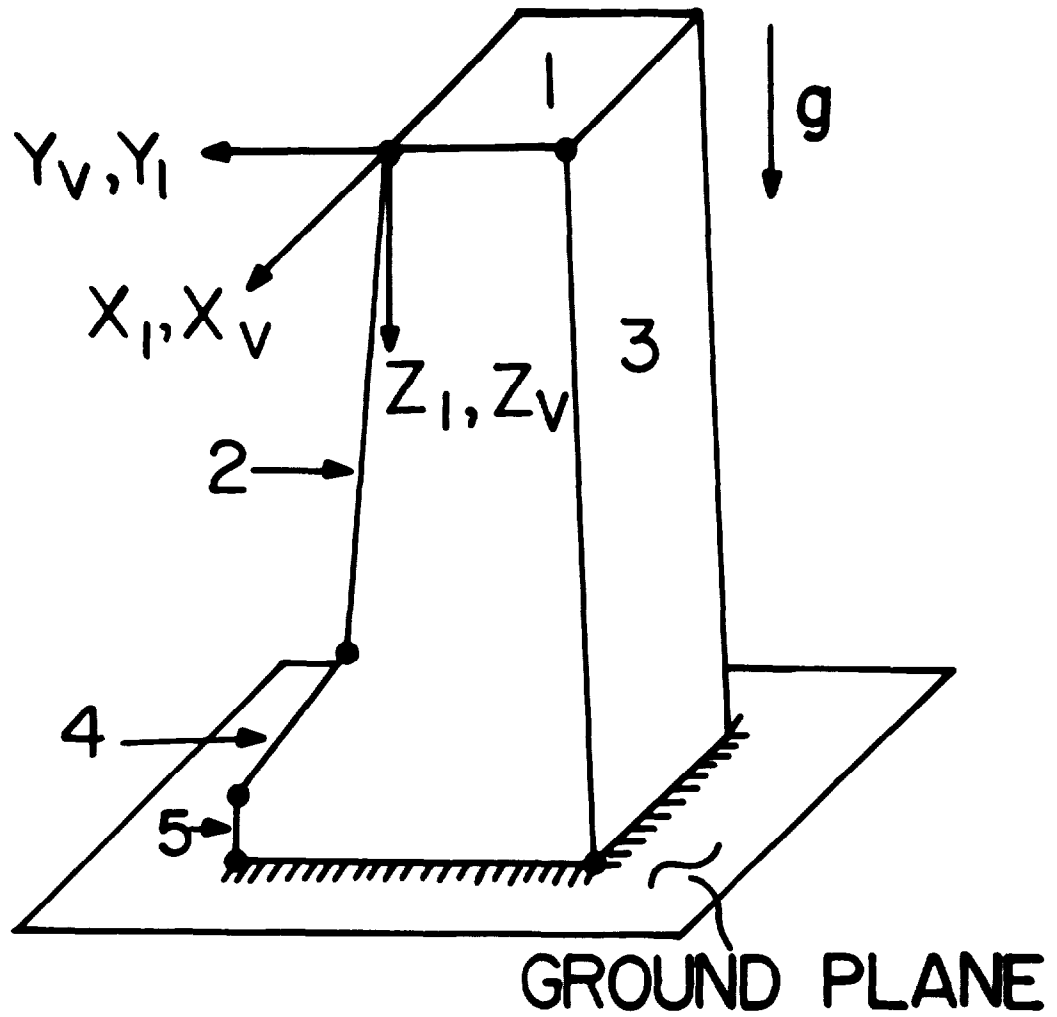


Figure 13.13 Vehicle Mock-Up Used by Texas Transportation Institute

TABLE 13.10

EXPECTED CONTACTS FOR TTI RUNS (FRONTAL-M1)

Segments	Planes
H	2, 4
N	
UT	2
CT	1, 2
LT	1, 2
RUL	1, 2, 3
RLL	1
RF	
LUL	1, 2, 3
LLL	1
LF	
RUA	
RLA	1
LUA	
LLA	1

For definitions of segments, refer to Tables 13.2 and 13.3.
 For definitions of plane numbers, refer to Figure 13.13.

One of the major problems in simulating the TTI drop tests was the differences in the definition of coordinate systems of the vehicle-fixed, inertial and body-fixed frames. Figure 13.14 shows the reference frames, as defined in CAL3-D model. In the TTI coordinate system, +Y- and +Z-axis are both opposite to that shown in Figure 13.14. Transformations were carried out to make the data compatible with the requirements of the CAL3-D program. The transformation matrix is:

$$\begin{array}{rcccl} X & & 1 & 0 & 0 & X_T \\ Y & = & 0 & -1 & 0 & Y_T \\ Z & & 0 & 0 & -1 & Z_T \end{array}$$

where, X_T , Y_T and Z_T are TTI coordinates.

Differences also arose in defining Euler angles. The order of rotation used by TTI is shown in Figure 13.14, while Calspan used roll, pitch and yaw. A computer program was written to relate the two sets of "Euler angles". They are related to the direction cosine matrix D_{ij} as follows:

$$\begin{aligned} D_{11} &= \cos\psi \cdot \cos\theta \cdot \cos\phi - \sin\psi \cdot \sin\phi \\ &= \cos\psi \cdot \cos\theta \\ D_{12} &= \cos\psi \cdot \cos\theta \cdot \sin\phi + \sin\psi \cdot \cos\phi \\ &= -(\cos\theta \cdot \sin\psi + \sin\theta \cdot \sin\psi \cdot \cos\psi) \\ D_{13} &= -\cos\psi \cdot \sin\theta = \\ &= -(\sin\theta \cdot \sin\psi - \sin\theta \cdot \cos\theta \cdot \cos\psi) \\ D_{21} &= -\sin\psi \cdot \cos\phi \cdot \cos\theta - \sin\phi \cdot \cos\psi \\ &= -(-\sin\psi \cdot \cos\theta) \\ D_{22} &= -\sin\phi \cdot \sin\psi \cdot \cos\theta + \cos\psi \cdot \cos\phi \\ &= \cos\psi \cdot \cos\theta - \sin\theta \cdot \sin\psi \cdot \sin\psi \\ D_{23} &= \sin\theta \cdot \sin\psi = \cos\psi \cdot \sin\theta + \sin\theta \cdot \sin\psi \cdot \cos\theta \\ D_{31} &= \sin\theta \cdot \cos\phi = -(\sin\theta) \\ D_{32} &= \sin\theta \cdot \sin\phi = -\sin\theta \cdot \cos\psi \\ D_{33} &= \cos\theta = \cos\theta \cdot \cos\psi \end{aligned}$$

Note that these relations transfer information contained in TTI coordinate system to suit the CAL3-D dataset (considering the peculiar order of rotation for input data).

13.5 Discussion on Integrator Input

Card A.4 in dataset provides important parameters which control the integrator. If proper values are assigned, they reduce cost and yield smooth output. They are identified as NDINT, NSTEPS, DT, HO, HMAX and HMIN. The following information was provided by Calspan Corporation in an input description document:

Card A.4 Format (2I4, 4F8.0)

NDINT Number of iterations for final convergence test of the integrator subroutine DINT (Minimum value = 2, suggested value = 4).

NSTEPS Number of integration steps (or output time points) for the integrator routine. May be zero to obtain initial conditions.

DT Main program time interval for integrator routine output (sec). Total time of run will be NSTEPS*DT seconds with main program Tape 1, printer plot and optional output produced every DT seconds.

HO Initial integrator step size (sec).

HMAX Maximum integrator step size (sec). For best efficiency DT should be an integral multiple of HMAX and HMAX a power of two multiple of HO. (Suggested value = 0.001 sec.)

HMIN Minimum integrator step size (sec). If a fixed step size is desired, set HMIN greater than HMAX, and step size will double from HO until HMAX is achieved.

For full-scale simulation of car-pedestrian impact, including the TTI drop tests, the total simulation time was determined from high-speed movies. Simulation was stopped shortly after significant contact has begun. For example, in the case of Wayne State University impact tests, simulation was carried out to 100 to 200 ms after initiation of head-hood contact. The following values were used for the pedestrian simulation:

NDINT = 4
 DT = 0.010 sec. *
 HO = 0.0005 sec.
 HMAX = 0.001 sec.
 HMIN = 0.0001 sec.

The total simulation time for the pedestrian impact tests is shown in Table 13.1.

* For a single segment impact DT = 0.005 sec.

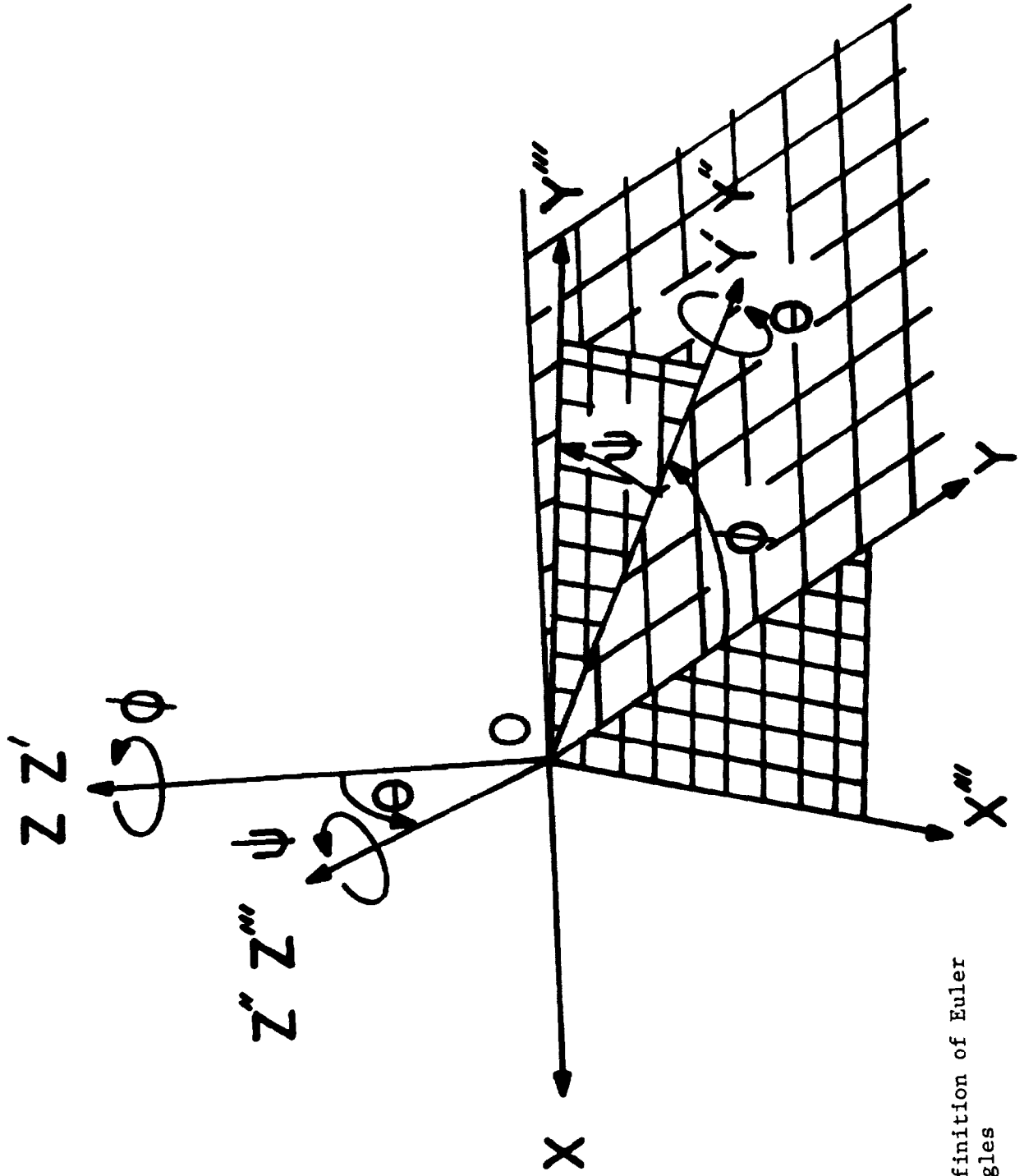


Figure 13.14 Definition of Euler Angles

MODEL VALIDATION FOR SINGLE SEGMENT IMPACT

14.1 Introduction

As a first step in the validation process, a single segment impact against a deformable surface was simulated and the results validated against experimental data. During pedestrian impact, the most significant contacts are of the head against the hood and the lower leg against the bumper.

Experimental data were acquired by dropping lower leg segments onto the bumper and heads onto hoods. These experiments served a dual purpose in that the force-deflection characteristics of these contacts were required as input data to the Cal3-D model. The experimental set-up for the leg-bumper impact is shown schematically in Figure 12.1. Both vehicle-fixed and segment-fixed coordinates are included for future reference. The drop height was selected to simulate the speed of impact during the 'pedestrian' experiments.

14.2 Leg-Bumper Contact Simulation

The right lower leg of a 95th percentile male dummy was dropped laterally onto the bumper of a 1973 Chevrolet. The impact site approximated that observed in full-scale impact runs. Naturally, a high value of roll angle is expected, as this was predominantly a 2-D motion. Figure 14.1 illustrates model output data on angular displacement relative to the vehicle-fixed axes. Figure 14.2 shows a comparison of the experimentally measured roll angle with that predicted by the model. The other two angles, yaw and pitch, were constant in the experiment, at 90° and 0° respectively, while in the model, yaw ranged between 86.5° to 92° and pitch varied from 0.5° to -5.5° . In view of the good correlation in angular displacement, a comparison of linear and angular acceleration can be made for this simulation. Obviously, the X-component of angular acceleration and Y-component of linear acceleration are dominant. Figure 14.3 demonstrates the relative magnitude of the X-component of angular acceleration with respect to the other 2 components. Figure 14.4 shows a comparison of this component in the model and experiment. A comparison of the Y-component of linear acceleration is shown in Figure 14.5. The pattern of both curves is similar but the experimental level is higher than that of the model prediction. X- and Z-components of linear displacements are shown in Figures 14.6 and 14.7 respectively. The actual rebound is higher than that predicted by the model. A comparison of the X-component of linear acceleration is shown in Figure 14.8. The correlation is obviously poor and cannot be explained by the existence of mechanical cross-axis sensitivity of accelerometers, which could be as high as 3 to 15%. The manufacturer guaranteed it to be less or equal to 5%.

14.3 Head-Hood Contact Simulation

The head of a 95th percentile male dummy was dropped laterally onto

RUN NO.: DN16-RLL

YAW MOD
PITCHMOD
ROLL MOD

○ — ○
▲ — ▲
+ — +

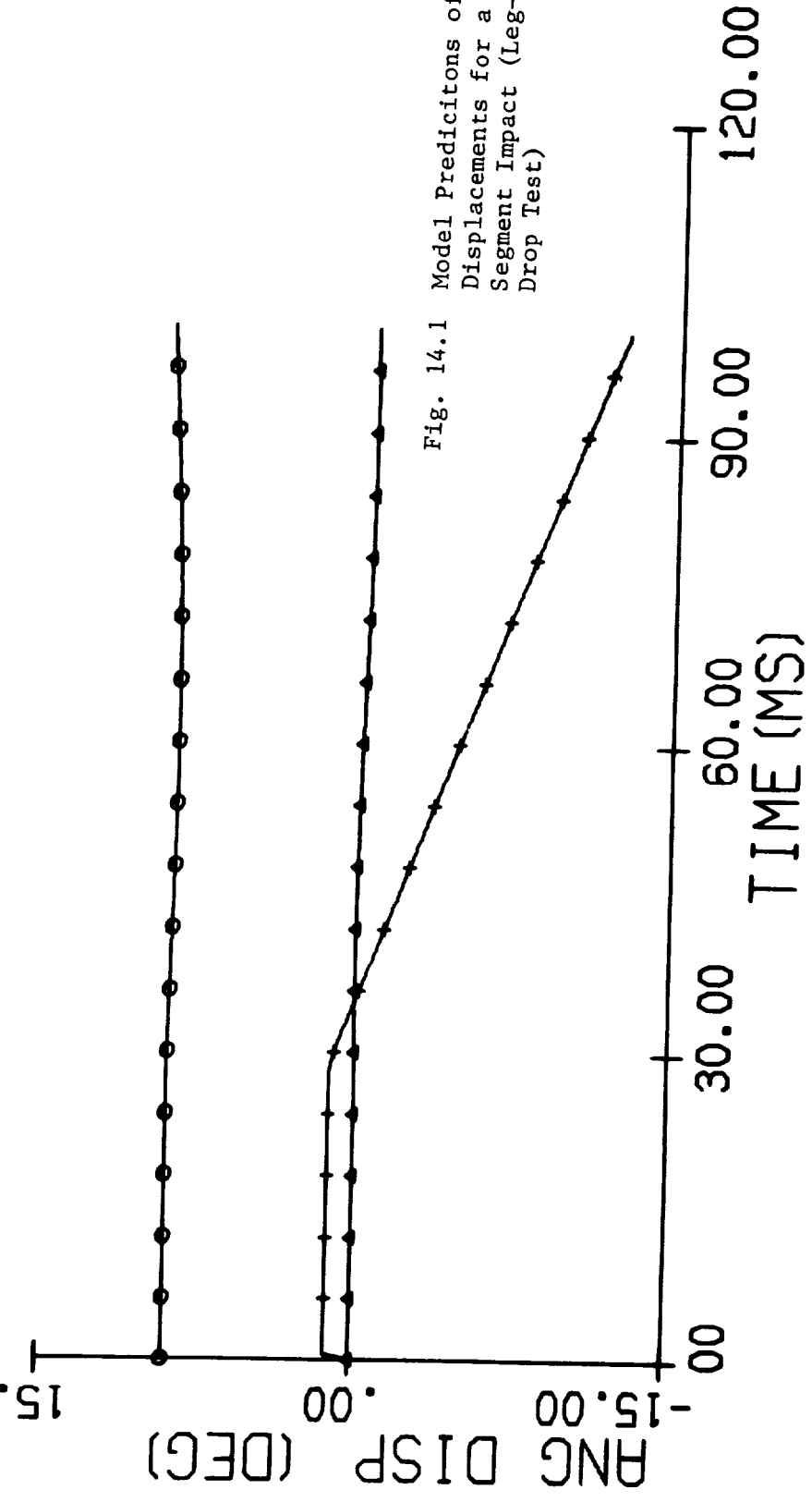


Fig. 14.1 Model Predictions of Angular Displacements for a Single Segment Impact (Leg-Bumper Drop Test)

MODEL
EXPT.

RUN NO.: DN16-RLL

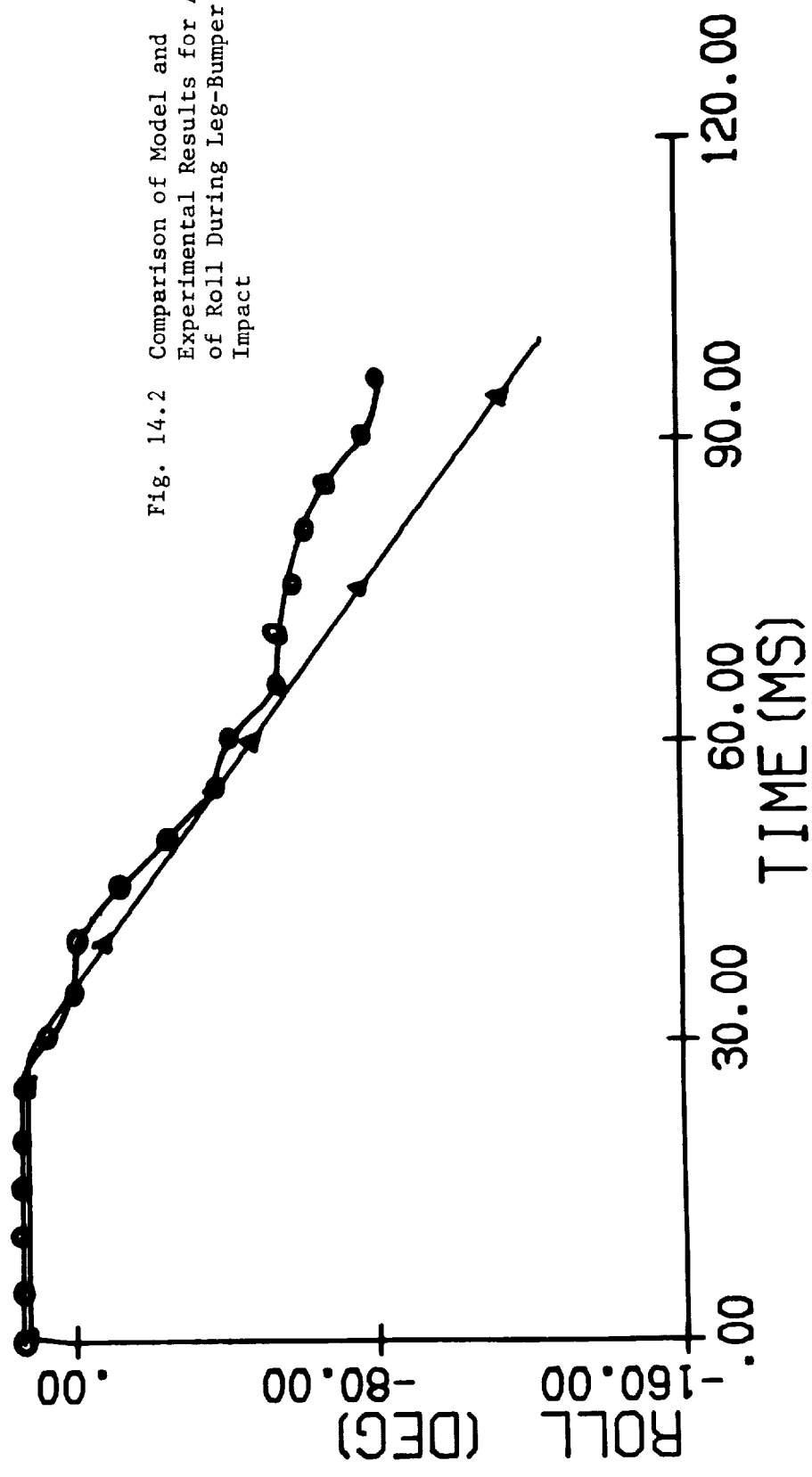


Fig. 14.2 Comparison of Model and Experimental Results for Angle of Roll During Leg-Bumper Impact

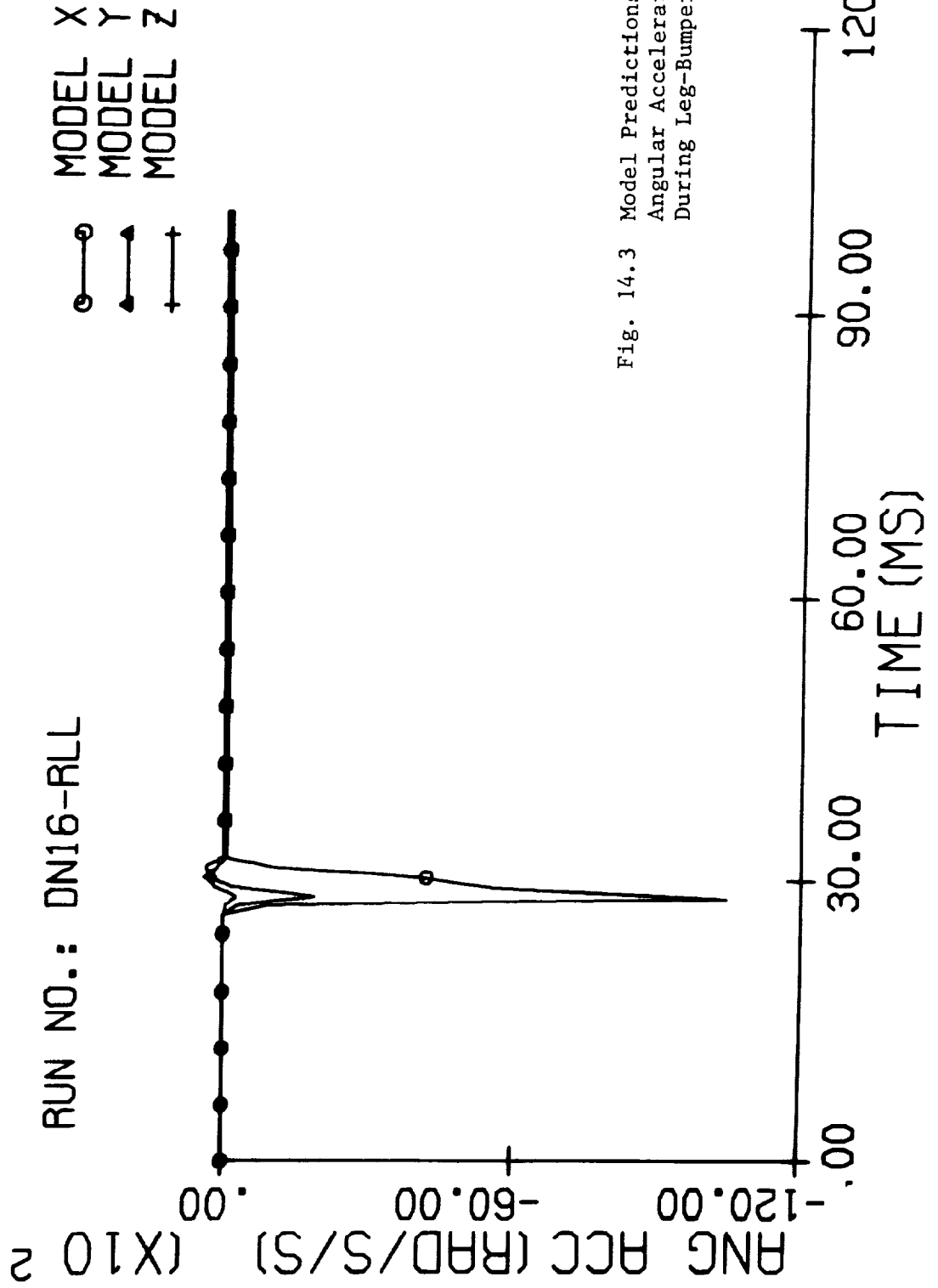


Fig. 14.3 Model Predictions of Segment Angular Acceleration Components During Leg-Bumper Impact

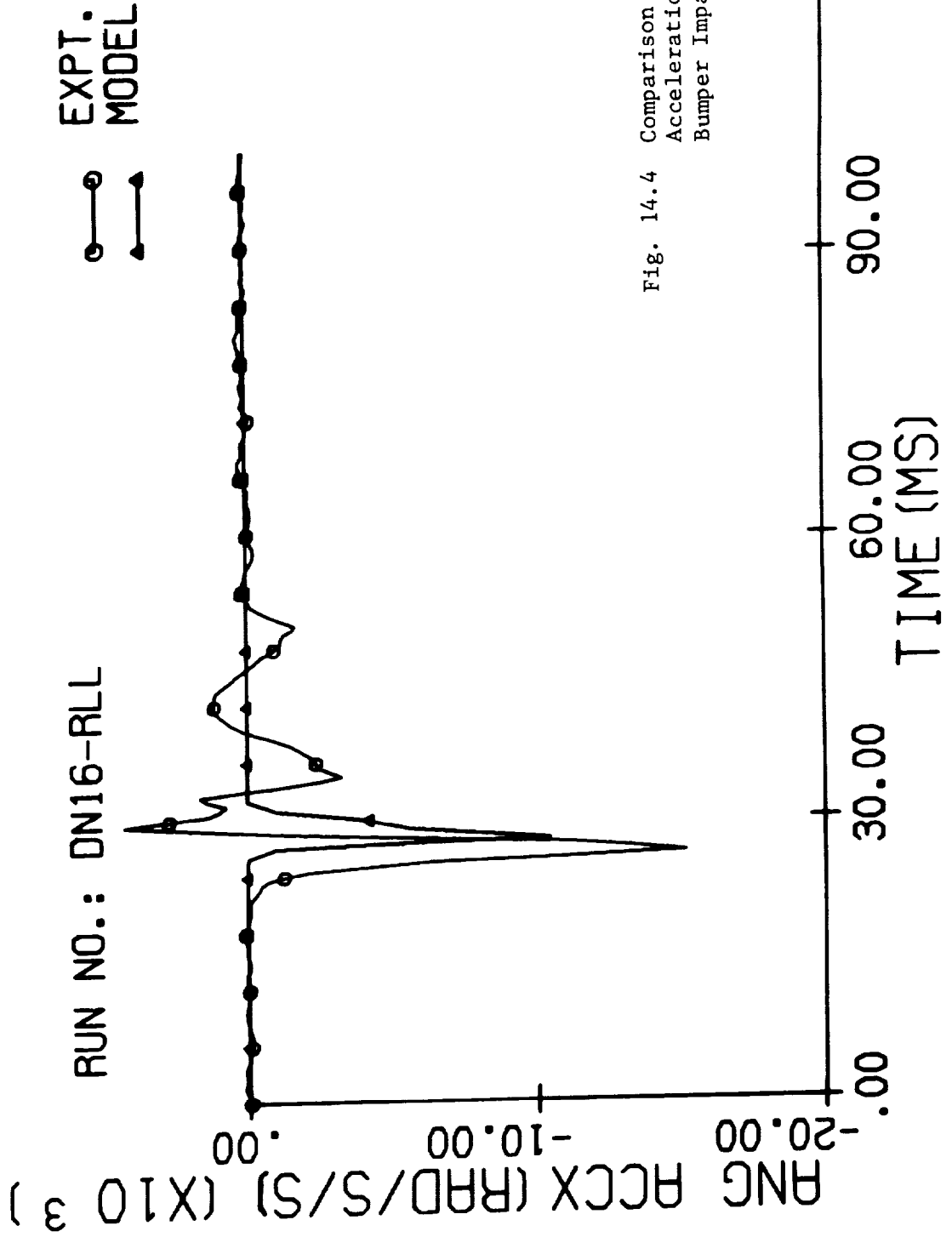
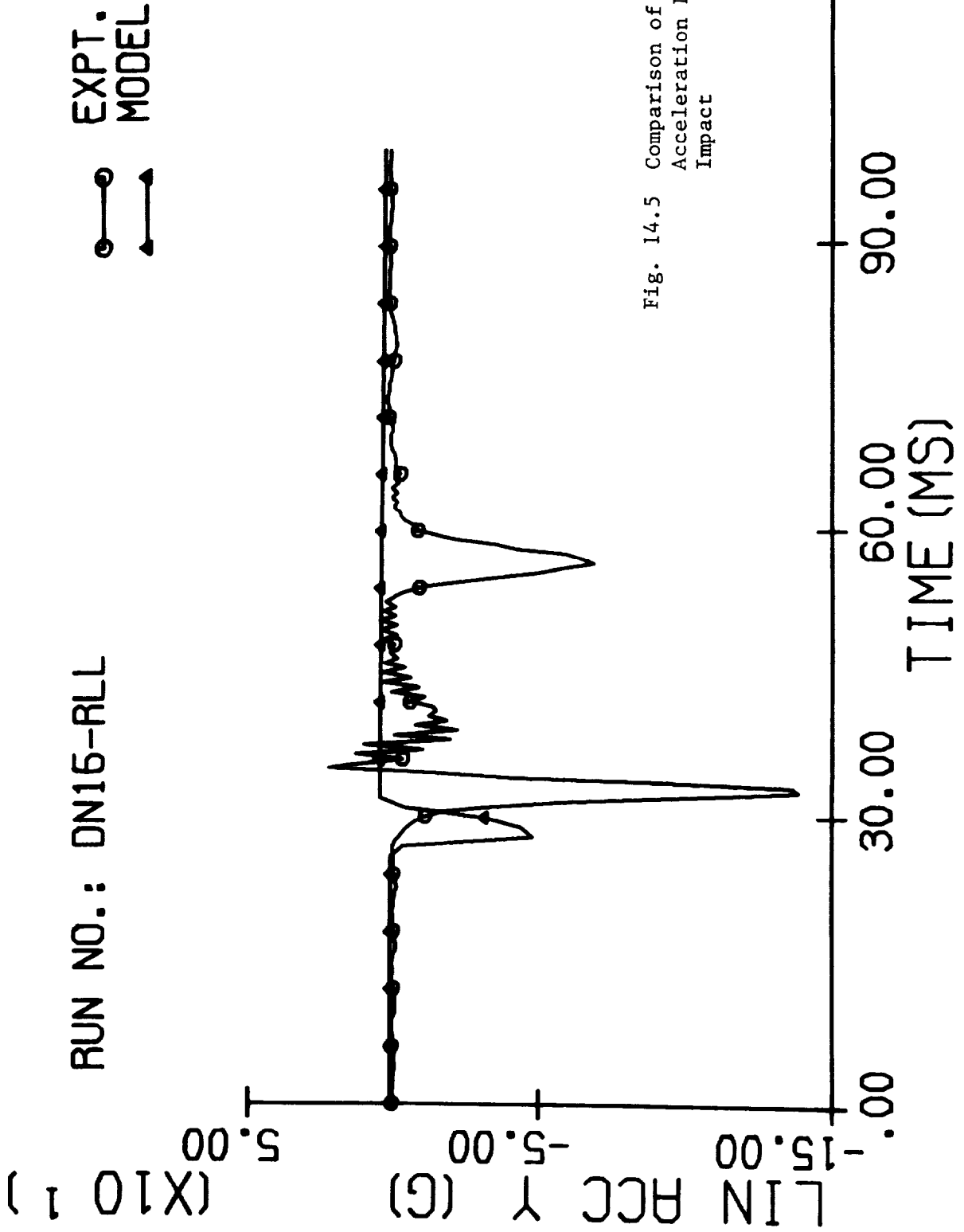


Fig. 14.4 Comparison of X-Axis Angular Acceleration During Leg-Bumper Impact



RUN NO.: DN16-RLL

▲ MODEL
○ EXPT.

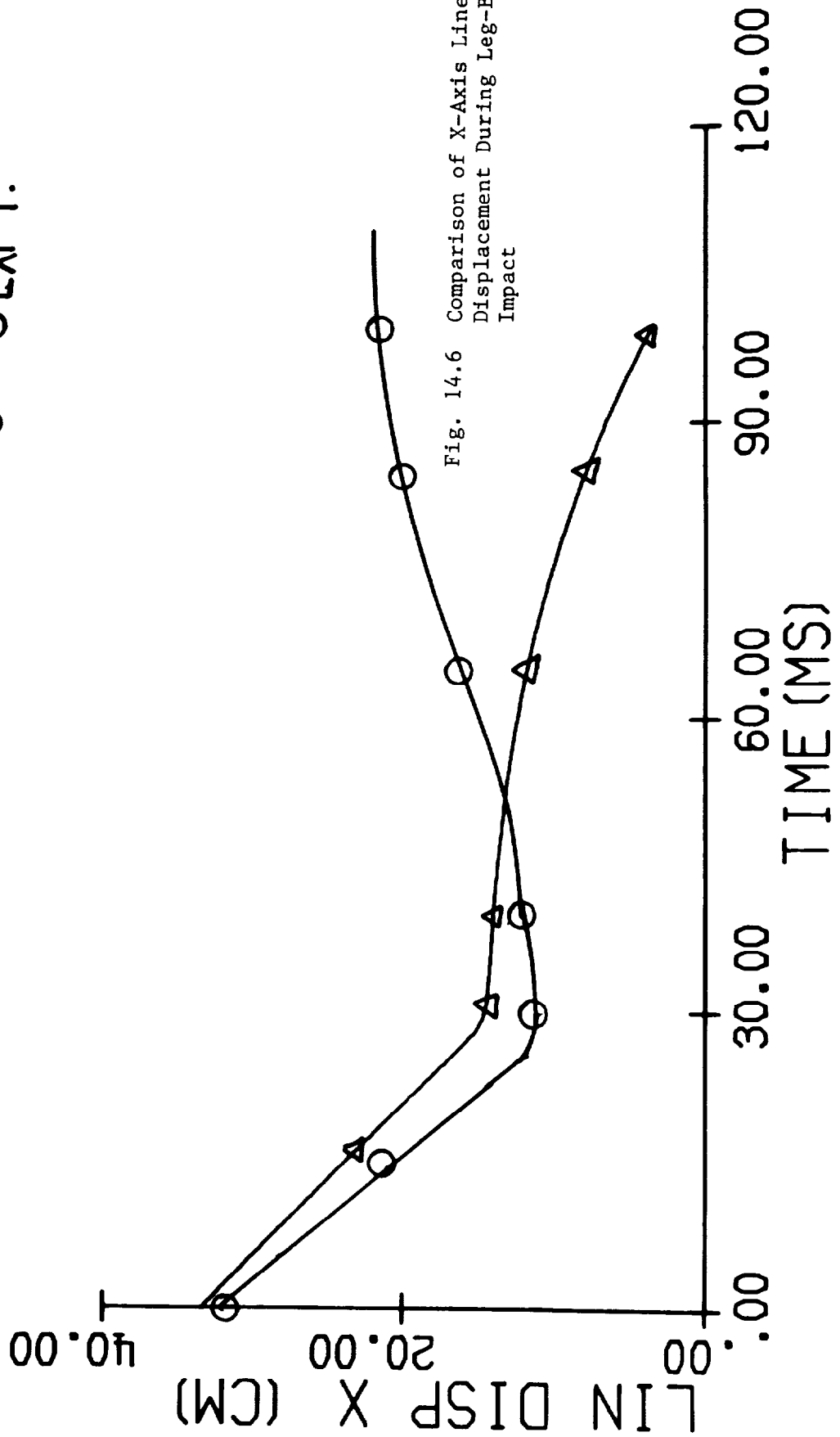


Fig. 14.6 Comparison of X-Axis Linear Displacement During Leg-Bumper Impact

MODEL
EXPT.

RUN NO.: DN16-RLL

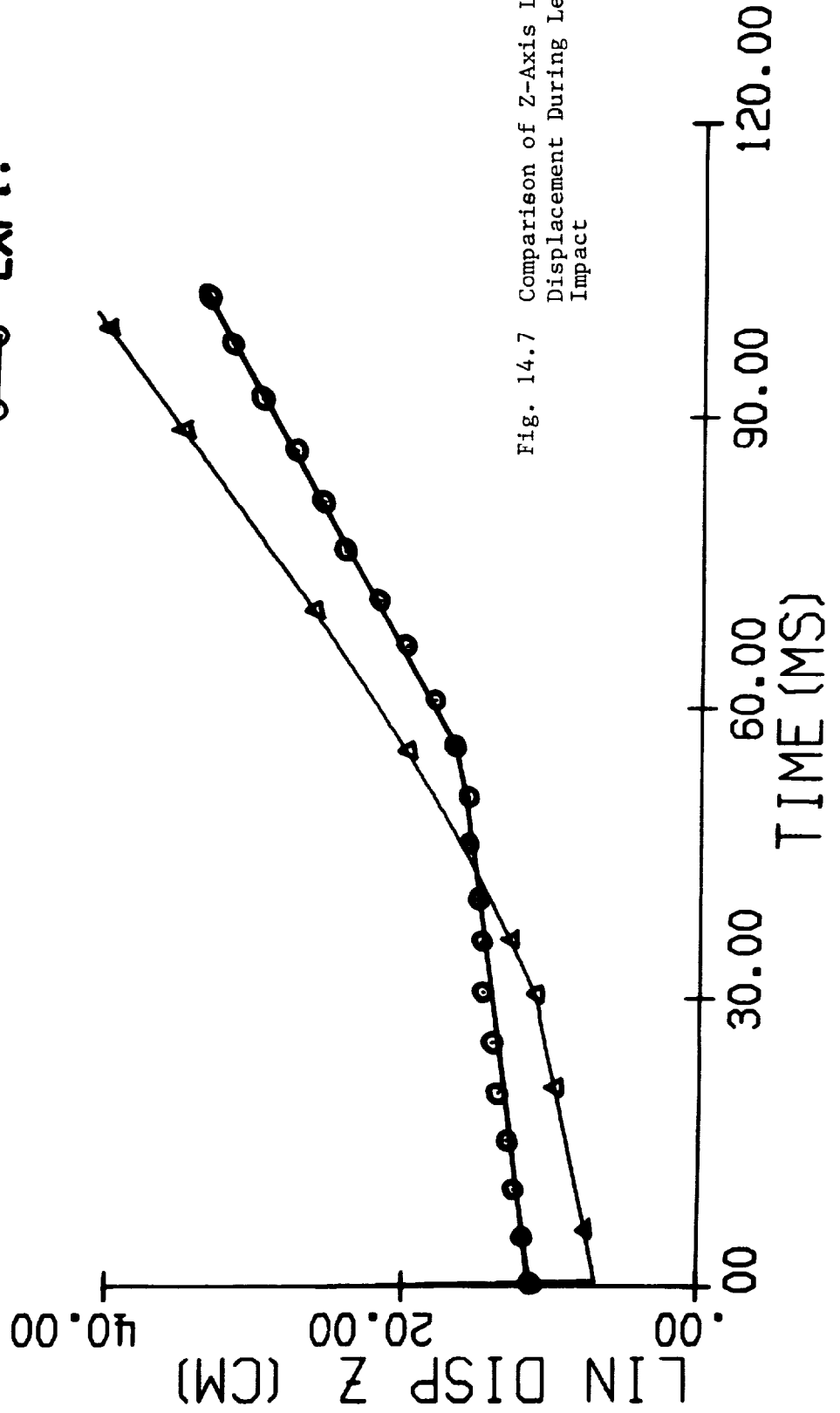


Fig. 14.7 Comparison of Z-Axis Linear Displacement During Leg-Bumper Impact

RUN NO.: DN16-RLL

EXPT. 
MODEL 

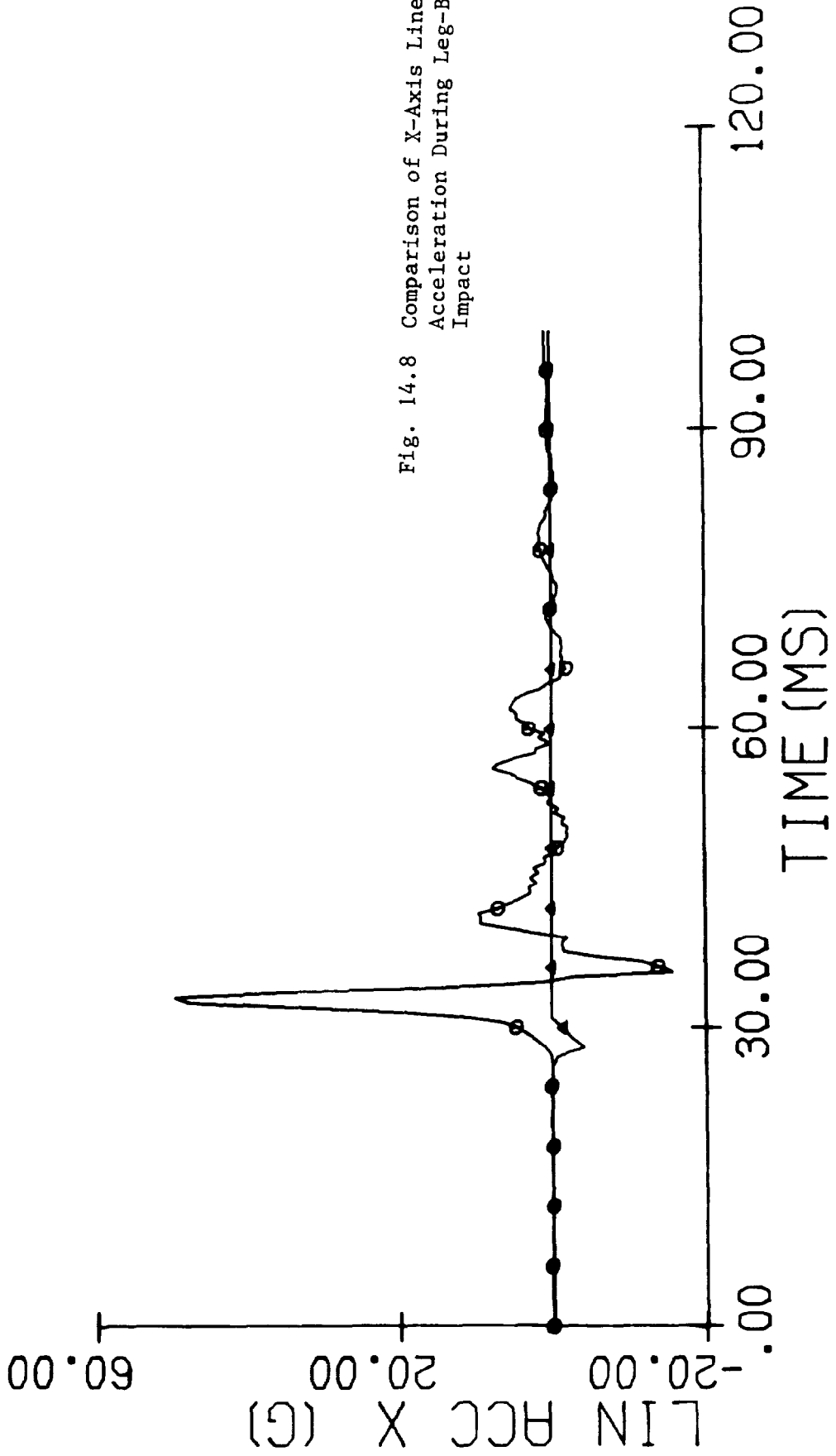


Fig. 14.8 Comparison of X-Axis Linear Acceleration During Leg-Bumper Impact

the hood of a 1973 Chevrolet used in the impact tests. Very little angular motion was expected. This was observed experimentally from the high-speed film. However, the model predicted a significant change in the angle of pitch, as shown in Figure 14.9. This would have a bearing on the comparison of model and experimental results at a later time. However, lack of angular motion, at impact, allows comparison of acceleration kinematics during this period of high acceleration levels. Little angular acceleration was expected. Clearly, from Figure 14.10, only the Z-component of angular acceleration showed any value at all. Figure 14.11 shows a comparison between experimental and model results for this component. The correlation is relatively good considering that the magnitudes involved are low for angular acceleration. As discussed in Chapter 3, angular acceleration is computed from the difference in two linear accelerations. At high impact levels of linear acceleration in the 100-g range, an angular acceleration of the order of 1000 rad/sec/sec can result from a 5 g difference. However, this difference could easily be the result of cross-talk inherent in accelerometers. Thus, it becomes extremely difficult to match low values of angular acceleration. Although experimental peak is higher, the model pulse has a longer duration causing larger angular displacement. Predictably, the Y-component of linear acceleration is the most significant, as illustrated in Figure 14.12. A comparison of the experimental and model results is shown in Figure 14.13. A comparison of the X-component of linear acceleration is shown in Figure 7.14. The correlation is still good, although it is not the dominant component. Figure 14.15 shows model predictions for all three components of linear displacements. The significant displacement is along the Z-axis. The segment comes down vertically, hits the hood and rebounds with very little displacement in the X-or Y-direction. In Figure 14.16 the comparison for Z-component is shown. Clearly, the rebound in the model is more than that observed experimentally. The Y-component of linear displacement is compared in Figure 14.17. Very good correlation is observed.

14.4 Discussion

In both cases, fairly good correlation is observed for linear as well as angular kinematics. Poor linear accelerometer resolution often makes it difficult to match low angular accelerations. However, good correlation has been observed for low values of linear acceleration. Mechanical cross-talk, electrical noise or a slight error in mount orientation can contribute to a poor match between experimental results and model output.

YAW-MOD
PITCHMOD
ROLL-MOD
PITCHEXPT

○
▲
+
●

RUN NO.: DN34HEAD

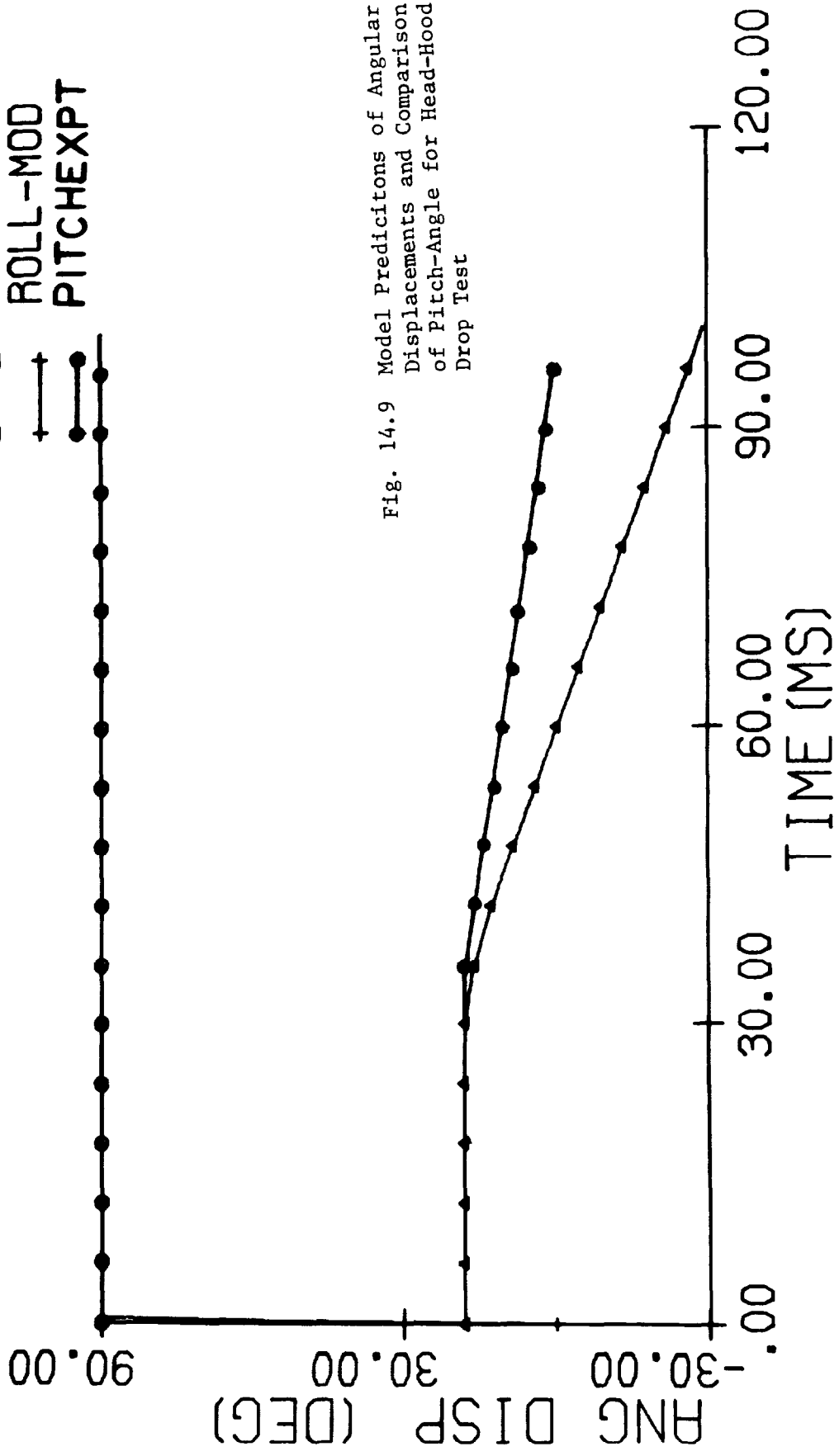


Fig. 14.9 Model Predictions of Angular Displacements and Comparison of Pitch-Angle for Head-Hood Drop Test

RUN NO.: DN34HEAD

MODEL X
 MODEL Y
 MODEL Z

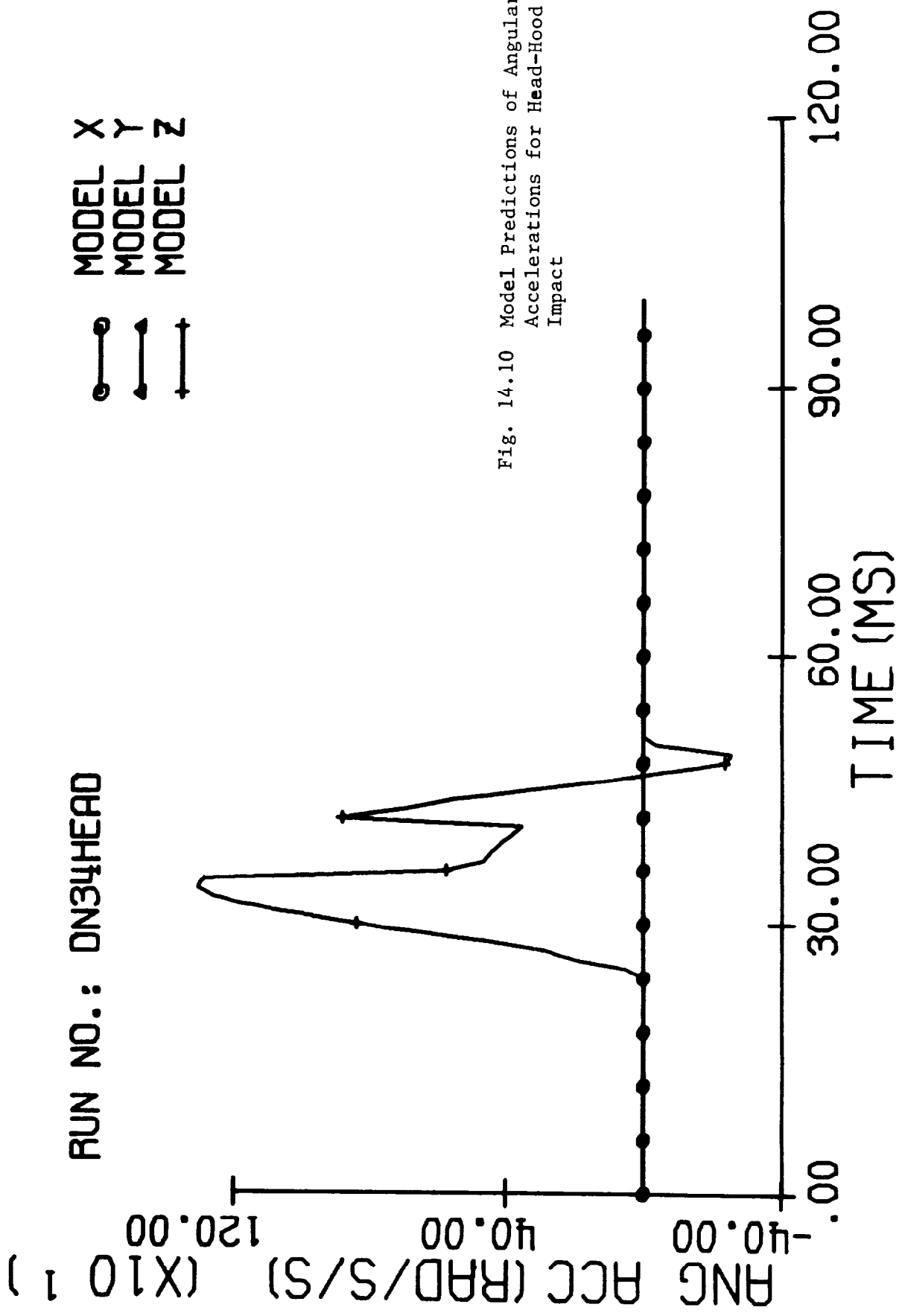
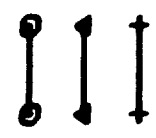


Fig. 14.10 Model Predictions of Angular Accelerations for Head-Hood Impact

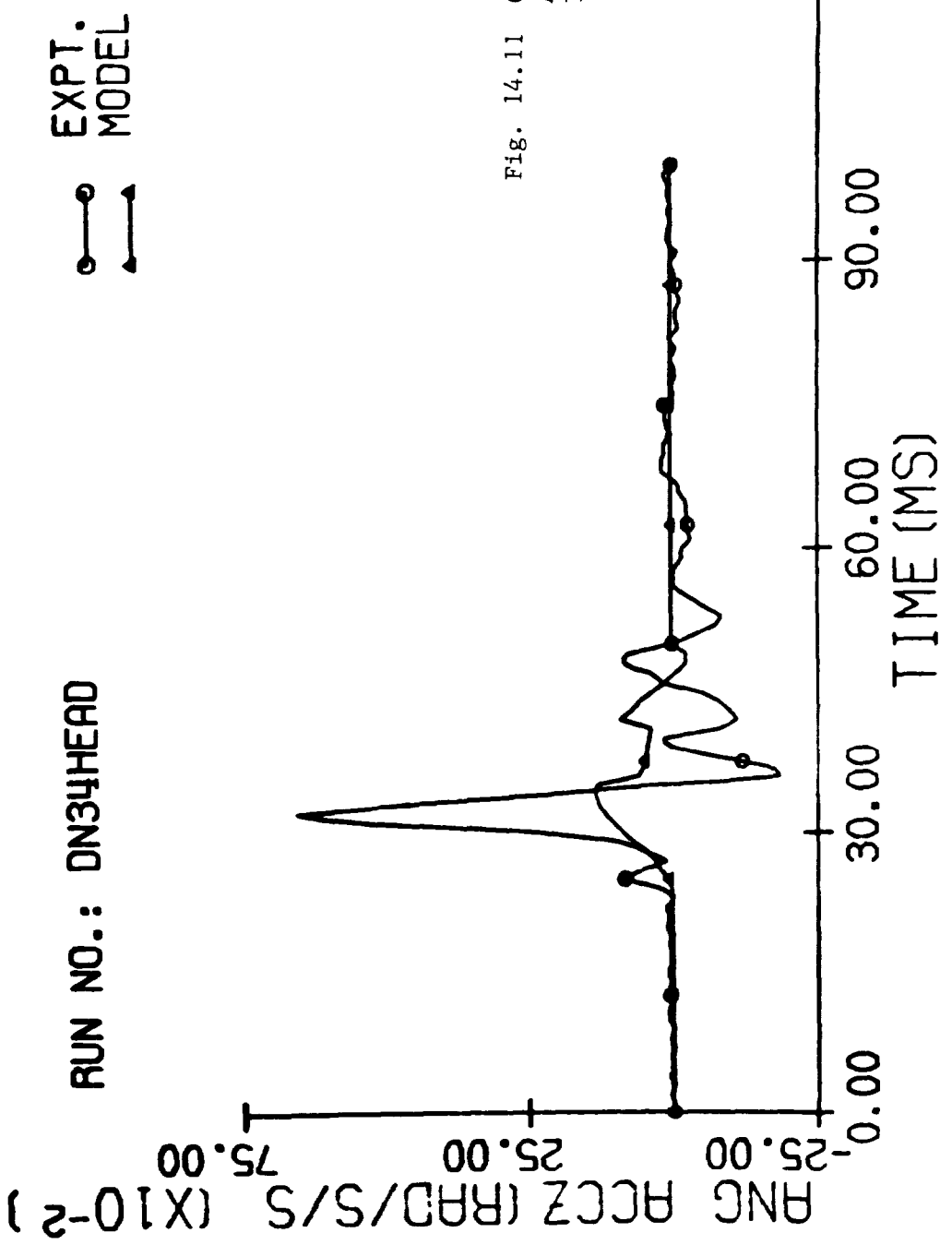


Fig. 14.11 Comparison of Z-Axis Angular Acceleration During Head-Hood Impact

MODEL X
MODEL Y
MODEL Z

○
▲
+

RUN NO.: DN34HEAD

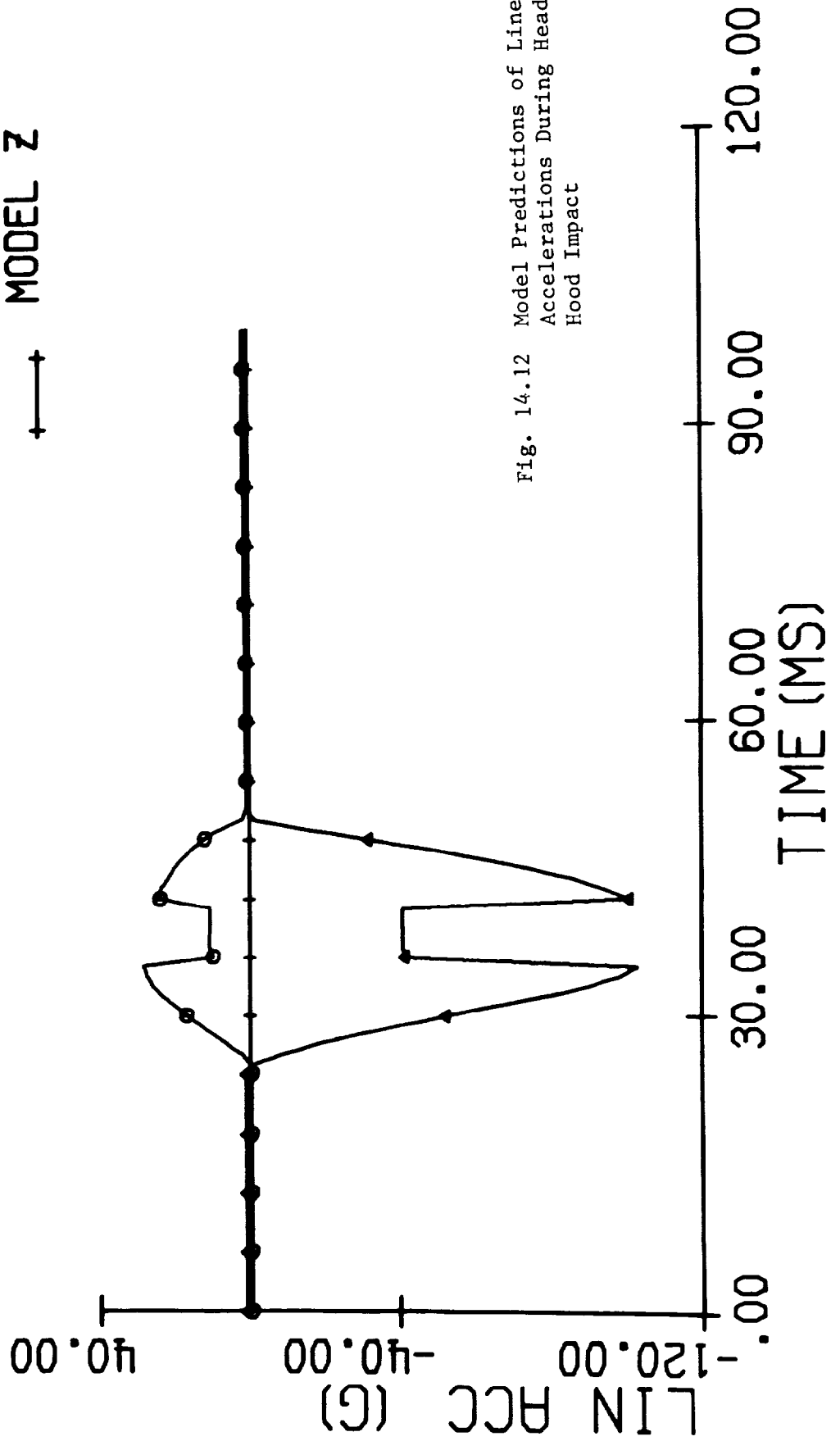


Fig. 14.12 Model Predictions of Linear Accelerations During Hood Impact

EXPT.
MODEL

RUN NO.: DN34HEAD

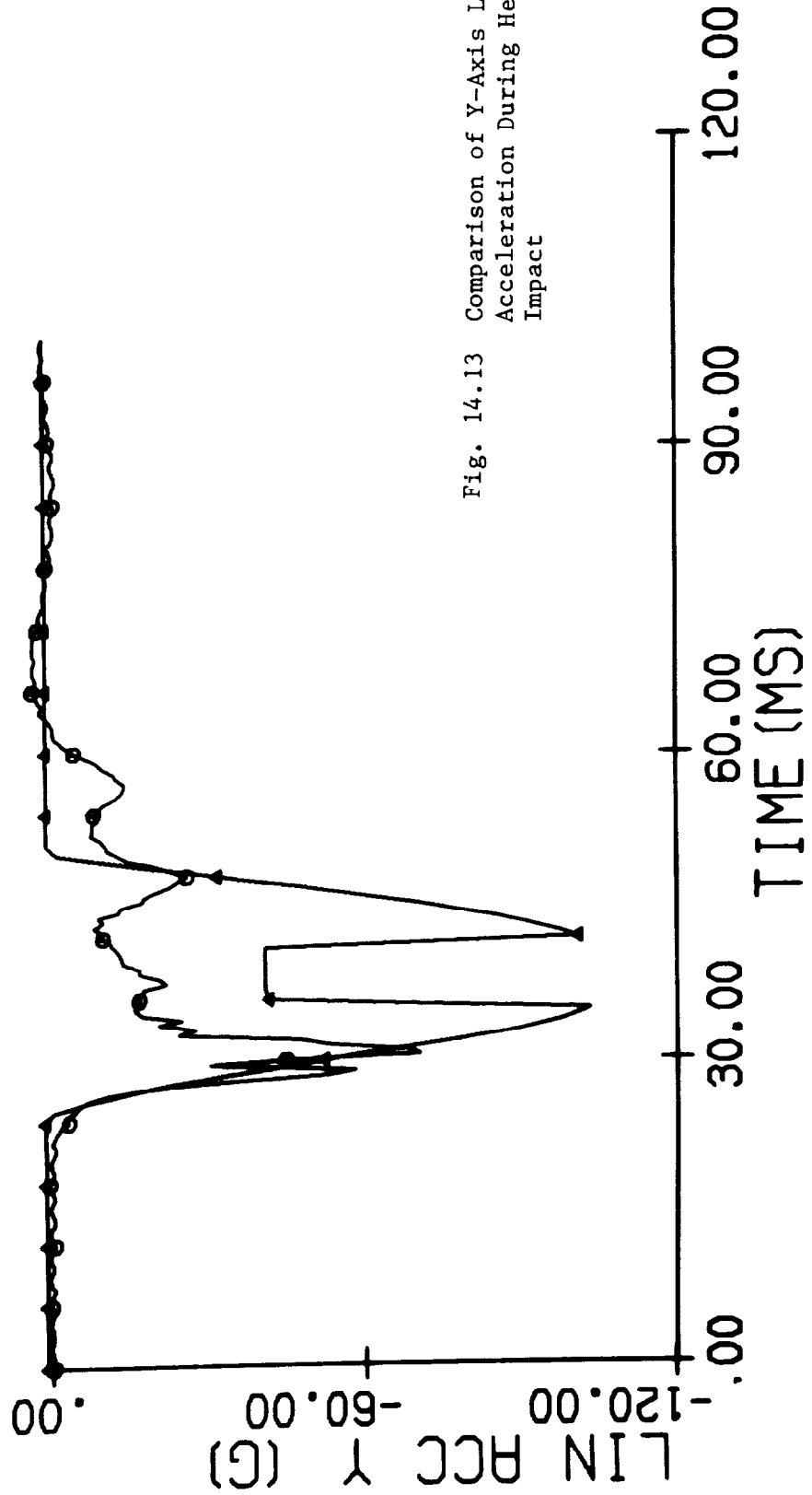
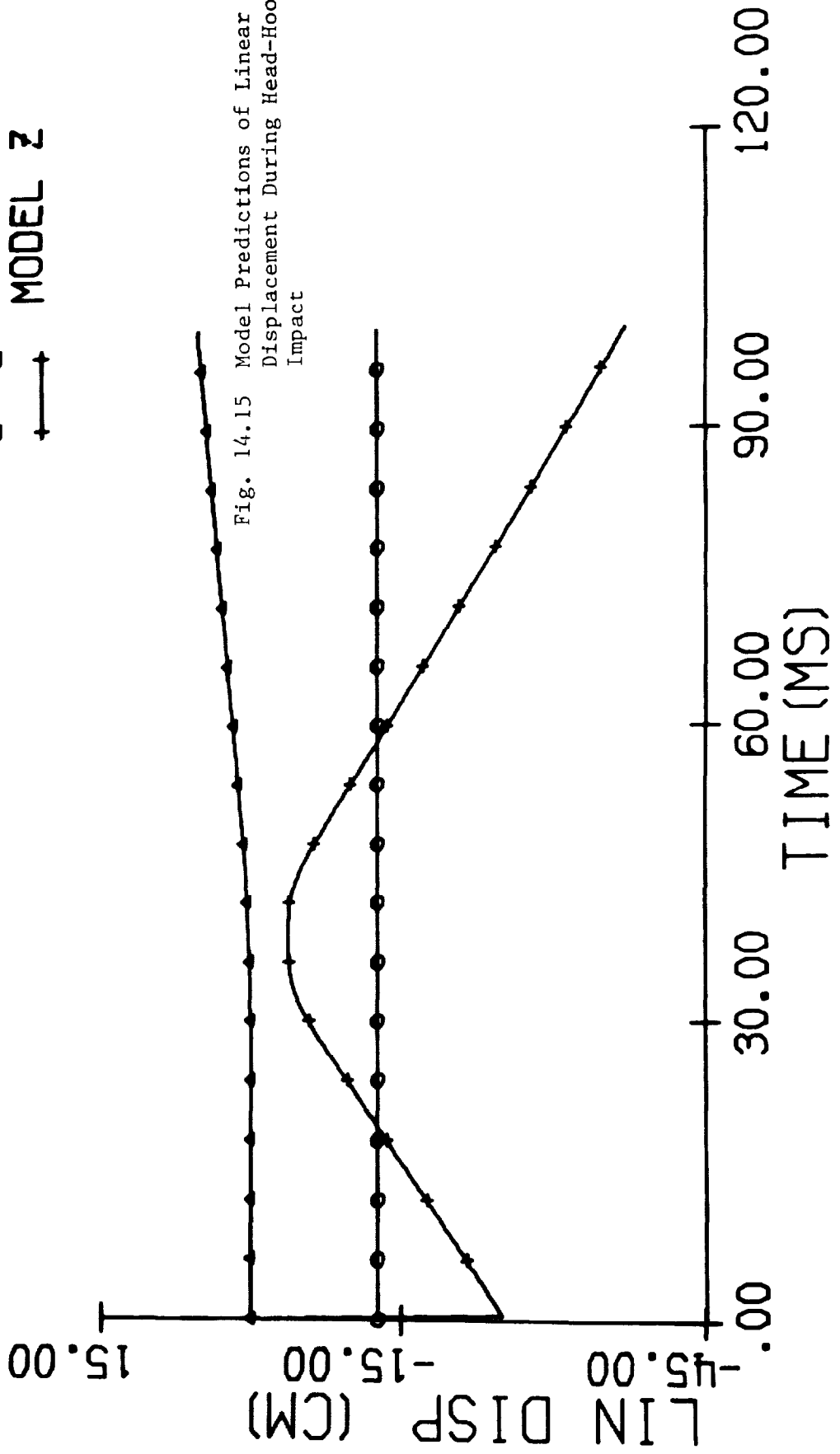


Fig. 14.13 Comparison of Y-Axis Linear Acceleration During Head-Hood Impact

RUN NO.: DN34HEAD

MODEL X
MODEL Y
MODEL Z

○
●
+



RUN NO.: DN34HEAD

MODEL
EXPT.

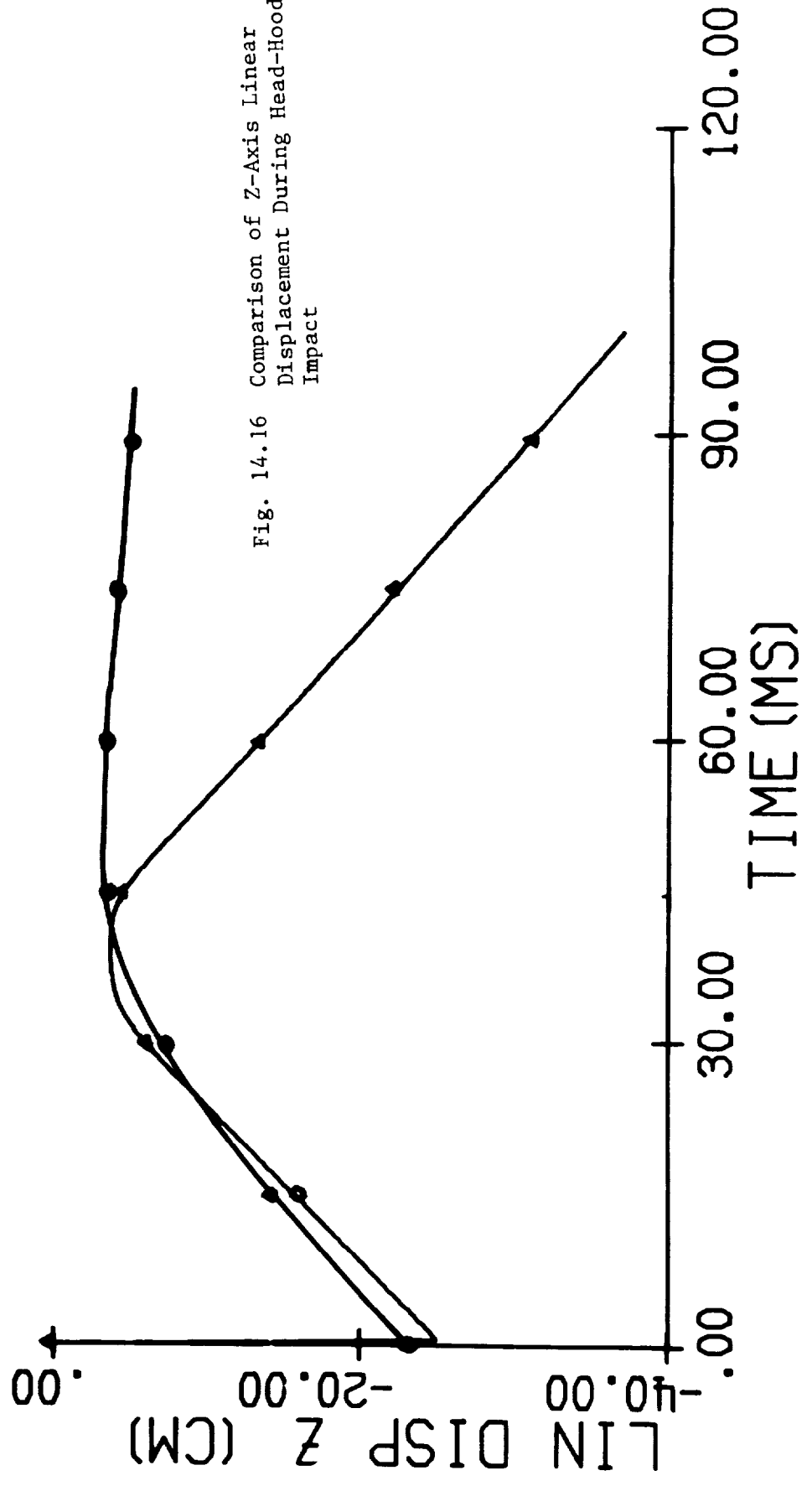


Fig. 14.16 Comparison of Z-Axis Linear Displacement During Head-Hood Impact

RUN NO.: DN34HEAD

MODEL
EXPT.

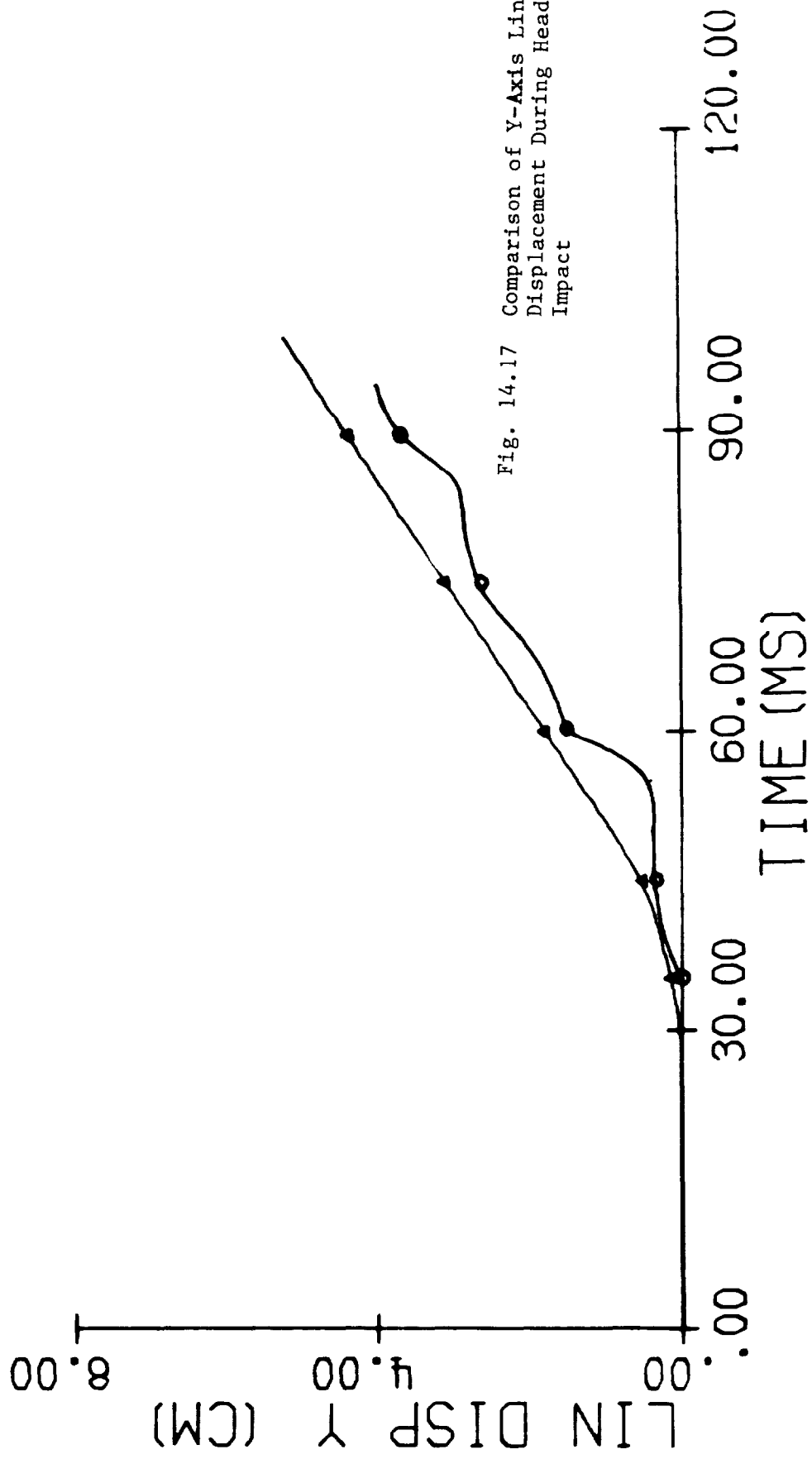


Fig. 14.17 Comparison of Y-Axis Linear Displacement During Head-Hood Impact

MODEL VALIDATION FOR ANTHROPOMORPHIC DUMMY IMPACTS

15.1 Introduction

For validation of dummy impacts, Runs D03, D05, D09 and D10 were simulated. In addition, the 9 TTI drop tests of a dummy against a vehicle were also simulated. For the full-scale impact tests carried out at Wayne State University, Runs D03 and D10 are almost identical and similar model kinematics are expected. Thus, detailed simulation of Runs D09 (39.4 km/h, lateral mode) and D10 (24.1 km/h, lateral mode) were performed to provide a kinematic study of lateral impacts and the effects of 15 km/h increase in impact speed. The frontal Run D05 (29.8 km/h), was also simulated.

It should be noted that displacements are expressed relative to the vehicle-fixed coordinate system shown in Figure 13.3. Both linear and angular acceleration are given with respect to segment-fixed axes, as illustrated in Figure 13.2. Typically, the positive X-axis is directed anteriorly. The positive Y-axis is towards the right and the Z-axis lies along the segment link with the positive direction pointing inferiorly.

15.2 Vehicular-Dummy Impact Simulation of TTI Drop Tests15.2.1 Comparison of Body Segment Displacements

In any validation, it is fundamentally important to compare model and experimental kinematics. Figure 15.1 shows a lateral view of whole-body linear displacements at 100 msec intervals, for 13.5 km/h impact (M1). Film and analog data were synchronized, based upon information on the delay time for the release mechanism given in the TTI report (May, 1973). The frontal view of the same Run is shown in Figure 15.2. Overall correlation is good.

15.2.2 Comparison of Linear Accelerations

The dummy was instrumented with three triaxial accelerometers, one each on the head, upper torso, and lower torso. Obviously, as discussed in Chapter 3, angular acceleration comparison cannot be made for this accelerometer configuration. Linear acceleration for the head and upper torso were made. Comparisons of the X-component of the head acceleration and the Z-component of the upper torso acceleration are illustrated in Figures 15.3 and 15.4 respectively. Overall patterns are similar but there exists a phase difference, possibly due to an erroneous estimate of the time of impact given in the TTI report.

15.3 Vehicular-Dummy Impact Simulation of Wayne State University Runs15.3.1 Comparison of Body Segment Displacement

Two runs were considered for comparison; Run D05 - which is a frontal impact at 29.8 km/h; and Run D10, a lateral impact at 24.1 km/h. Figure 15.5

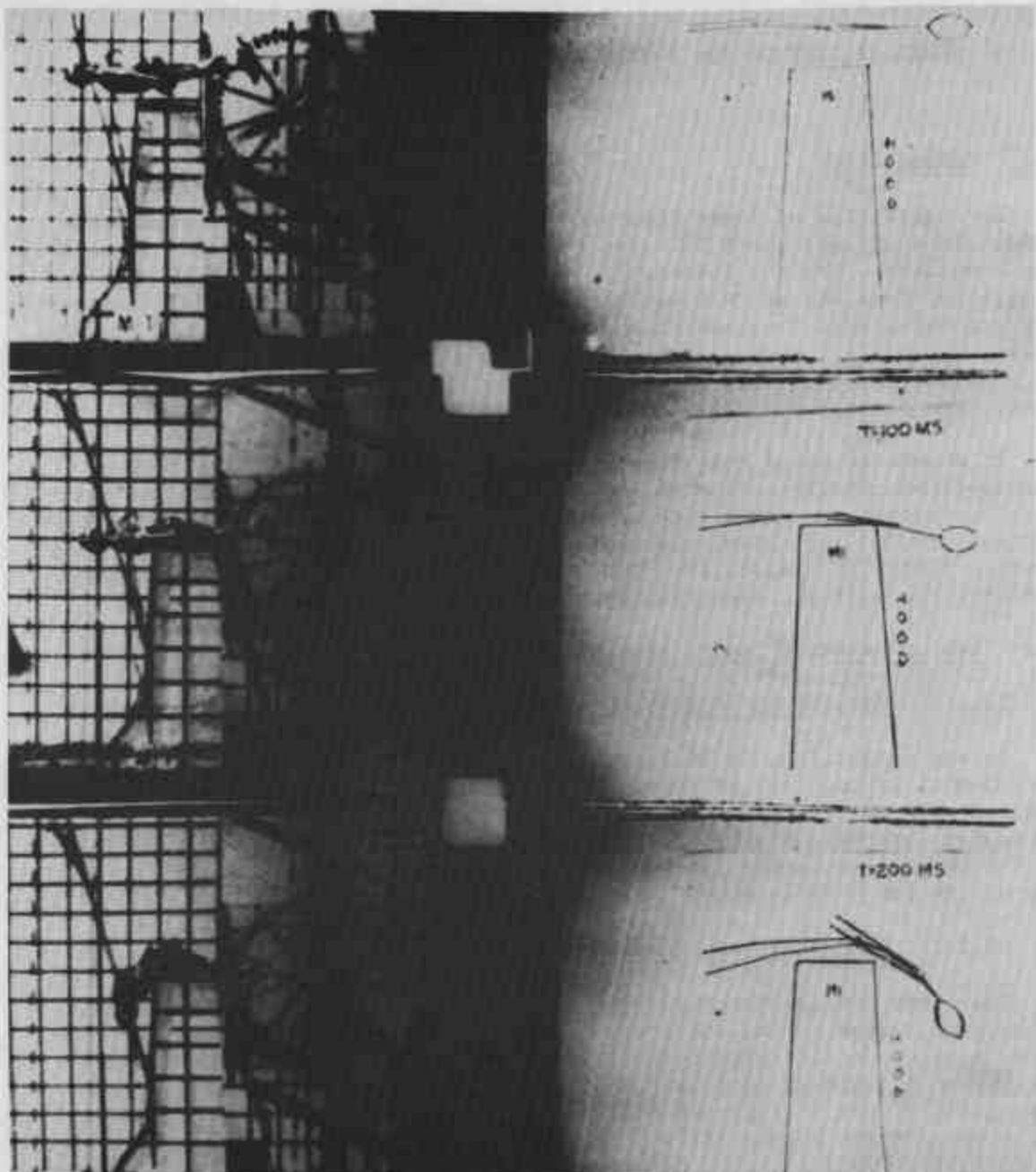


Fig. 15.1(a) Comparison of Whole Body Displacement for a Dummy Drop Test at 13.5 Km/h (M1)- Lateral View (0-200 ms) Mirror Image

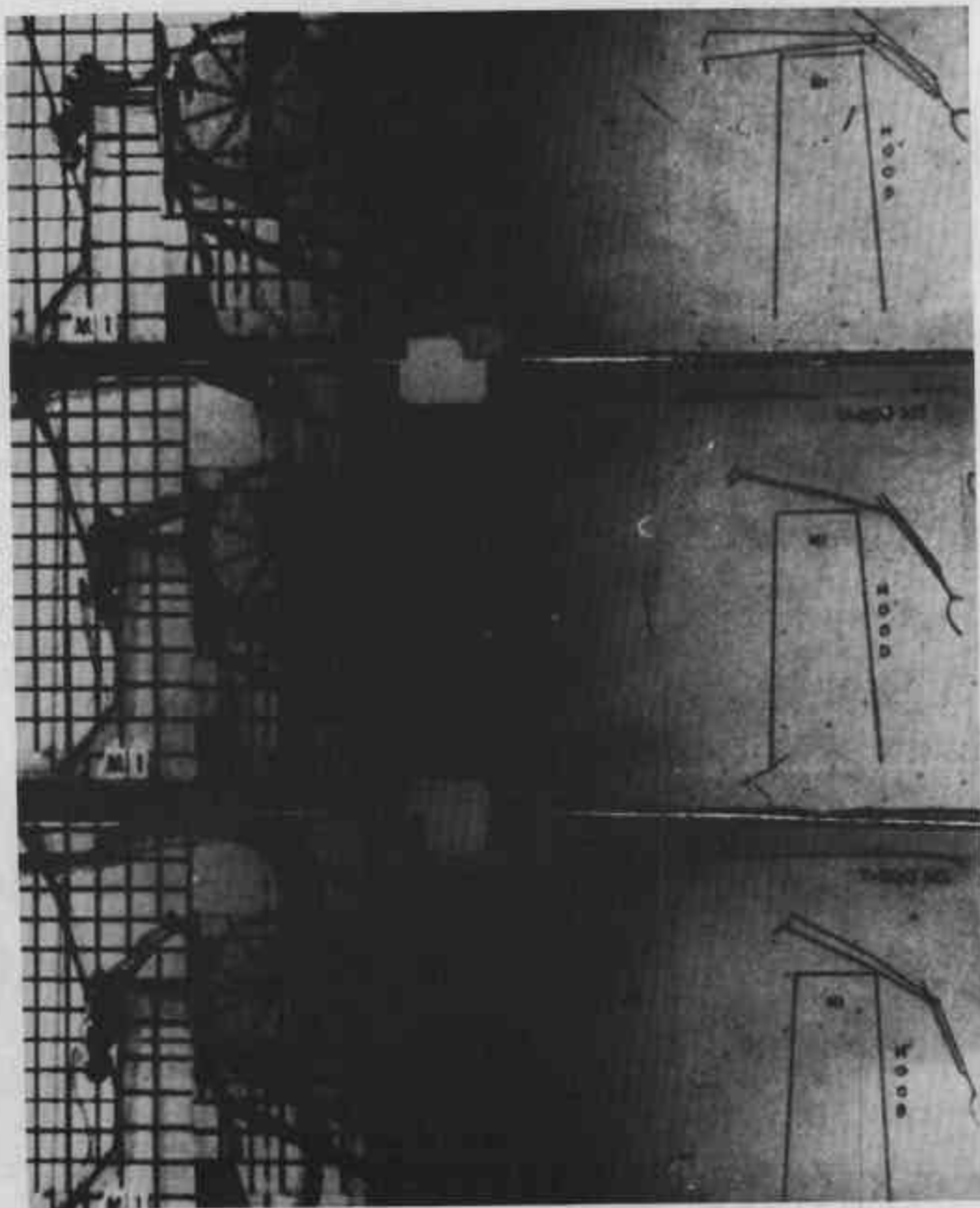


Fig. 15.1(b) Comparison of Whole Body Displacement for a Dummy Drop Test at 13.5 Km/h (M1)- Lateral View (300-500 ms) Mirror Image

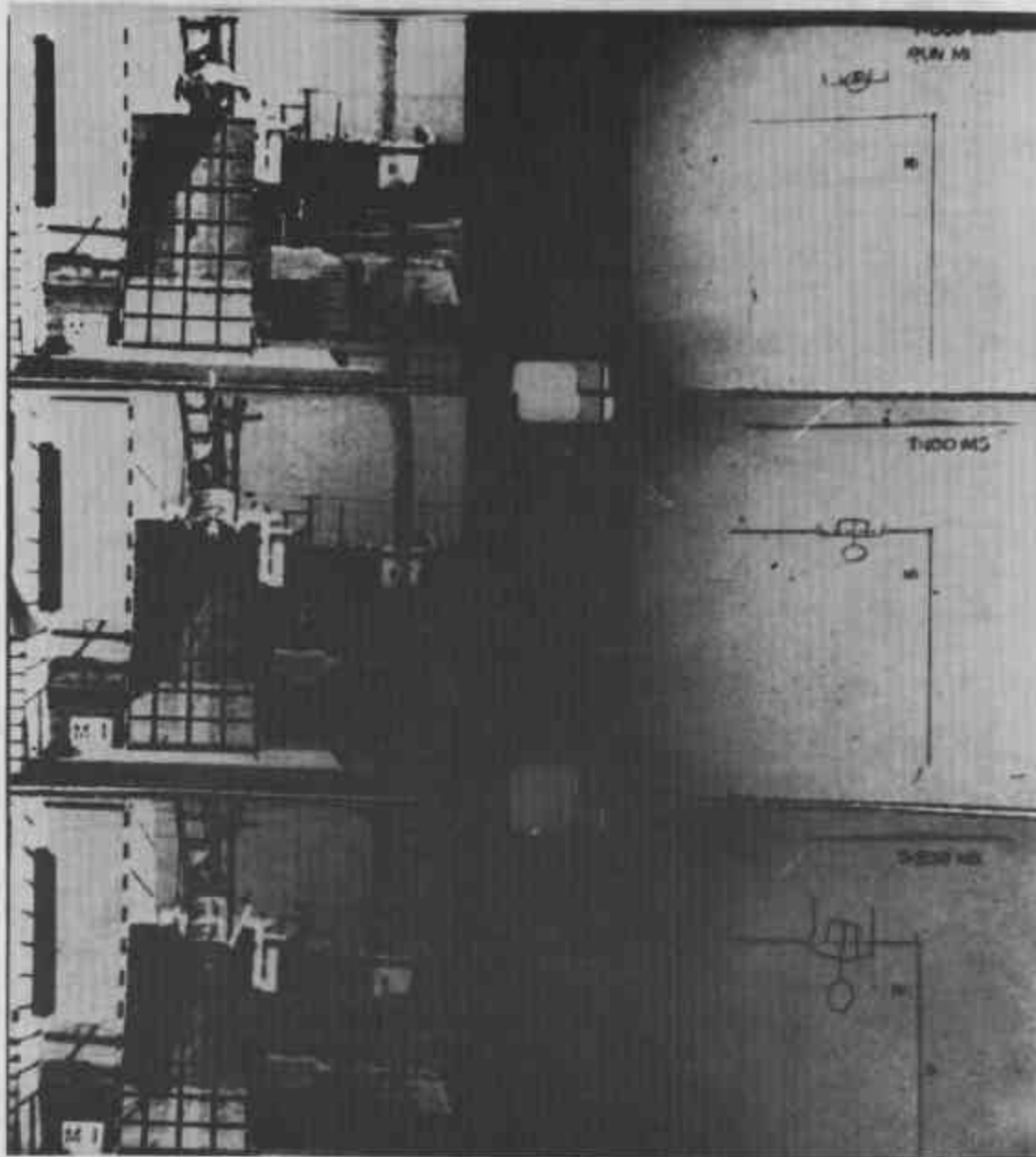


Fig. 15.2(a) Comparison of Whole Body Displacement for a Dummy Drop Test at 13.5 Km/h (M1)- Frontal View (0-200 ms)

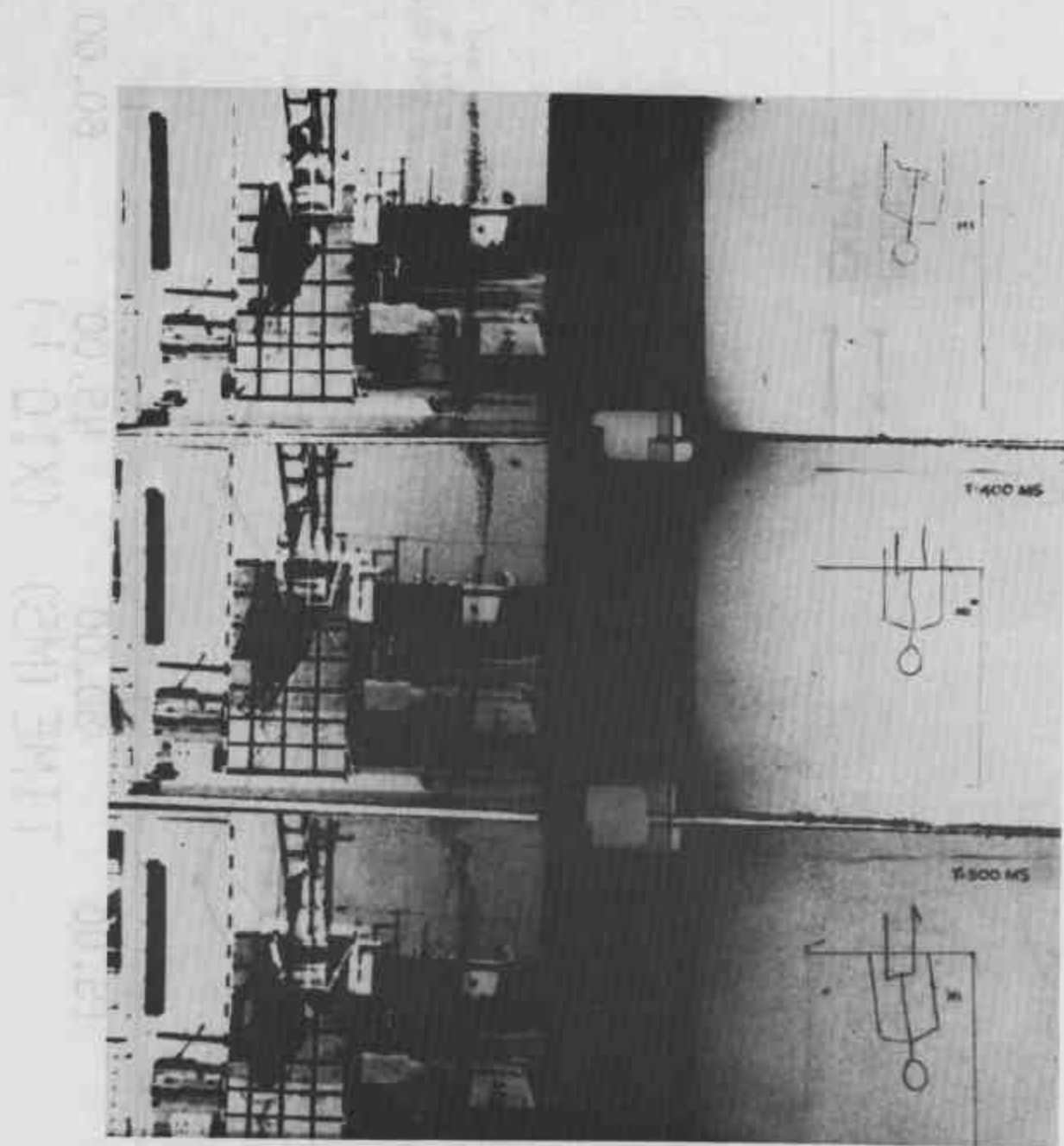


Fig. 15.2(b) Comparison of Whole Body Displacement for a Dummy Drop Test at 13.5 Km/h (M1)- Frontal View (300-500 ms)

RUN NO.: M1-HEAD

MODEL
EXPT.

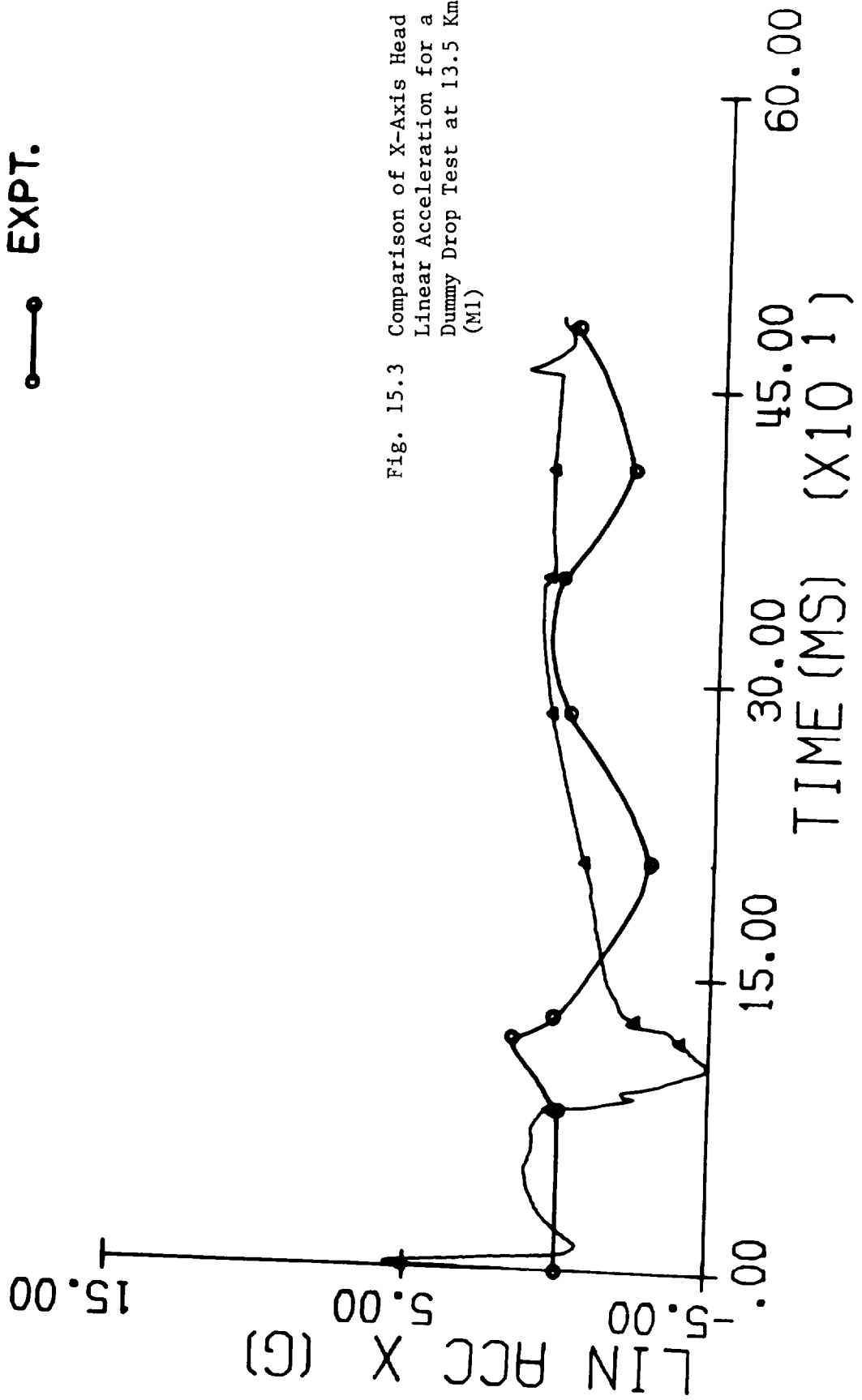


Fig. 15.3 Comparison of X-Axis Head Linear Acceleration for a Dummy Drop Test at 13.5 Km/h (M1)

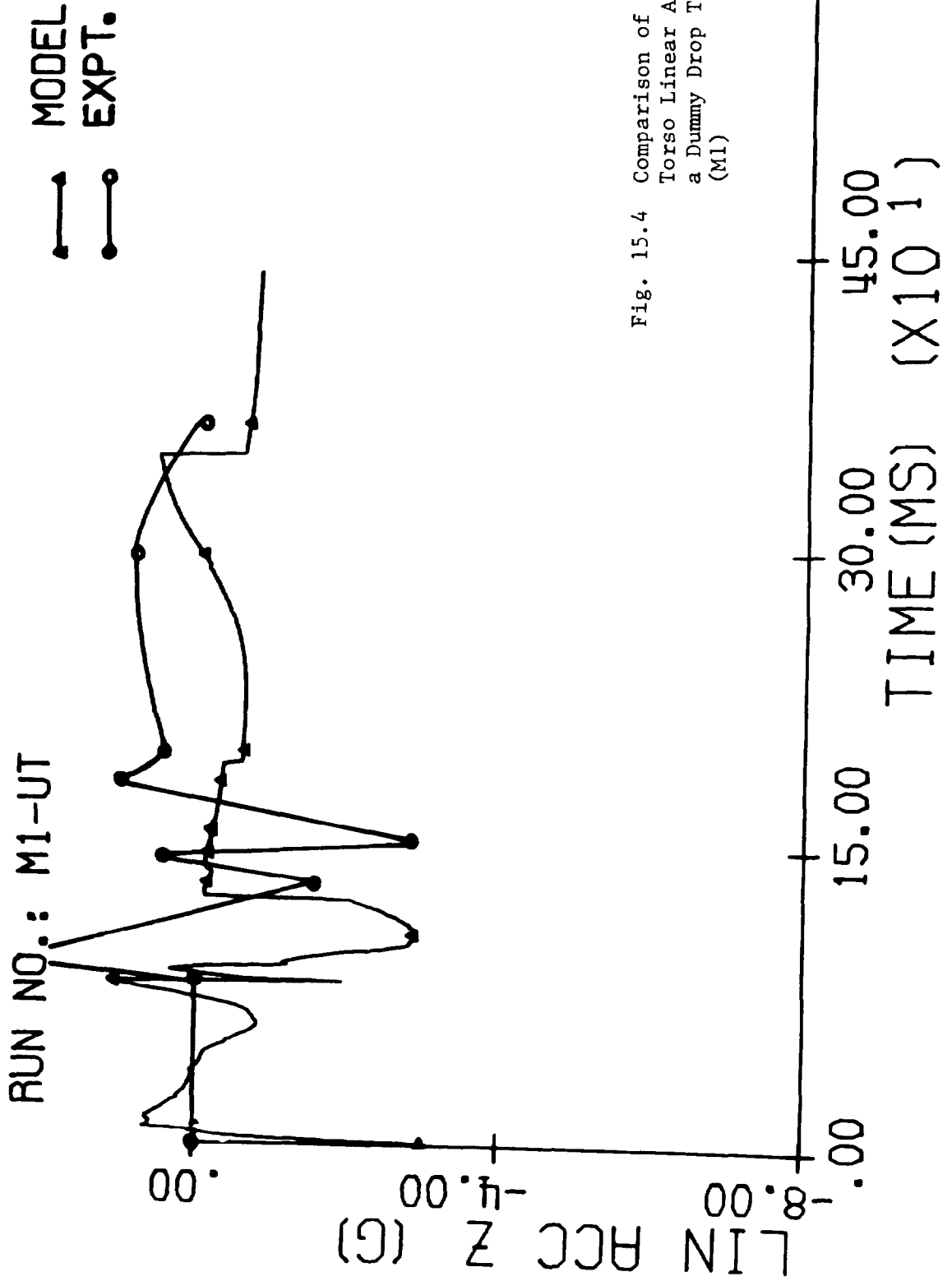


Fig. 15.4 Comparison of Z-Axis Upper Torso Linear Acceleration for a Dummy Drop Test at 13.5 Km/h (M1)

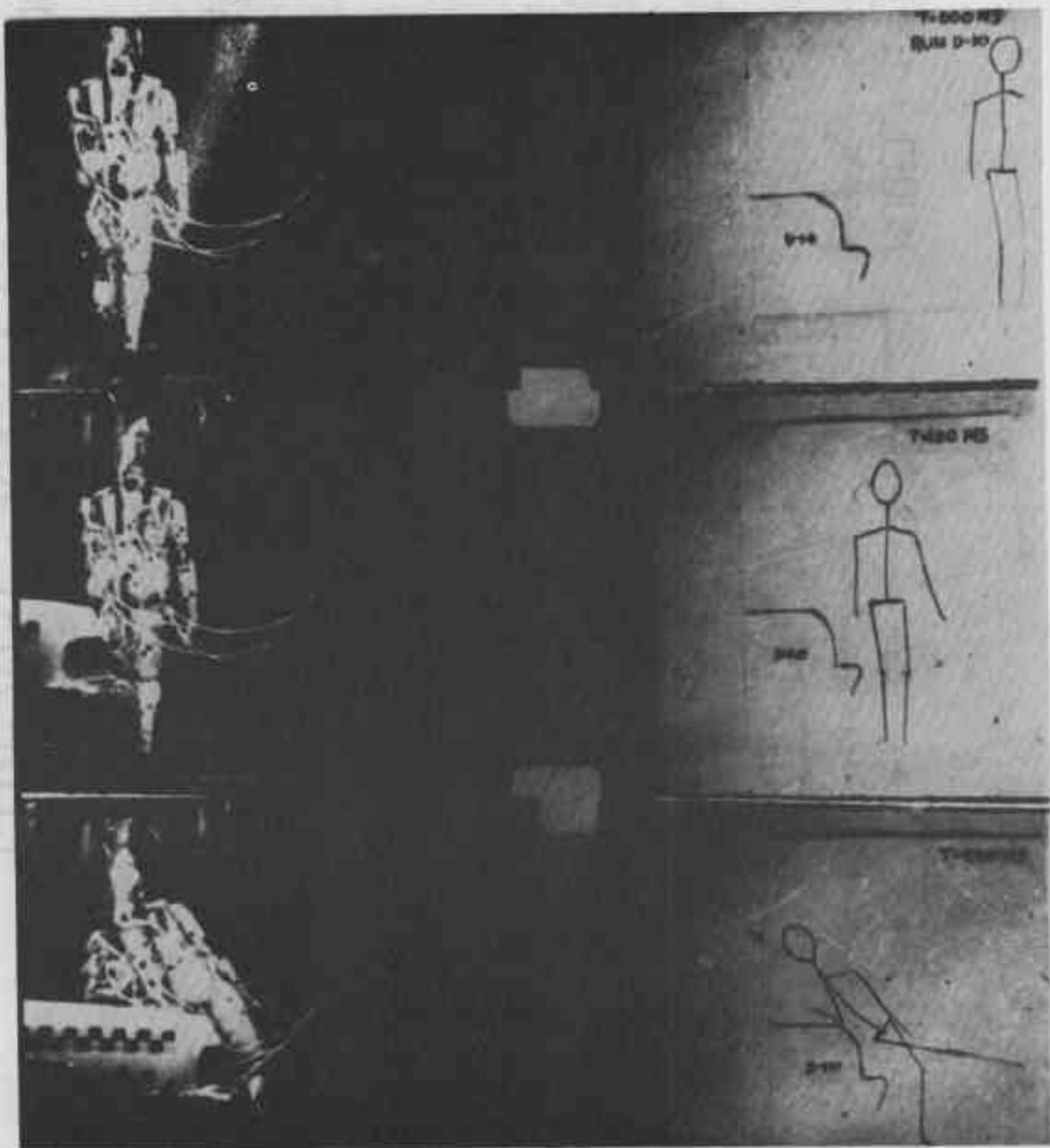


Fig. 15.5(a) Comparison of Whole Body Displacement for a Dummy (Lateral) Impact Test at 24.1 Km/h (D10)-Lateral View (0-200 ms)

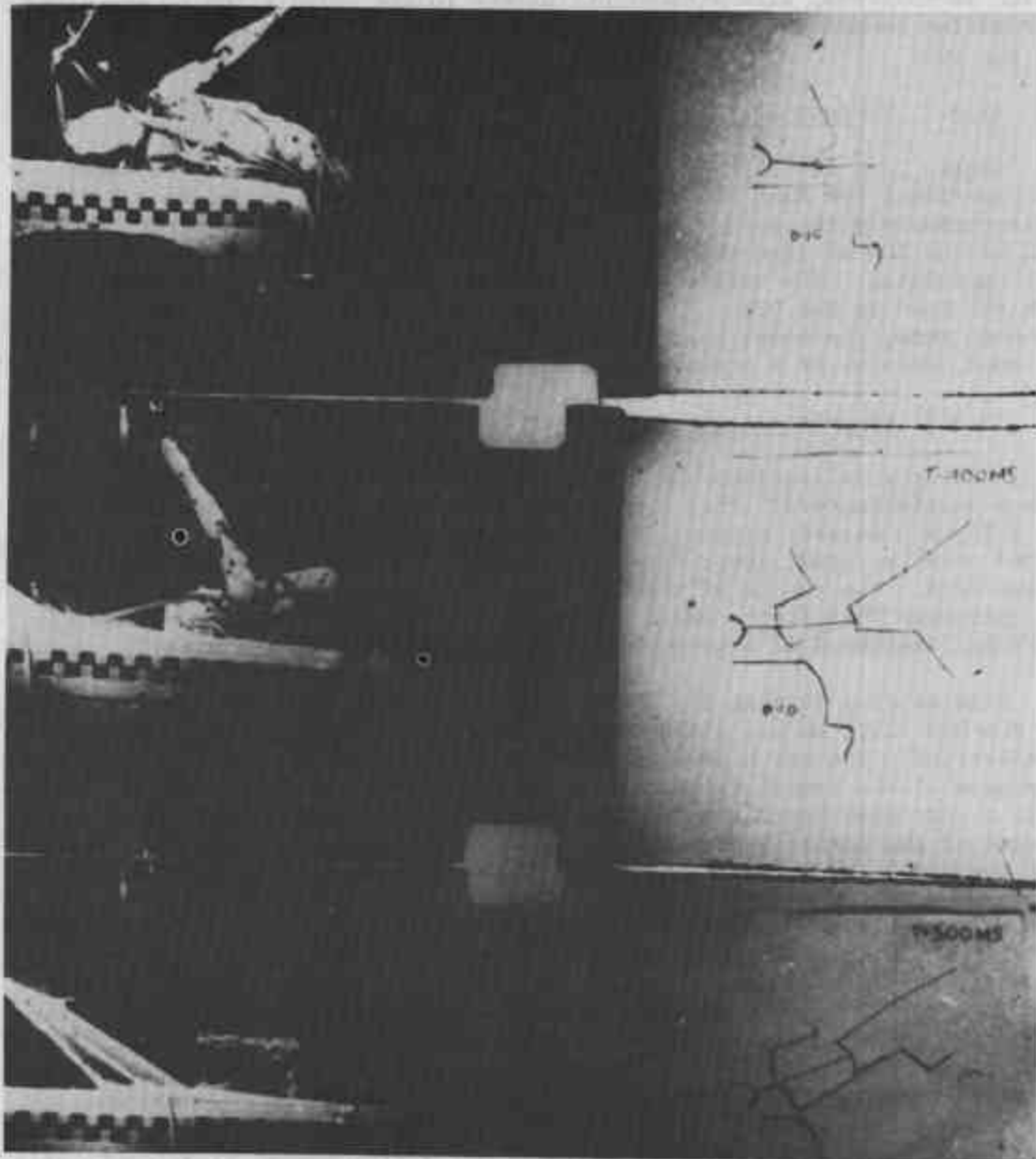


Fig. 15.5(b) Comparison of Whole Body Displacement for a Dummy (Lateral) Impact Test at 24.1 Km/h (D10)-Lateral View (300-500 ms)

compares the lateral views of body segment motion for Run D10 (24.1 km/h). Figure 15.6 shows a similar view for Run D05 (29.8 km/h). Again good correlation is observed, with minimal difference in the orientation of the lower extremities toward the end of the impact for Run D10 and a higher rebound for Run D05.

15.3.2 Contact History

Tables 15.1 and 15.2 compare contact duration observed in the model and experiment for Runs D10 and D05 respectively. Clearly, contact begins at approximately the same time, even for the head which impacts the hood well beyond 200 ms into the run. Duration of contact also appears to be well-correlated. The only mismatch is the contact of the right upper arm with the hood in Run D10. The model did not predict contact. Furthermore, for both runs, the model head did not have a second prolonged contact with the hood, because of a strong rebound.

15.3.3 Kinematic Analysis

Angular accelerations can only be compared for segments instrumented with 9 accelerometers. This configuration was first used in Run D10 which was a 24 km/h lateral impact. Four prominent segments that were so instrumented were the head, lower torso, left upper leg and left lower leg (impacted leg). The choice of the two extreme segments, the head and lower leg, presumes that if the model can match the kinematics of the two ends, there is likelihood of a good match for the intermediate segments.

Figures 15.7 through 15.16 compare experimental data and model output for Run D10 (24.1 km/h). Figure 15.7 compares the Z-component of angular acceleration. The match is good, even though the values were low. The Z-component of the linear acceleration for the head is shown in Figure 15.8. It is a very good correlation. Figures 15.9 and 15.10 compare X- and Y-components of the linear head acceleration. These figures clearly indicate that the model predicted a much higher level of acceleration in both directions, as compared to the experimental results. As a matter of fact, in the experiment, the head hit the hood on its side resulting in a comparatively high lateral Y-axis acceleration. The model predicted an oblique contact. Moreover, the high acceleration level in the model resulted in larger displacements, and hence, a stronger rebound. Figure 15.11 shows the resultant accelerations and confirms the large peak in the model results. Figure 15.12 illustrates the Y-component of the angular acceleration for the lower torso. In Figure 15.13 the Z-component of its linear acceleration is compared. Figure 15.14 also compares resultant values of linear acceleration for the lower torso. All three plots (Figures 15.13, 15.14, 15.15) illustrate fairly good correlation. The Y-component of the linear acceleration for the left upper leg is shown in Figure 15.15. While Figure 15.16 compares the Y-component of linear acceleration for the left leg. Essentially, Figures 15.15 and 15.16 compare acceleration of the impacted leg, in the direction of impact; a good correlation has been obtained. Predicted values of angular acceleration for all 3 components of impacted left lower leg are given in Figure 15.17. The relative magnitudes correspond with the anticipated

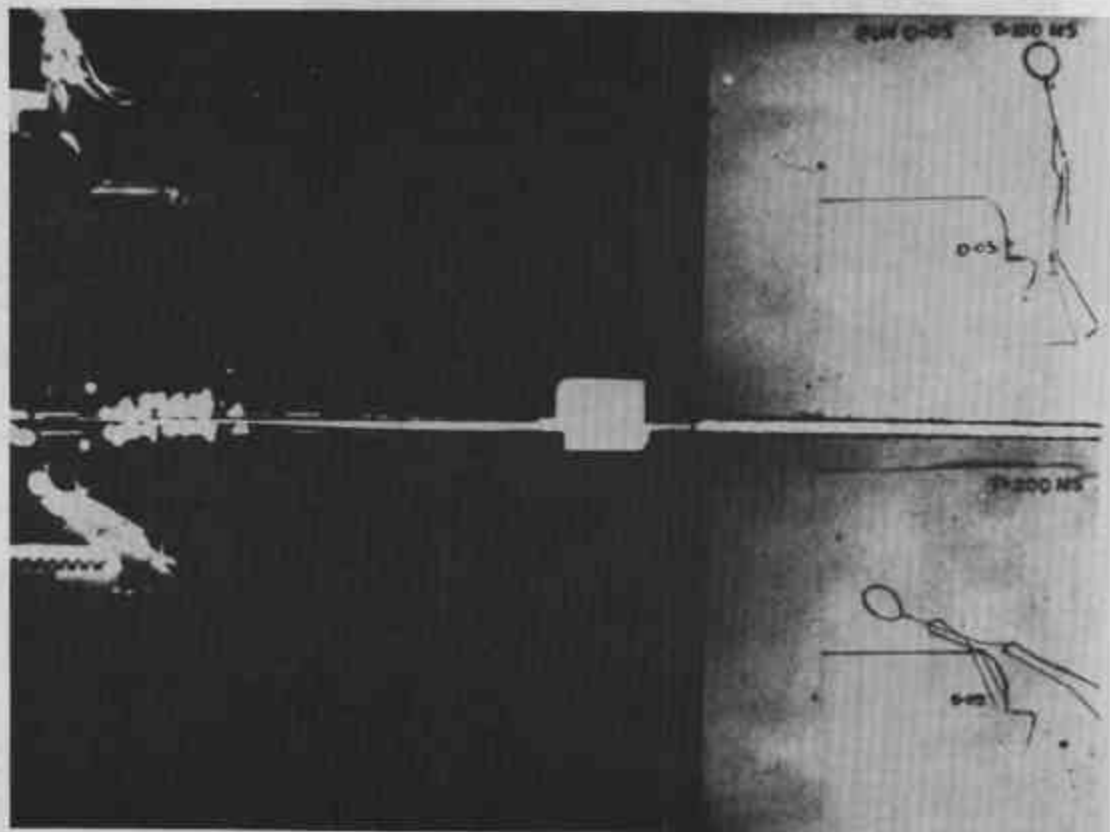


Fig. 15.6(a) Comparison of Whole Body Displacement for a Dummy (Frontal) Impact Test at 29.8 Km/h (D05)-Lateral View (100-200 ms)

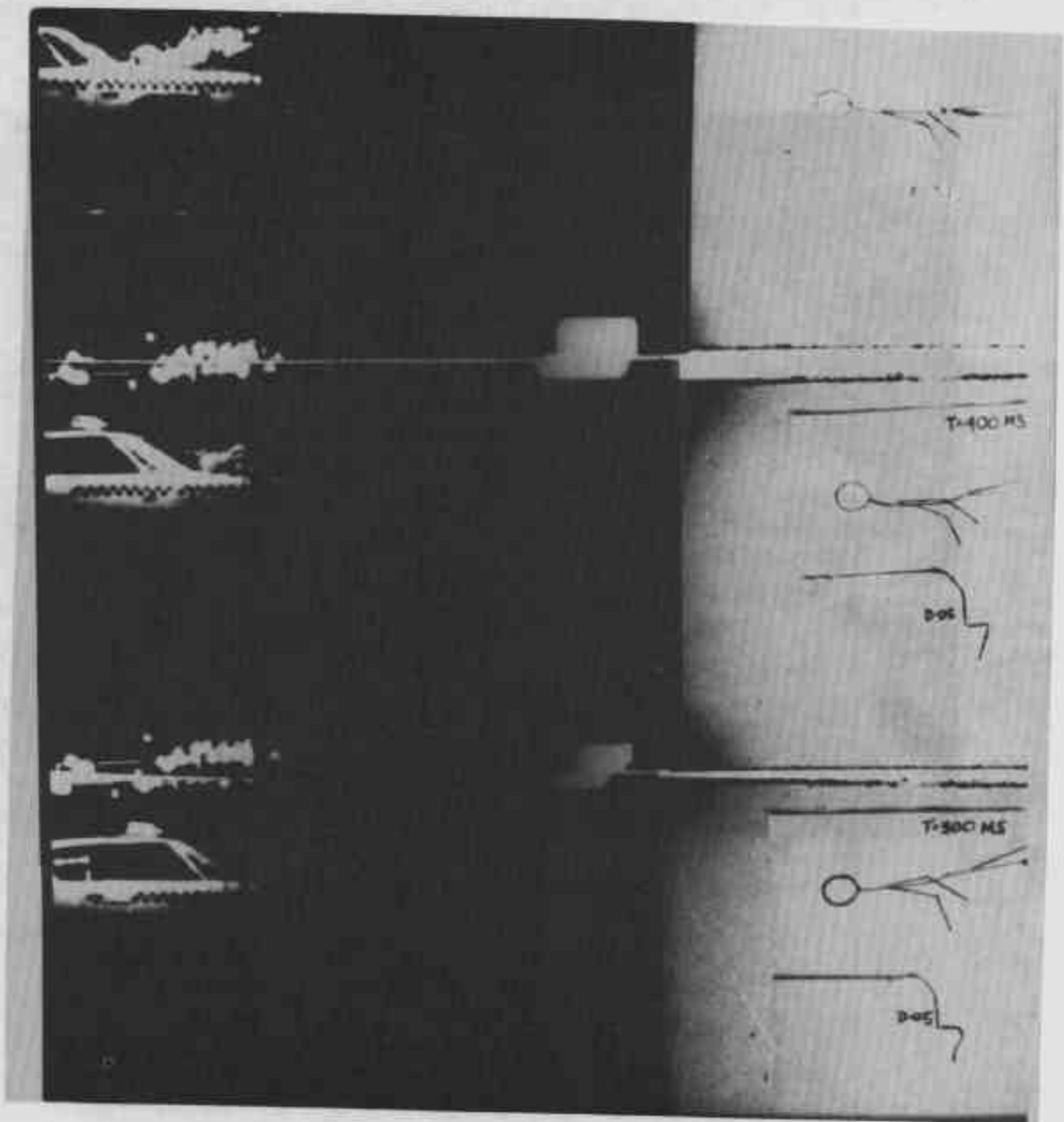


Fig. 15.6(b) Comparison of Whole Body Displacement for a Dummy (Frontal) Impact Test at 29.8 Km/h (D05)-Lateral View (300-500 ms)

TABLE 15.1

CONTACT HISTORY FOR RUN D10

Segment	Plane*	Contact Duration (ms)			
		Experiment		Model	
		Begins	Ends	Begins	Ends
Head	12	260	282	265	285
		336	beyond 500	-	-
Left Upper Leg	10 (20)	92	260	125	206
Left Lower Leg	4 (17)	80	114	100	141
Right Upper Arm	13	388	500	-	-

* Number in brackets represent the equivalent ellipsoidal number.

TABLE 15.2

CONTACT HISTORY FOR RUN D05

Segment	Plane	Contact Duration (ms)			
		Experiment		Model	
		Begins	Ends	Begins	Ends
Head	13	266	326	214	261
	13	354	Beyond 500	-	-
Left Upper Leg*	16	-	-	135	235
	17	114	255	-	-
Left Lower Leg†	22	-	-	108	155
	23	100	160	-	-
Right Upper Arm	13	-	-	223	228

† Planes 22 and 23 constitute the header

* Planes 16 and 17 constitute the bumper

The reason of contacts with different planes is generated due to slight lateral offset.

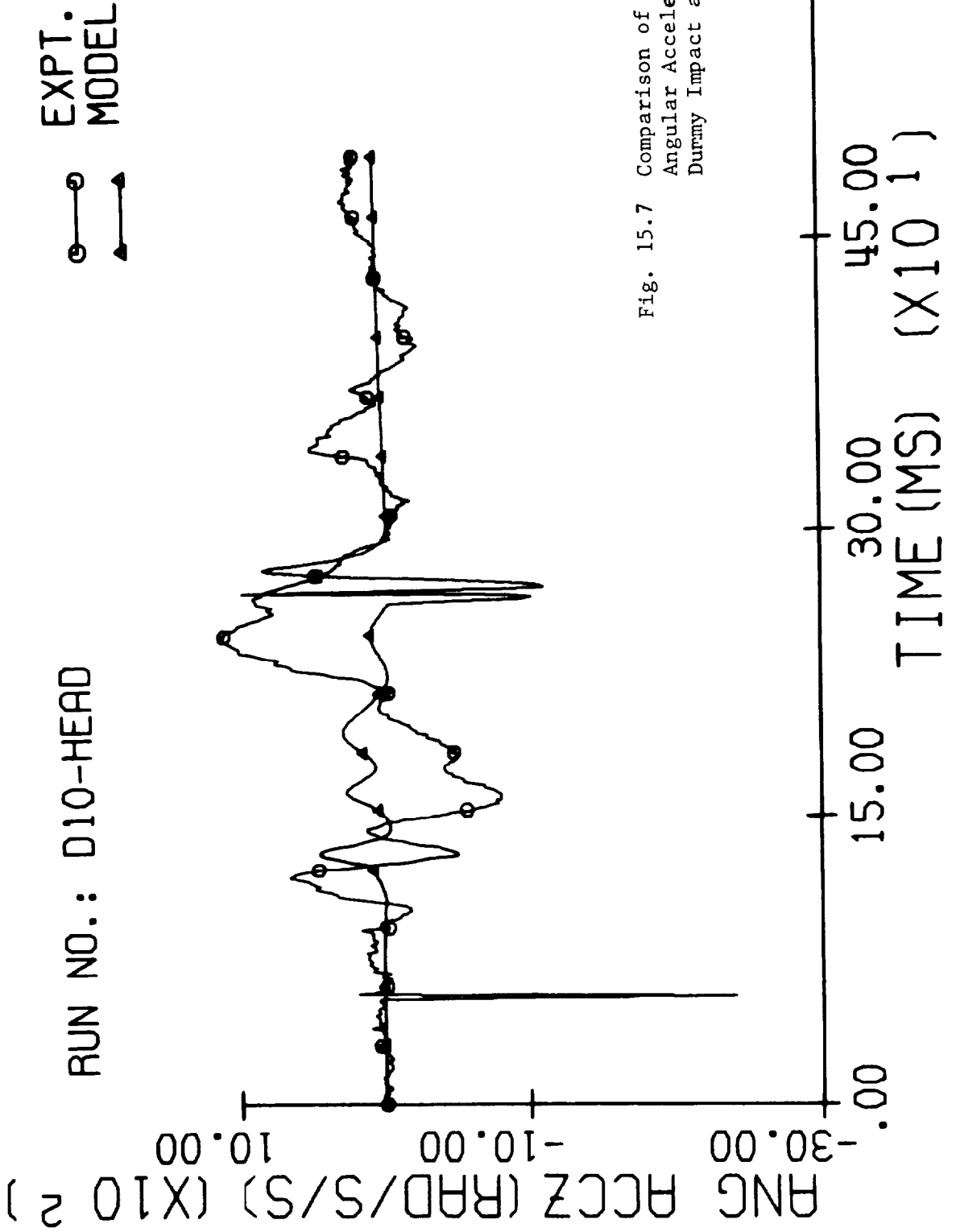


Fig. 15.7 Comparison of Z-Axis Head Angular Acceleration for a Car-Dummy Impact at 24.1 Km/h (D10)

RUN NO.: D10-HEAD

EXPT. MODEL

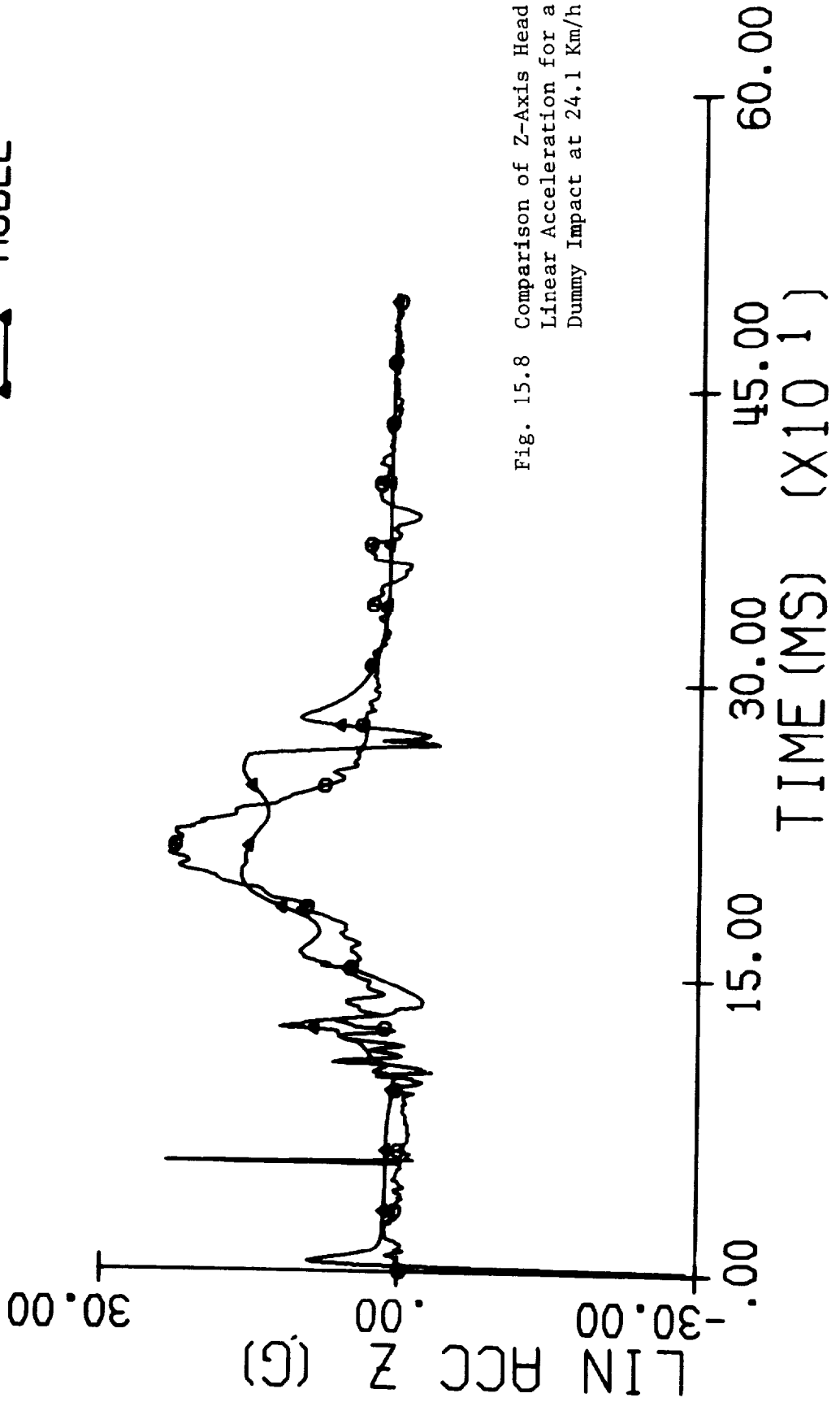


Fig. 15.8 Comparison of Z-Axis Head Linear Acceleration for a Car-Dummy Impact at 24.1 Km/h (D10)

RUN NO.: D10-HEAD

EXPT.
MODEL

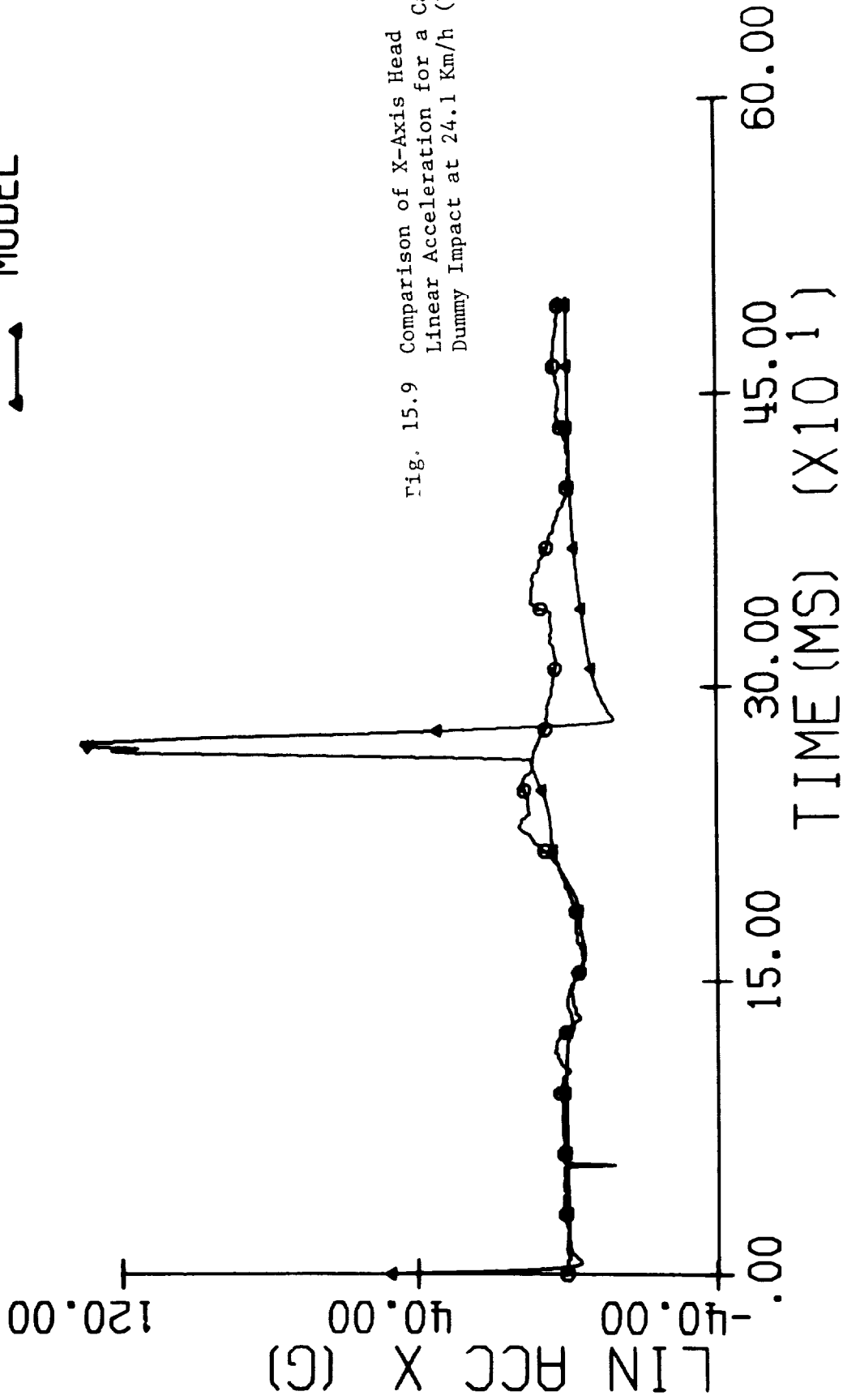


Fig. 15.9 Comparison of X-Axis Head Linear Acceleration for a Car-Dummy Impact at 24.1 Km/h (D10)

RUN NO.: D10-HEAD

EXPT.
MODEL

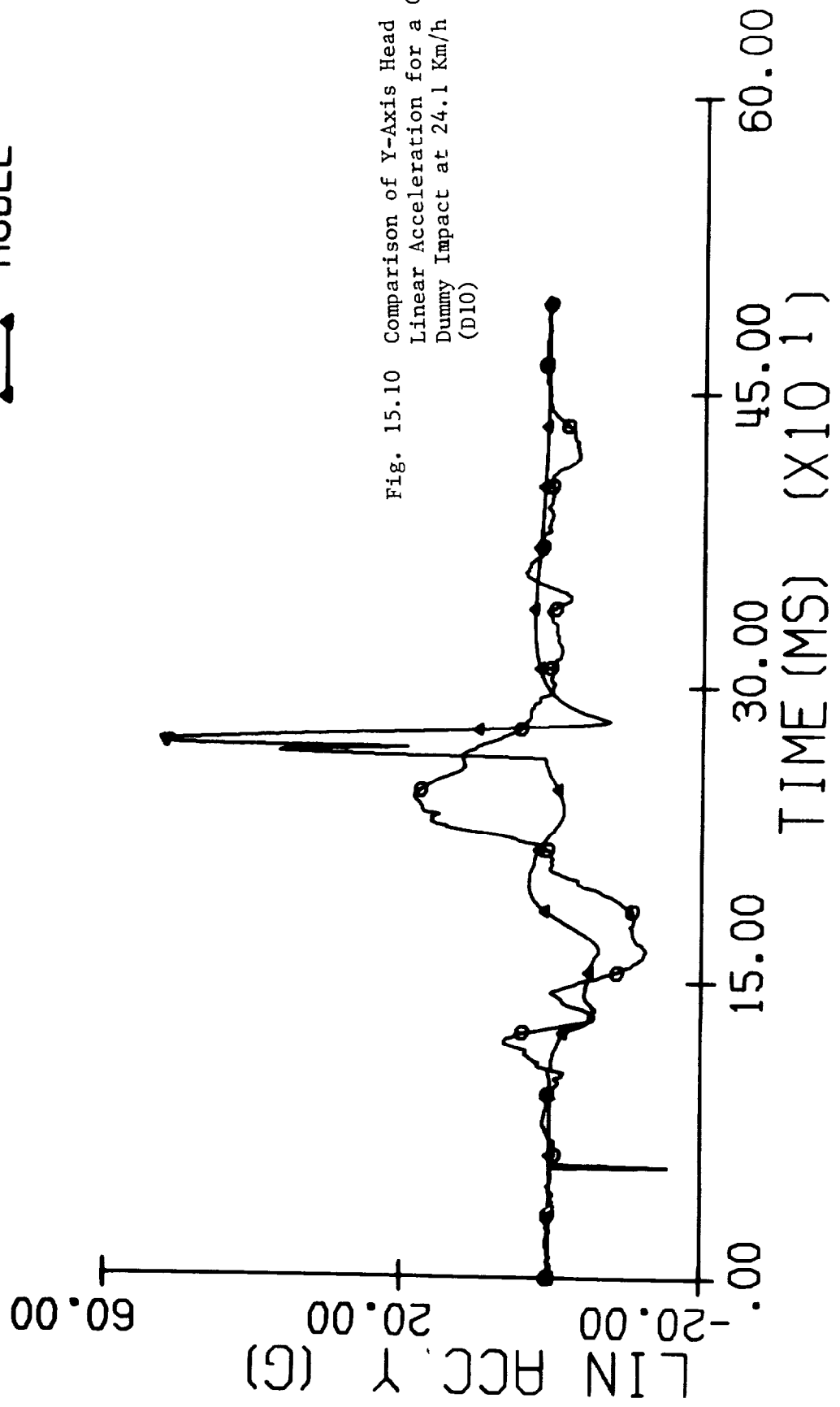
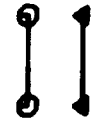


Fig. 15.10 Comparison of Y-Axis Head Linear Acceleration for a Car-Dummy Impact at 24.1 Km/h (D10)

EXPT. RES
MODEL RES



RUN NO.: D10-HEAD

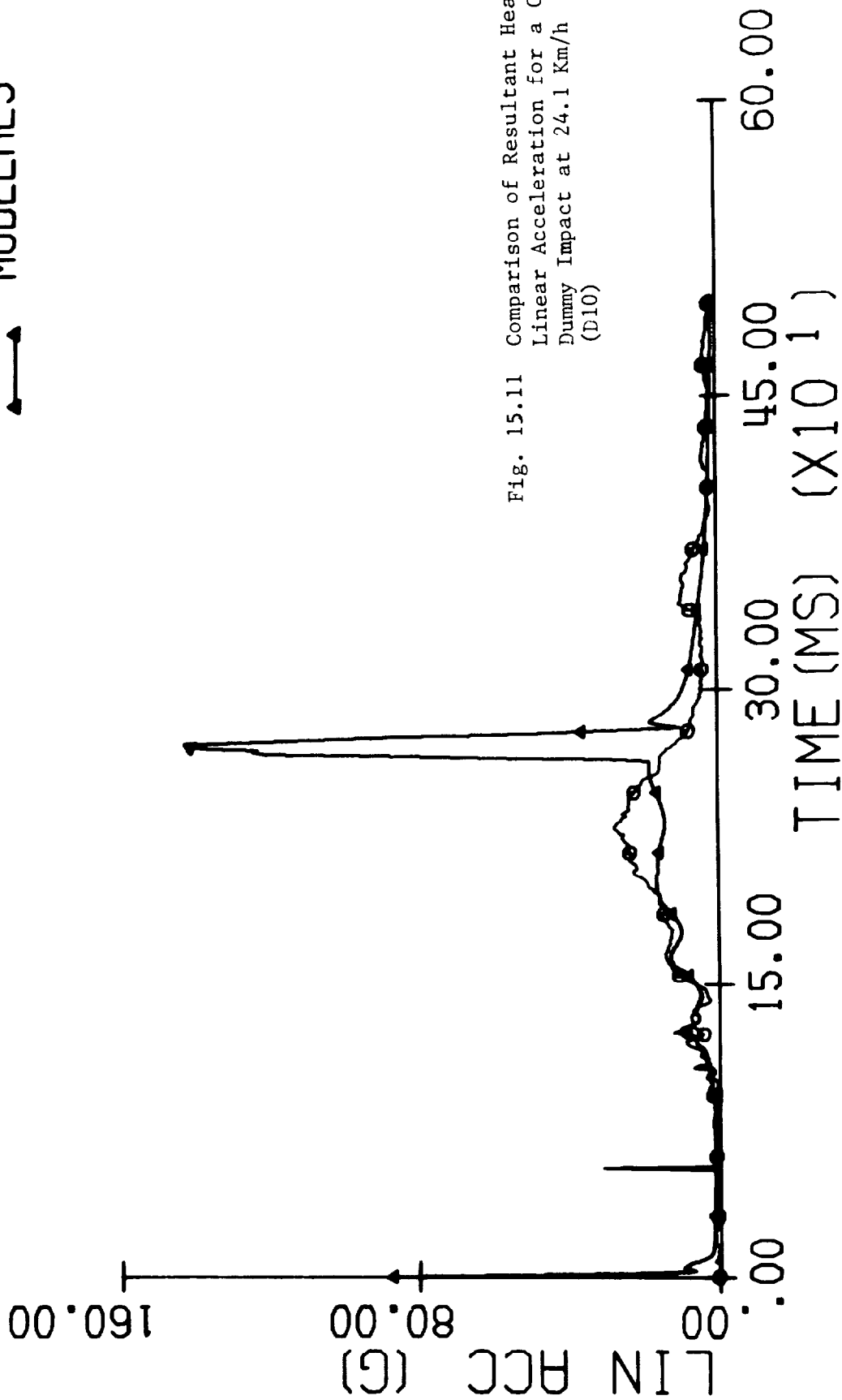


Fig. 15.11 Comparison of Resultant Head Linear Acceleration for a Car-Dummy Impact at 24.1 Km/h (D10)

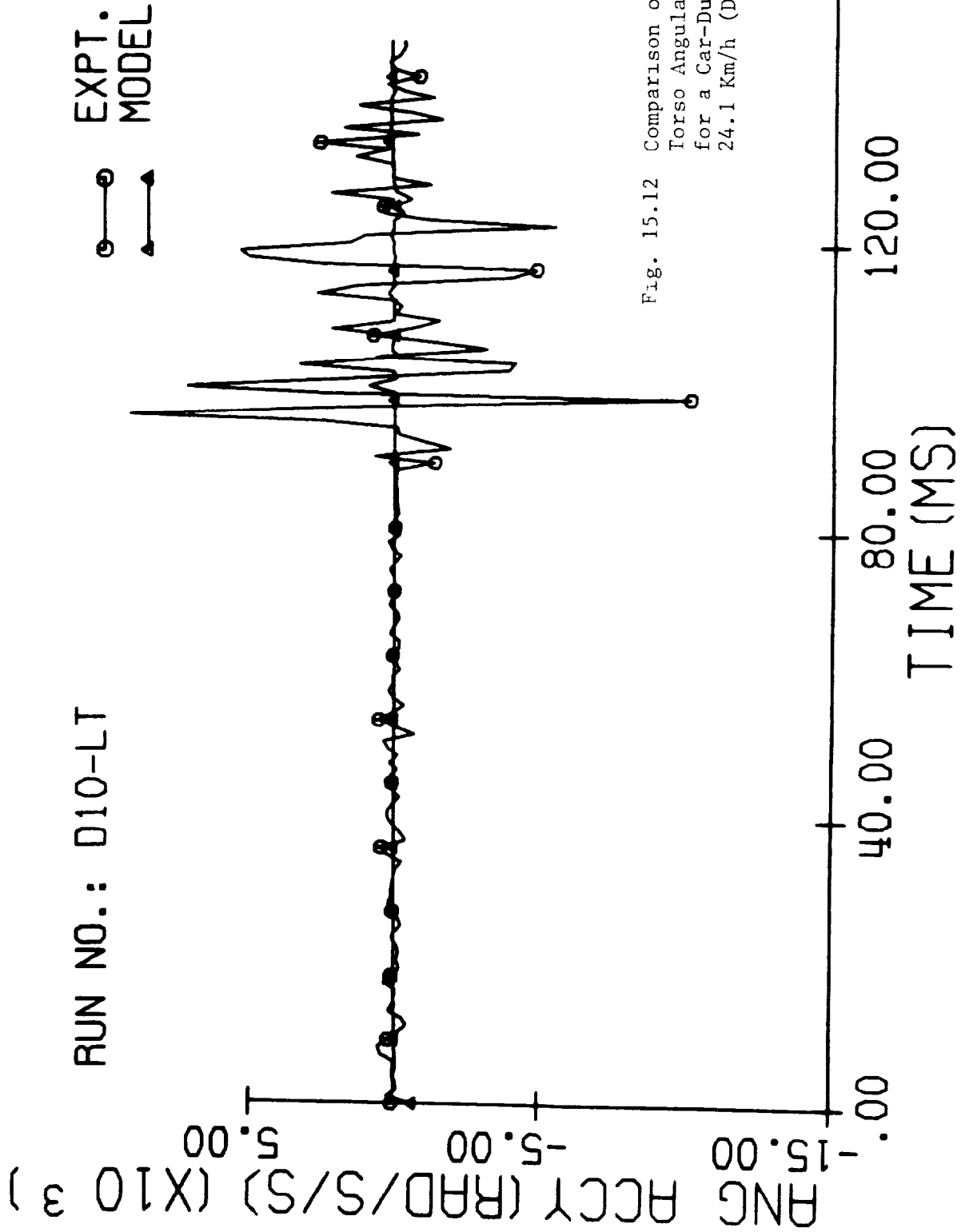


Fig. 15.12 Comparison of Y-Axis Lower Torso Angular Acceleration for a Car-Dummy Impact at 24.1 Km/h (D10)

RUN NO.: D10-LT

EXPT.
MODEL

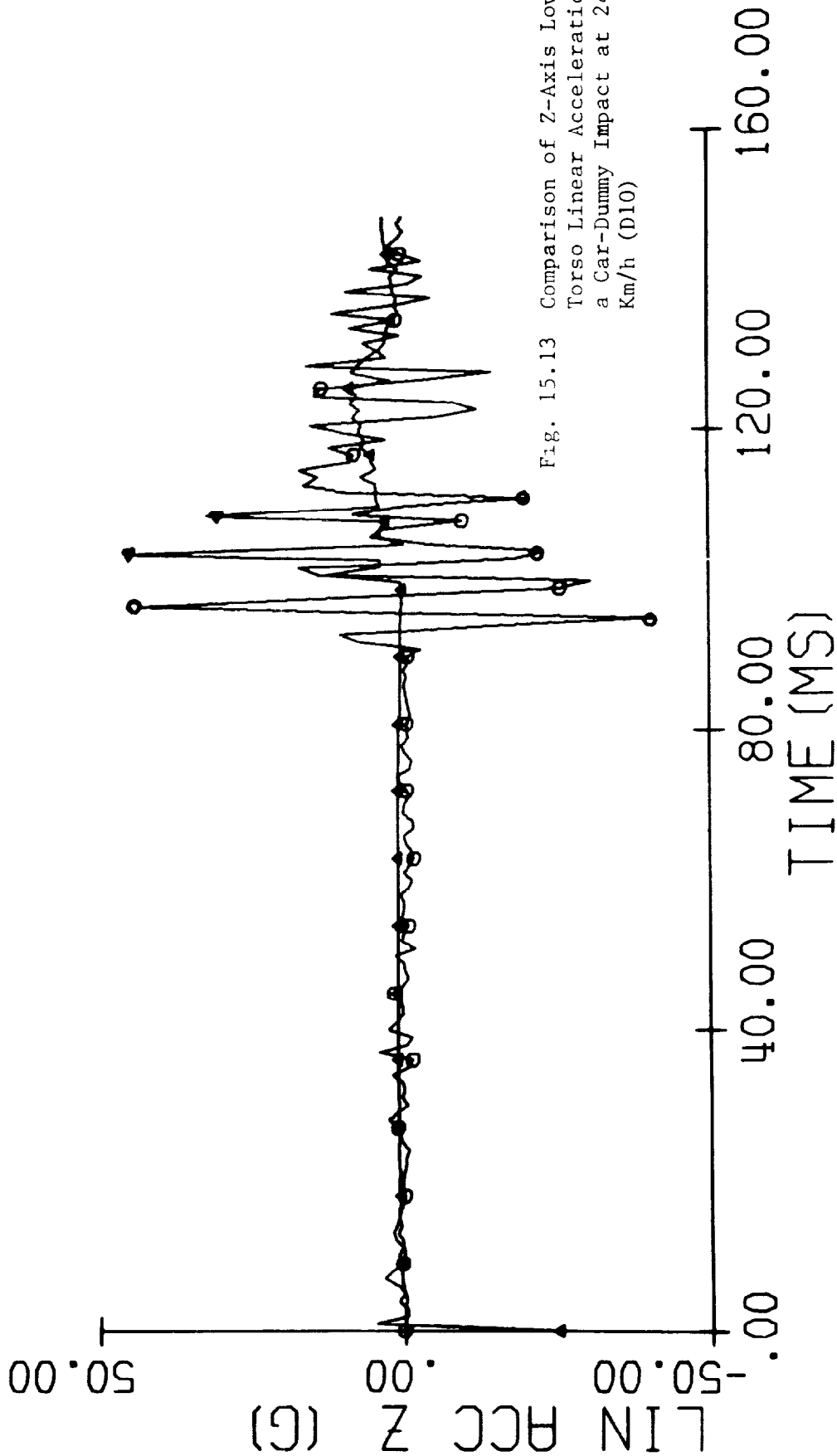


Fig. 15.13 Comparison of Z-Axis Lower Torso Linear Acceleration for a Car-Dummy Impact at 24.1 Km/h (D10)

RUN NO.: D10-LT

EXPT. RES
MODEL RES

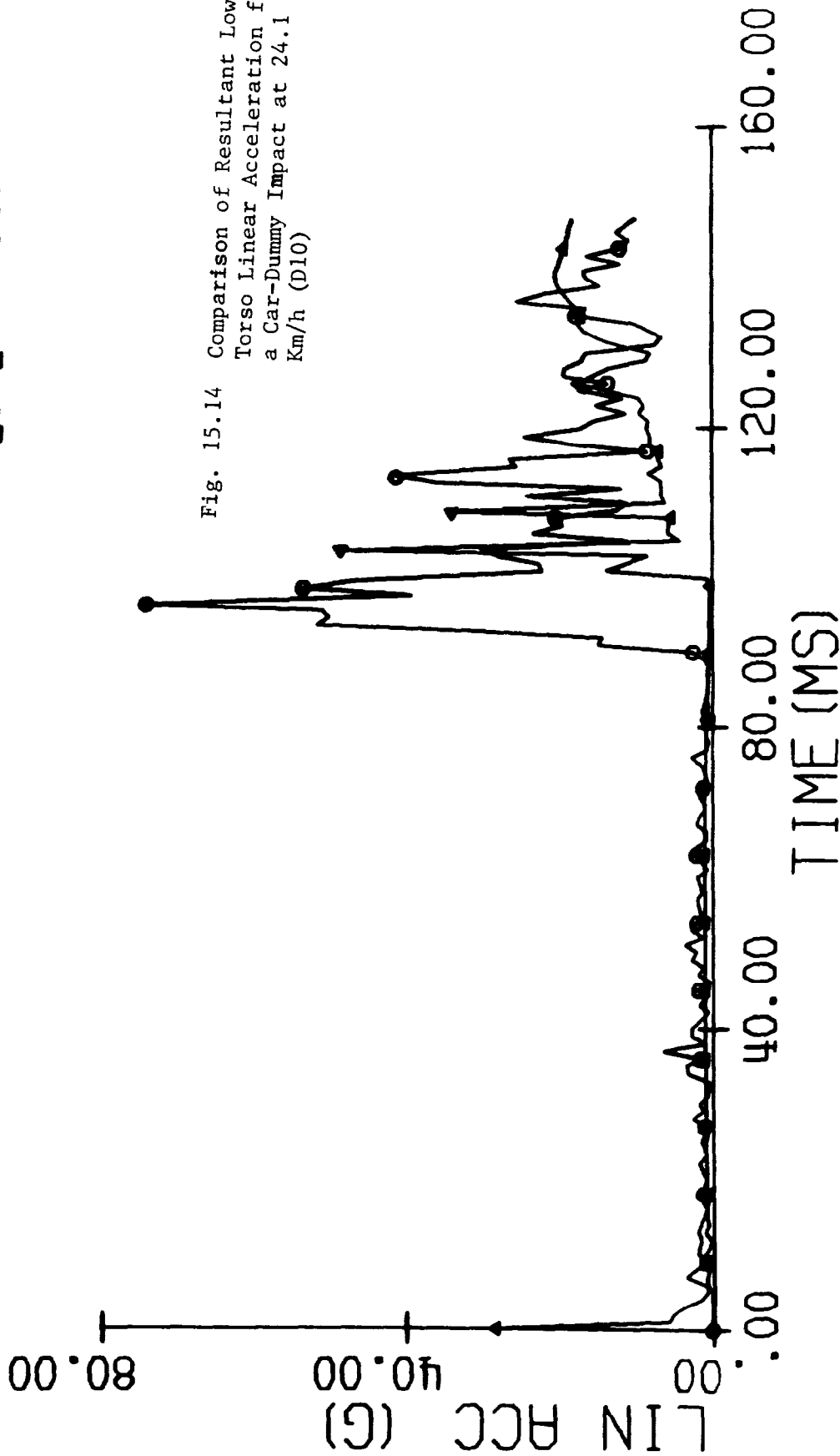


Fig. 15.14 Comparison of Resultant Lower Torso Linear Acceleration for a Car-Dummy Impact at 24.1 Km/h (D10)

RUN NO.: D10-LUL

EXPT.
MODEL

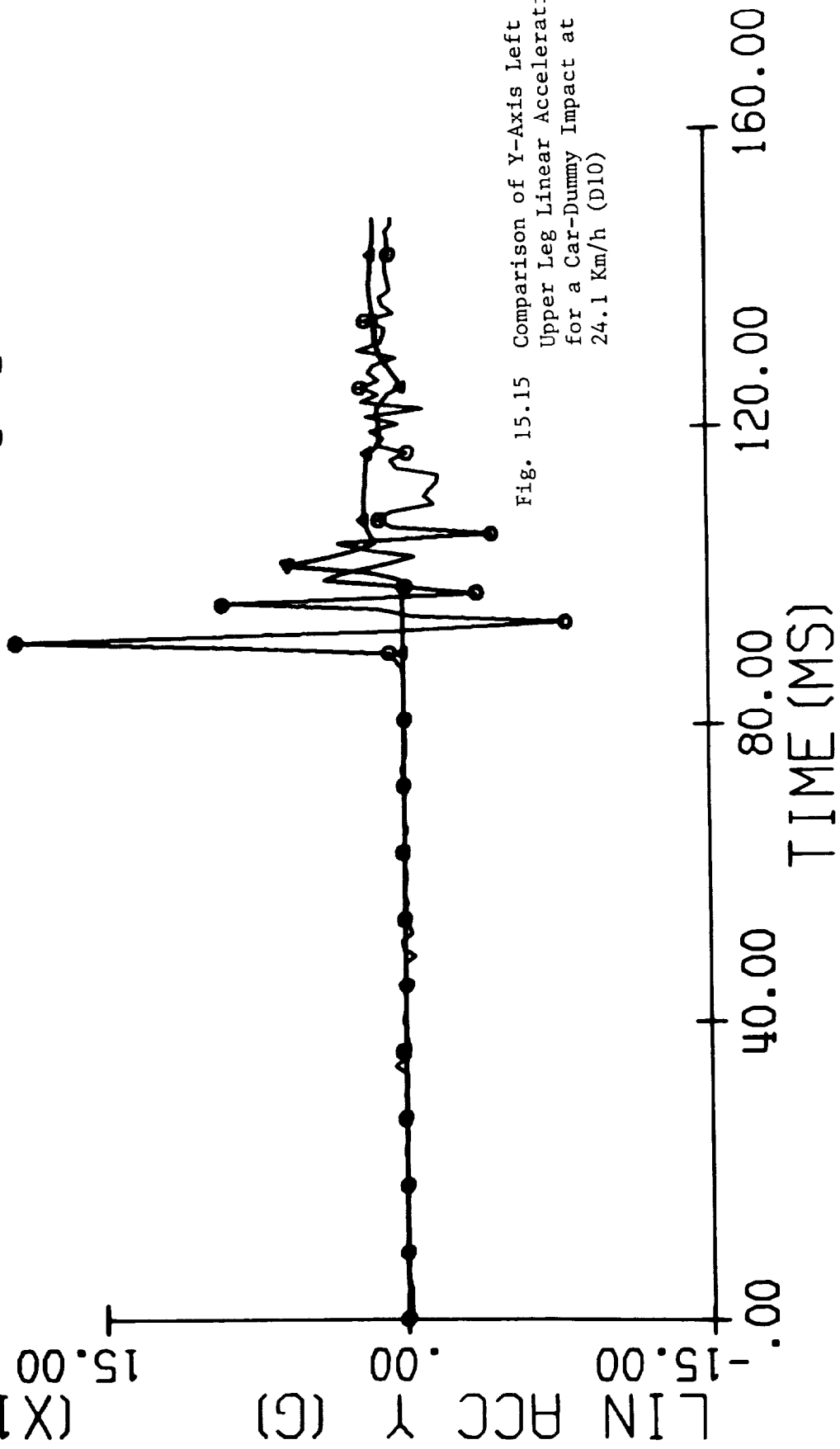
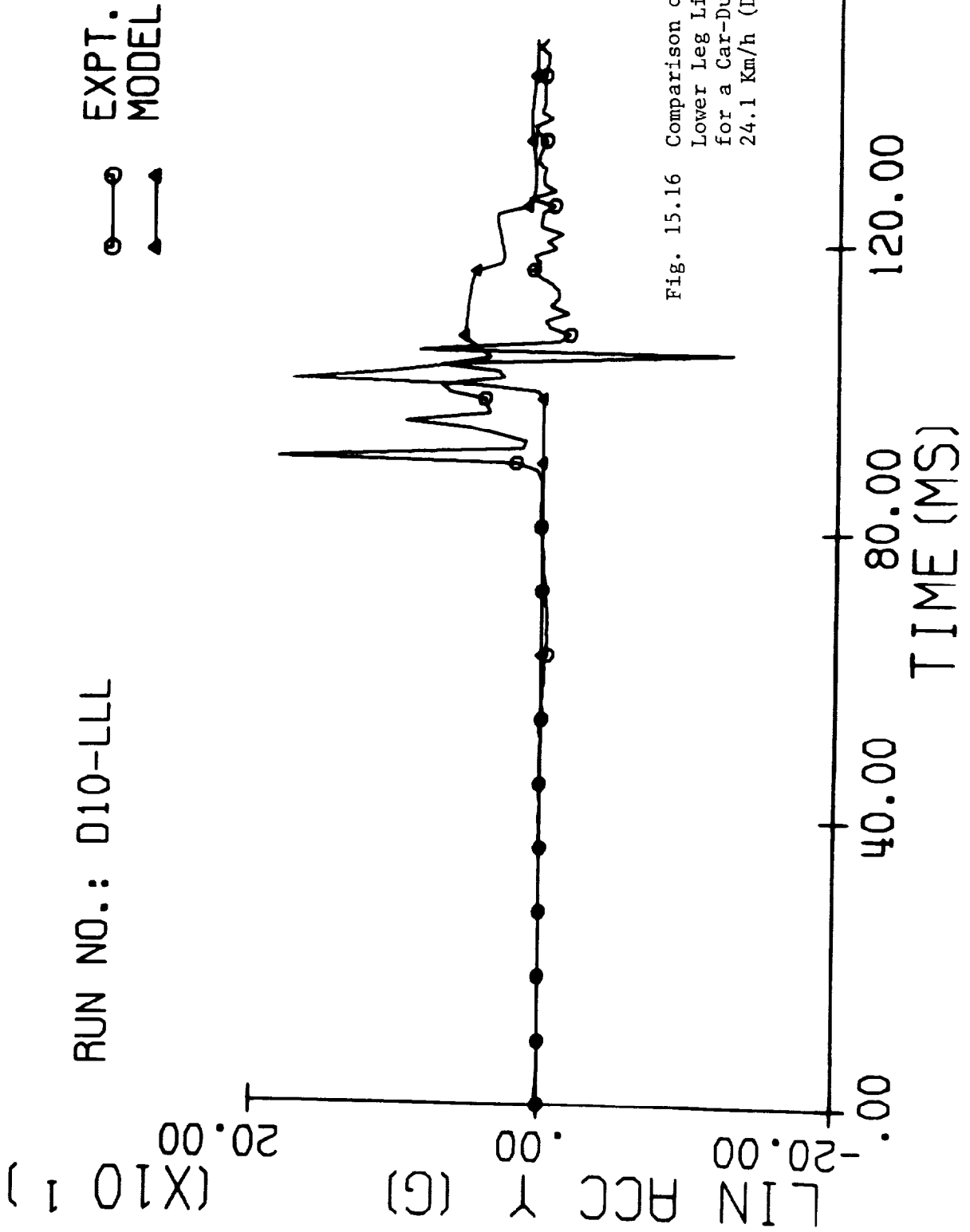


Fig. 15.15 Comparison of Y-Axis Left Upper Leg Linear Acceleration for a Car-Dummy Impact at 24.1 Km/h (D10)



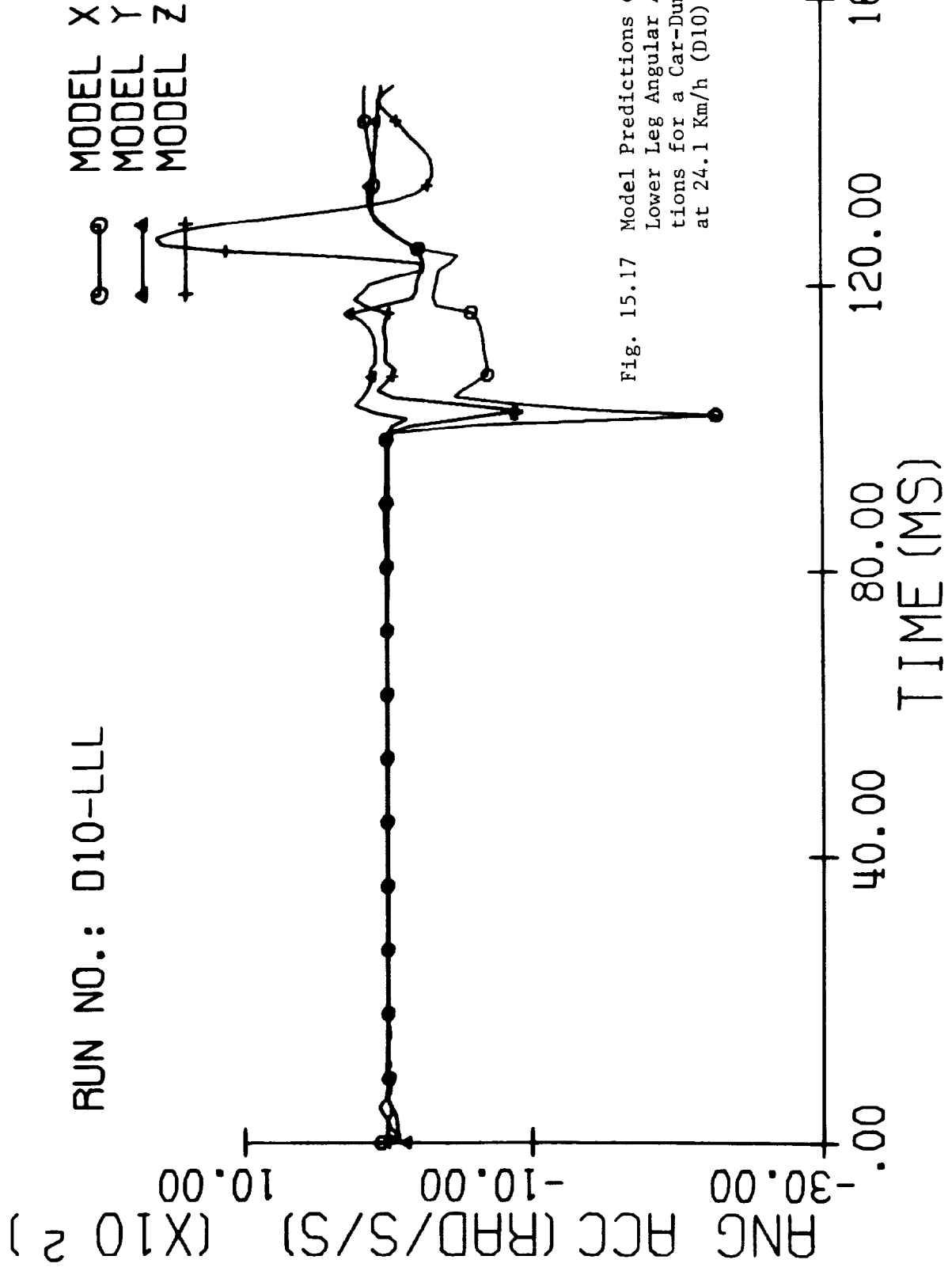


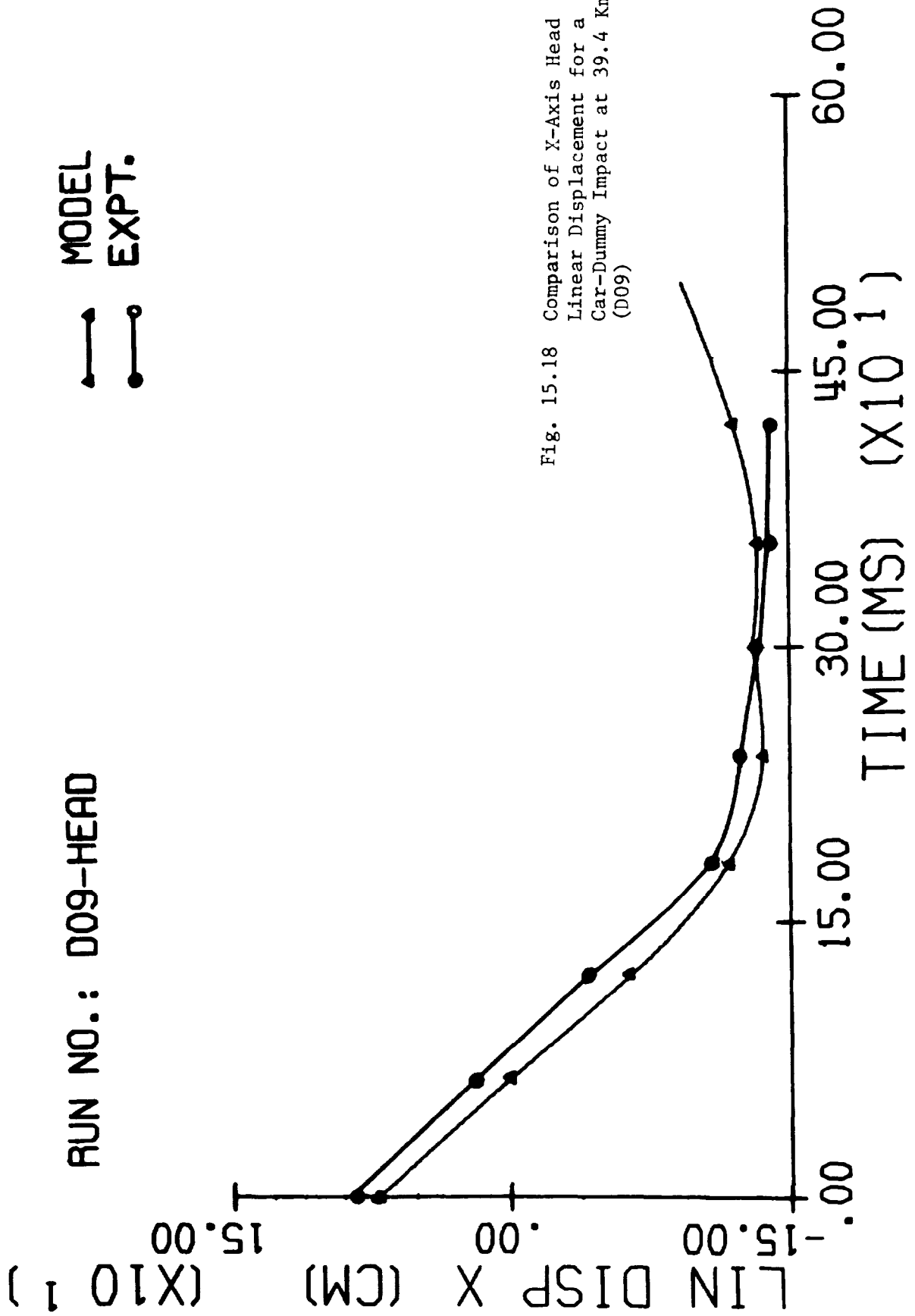
Fig. 15.17 Model Predictions of Left Lower Leg Angular Accelerations for a Car-Dummy Impact at 24.1 Km/h (D10)

motion of this segment. The dominant angular motion for lateral impact will be around the X-axis, which is coupled with a lower level spin around the Z-axis. Minimal rotation occurs around the Y-axis throughout the impact.

For Runs D05 and D09, most of the attention was given to displacement kinematics, since angular acceleration data were not available for these runs. Whole-body motion for D05 has already been compared. Thus, linear displacement comparisons for the head for D09 are included. The X- and Z-components of linear displacement are shown in Figures 15.18 and 15.19. These figures are indications of a good correlation.

15.4 Discussion

It has been demonstrated that a good correlation can be obtained in both the vertical drop tests and the horizontal impacts. The lateral as well as frontal mode was compared. In general, the simulation was carried out to about 500 ms, although some curves only show a part of that simulation as there is very little to compare after that. Some of the comparisons show a phase shift or a mismatch in time, represented more prominently in expanded curves plotted for a shorter duration. There can be many reasons for this shift, some, of which are rather insignificant by themselves but can result in a total shift of about 10 to 15 ms. For example, errors due to lateral parallax in movie analysis, though negligible, and representation of planes by ellipsoids etc., should not be treated as a serious mismatch. No attempt was made to synchronize the time for model and experimental impact.



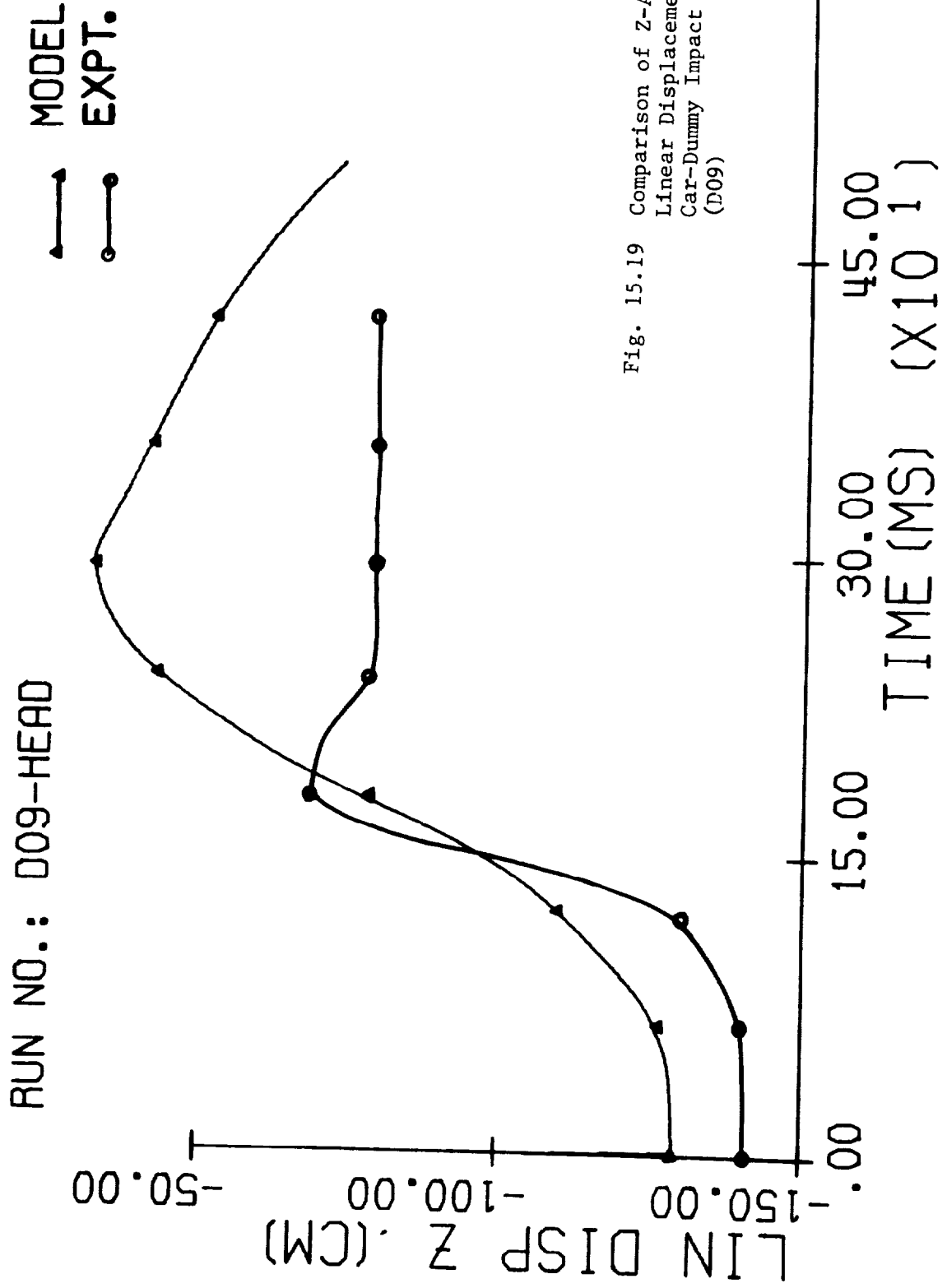


Fig. 15.19 Comparison of Z-Axis Head Linear Displacement for a Car-Dummy Impact at 39.4 Km/h (D09)

MODEL VALIDATION OF CADAVER IMPACTS

16.1 Comparison of Body Segment Displacements

Again the validation attempt begins with a comparison of model and experimental displacement kinematics. Figure 16.1 shows whole-body linear displacements at 100 ms intervals for a 24.1 km/h cadaver impact (Run C03). The simulation was initiated at the time of actuation of the release mechanism. Overall correlation is good.

16.2 Contact History

Table 16.1 compares the contact duration observed in the experiment and model (for 4 body segments) for a 37.3 km/h impact (Run C06). Contact begins at approximately the same instant in both cases, with the exception of the right upper arm. However, the duration is shorter in the model. The right upper arm contact-time history is not well correlated.

16.3 Kinematic Analysis

Correlating acceleration kinematics is emphasized. At impact, the angular position is identical in model and experiment, for the lower torso, left upper leg and left lower leg. Thus, comparison of linear acceleration can be made. Moreover, the acceleration pulse has significant magnitude for only a short post-impact duration. Figures 16.2 through 16.7 compare accelerations for Run C03 (24.1 km/h) and Figures 16.9 through 16.15 represent Run C06 (37.3 km/h). It should be noted that both are lateral impacts and that in Run C06, the front-end was covered with a 15 cm thick layer of foam rubber. Comparisons for a 32.4 km/h frontal impact (Run C05) are given in Figures 16.16 through 16.19.

Figure 16.2 compares the Z-component of head angular acceleration. It appears to be a very good correlation, except for the spike observed at about 280 ms. This can be attributed to the ringing of the accelerometers. Figure 16.3 shows a good correlation of the X-components of head linear acceleration. As seen in Figure 16.4 the Z component of angular acceleration of the lower torso, as predicted by the model is very low in magnitude in comparison with experimental data. In Figure 16.5 a comparison of the Y-component of the linear acceleration of the lower torso is made. Figure 16.6 compares the Y-component of linear acceleration of the left upper leg. There exists a time shift and the experimental peak is higher. However, the overall pattern is similar. The same comparison is made for the left lower leg, the impacted leg, as shown in Figure 16.7. Although the pattern is similar in both experiment and model, there is a time shift, thus the model peak value is lower and of longer duration. The negative peaks in the experimental data are again indicative of accelerometer ringing. Pre-

TABLE 16-1

CONTACT HISTORY FOR RUN C06

Segment	Plane*	Contact Duration			
		Experiment		Model	
		Begins	Ends	Begins	Ends
Head	12	240	beyond 500	213	272
Left Upper Leg	10	98	269	71	142
Left Lower Leg	4	65	202	72	109
Right Upper Arm	12	630	beyond 1000	229	260

*These plane numbers relate to Figure 13.3. In the actual dataset for Run C06, plane numbers were different.

dicted values of all three components of angular acceleration for the left upper leg are plotted in Figure 16.8. They are reasonable for a lateral impact. As expected, the X-component is the largest and there is a lower level spin about the Z-axis. The Y-component is very small.

For Run C06, the Y-component of the head angular acceleration is compared in Figure 16.9. The first positive peak is absent from the model output. Linear components of head acceleration along the X- and Y-axis are compared in Figure 16.10 and 16.11. Clearly, the magnitude of the peaks of the X-component are roughly comparable, but the Y-component experimental value is much higher in magnitude. This is a clear indication of orientation mismatch and is confirmed by movie analysis. Y- and Z-components of the lower torso linear acceleration are plotted in Figure 16.12 and 16.13. Correlation is fair for both components. Figures 16.14 and 16.15 illustrate the X-component of angular acceleration of the left upper leg and Y-components of linear acceleration of left lower leg respectively. Both are predominant components and the correlation is reasonably good.

The major component of head acceleration during Run C05 was along the X-axis. Figure 16.16 shows excellent correlation between model and output experimental results. The head angular acceleration about the Y-axis is compared in Figure 16.17. The experimental data showed an additional oscillation which was not predicted by the model. However, the predominant peak for both cases occurred at about the same time. There was reasonable correlation between the Z-axis lower torso acceleration, as shown in Figure 16.18. The X-axis acceleration of the left lower leg (impacted leg) is compared in Figure 16.19. Although there is a 20 ms shift in time, the pulse shapes for the predominant peak are similar.

Based on the comparison made in this chapter and Chapters 14 and 15, it can be said that the Calspan model is capable of simulating pedestrian-vehicle impact in three different modes. It can give reasonable kinematic predictions for both cadaver and dummy segments. Although force-deflection data were not completely available, the resulting kinematics were reasonably realistic. However, not all segment kinematics correlate as well as the examples shown. Some of the poorer correlations are also represented. Matching low values of angular acceleration was difficult, as discussed in Chapter 14. Care must be exercised in comparing linear accelerations, since a pre-condition for good correlation is matching the angular orientation of the segment. As mentioned in Chapter 15, no attempt was made to adjust the observed time shift.

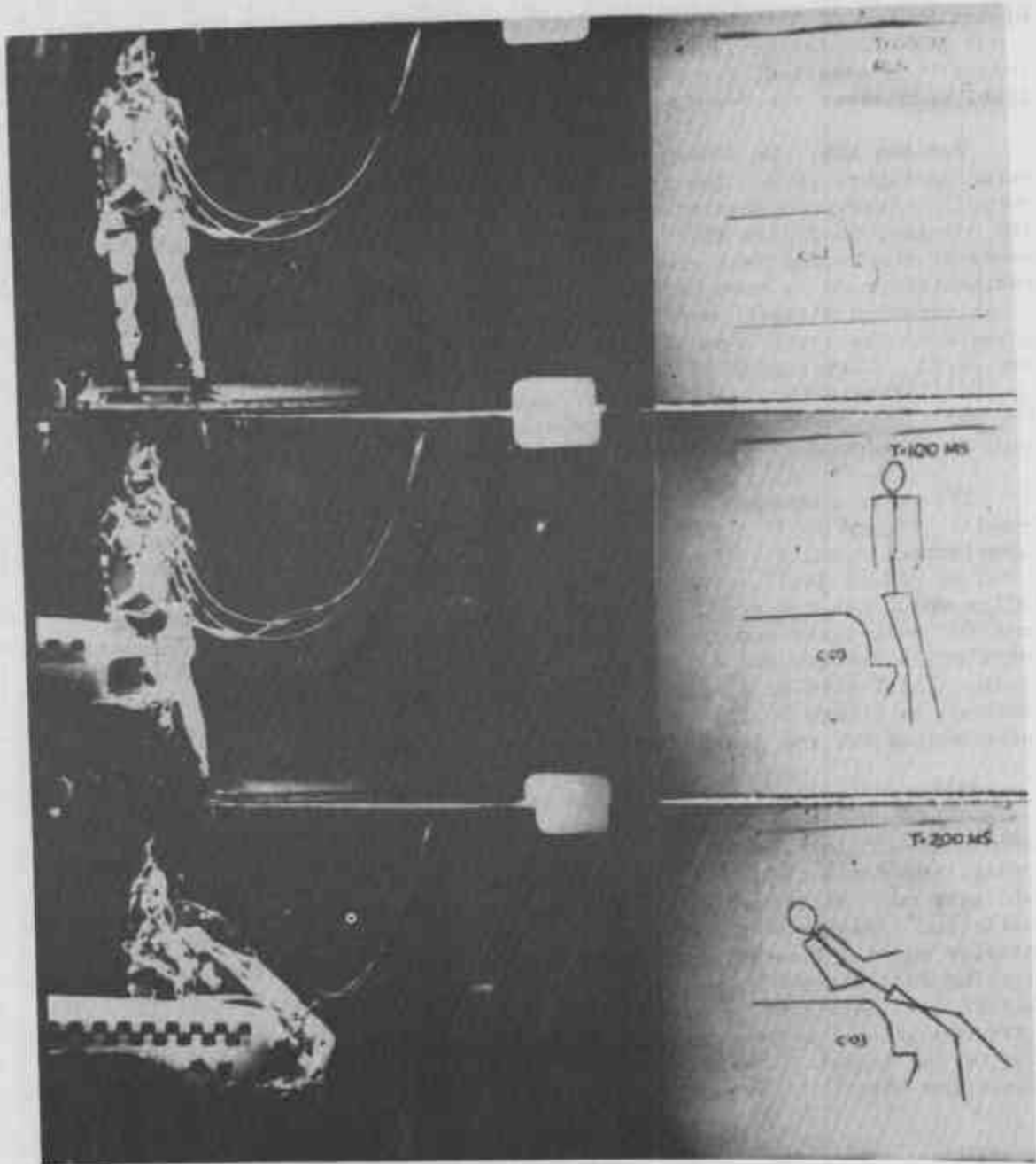


Fig. 16.1(a) Comparison of Whole Body Displacement for a Cadaver (Lateral) Impact Test at 24.1 Km/h (C03)-Lateral View (0-200 ms)

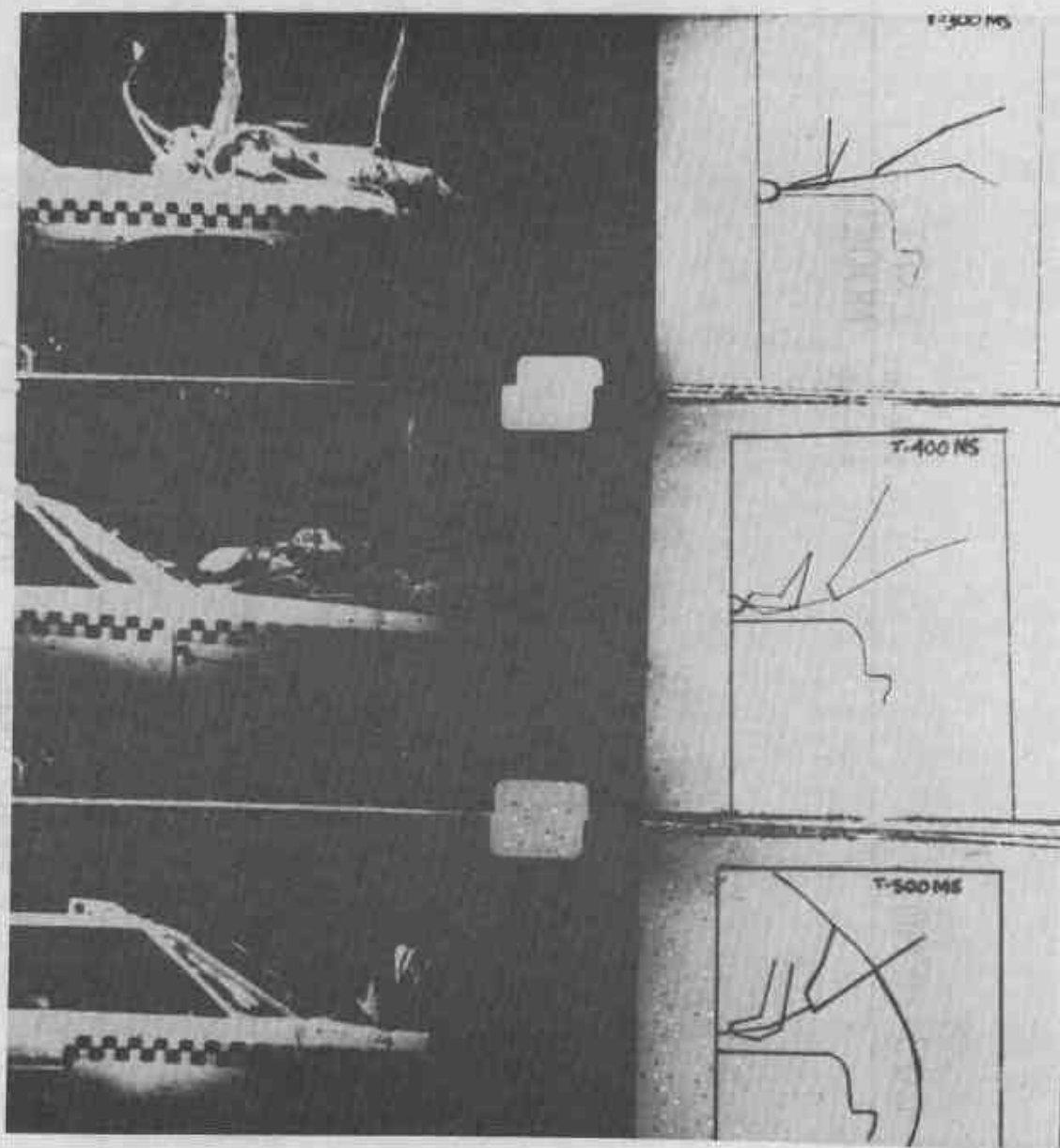
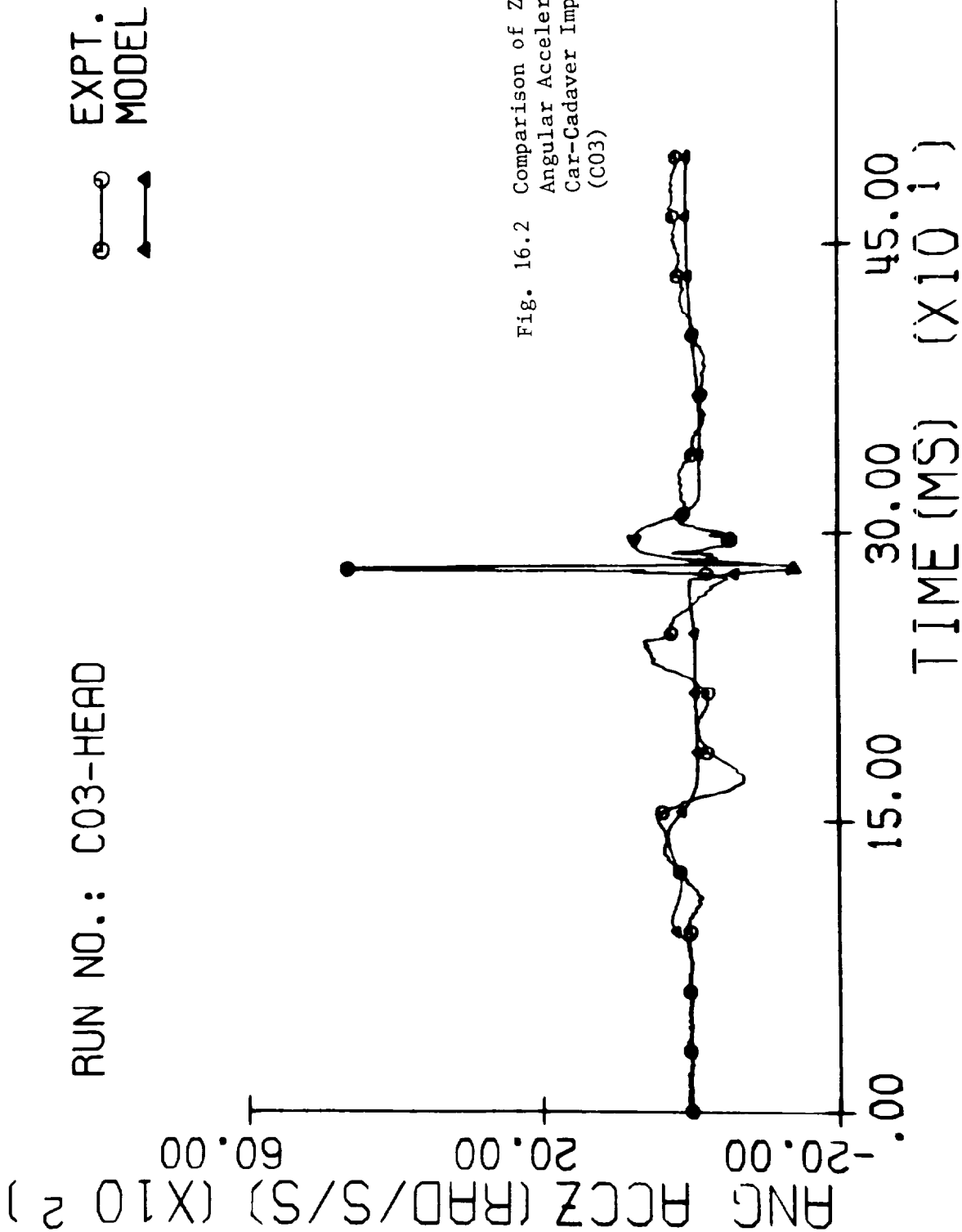


Fig. 16.1(b) Comparison of Whole Body Displacement for a Cadaver (Lateral) Impact Test at 24.1 Km/h (C03)-Lateral View (300-500 ms)



EXPT.
MODEL

RUN NO.: C03-HEAD

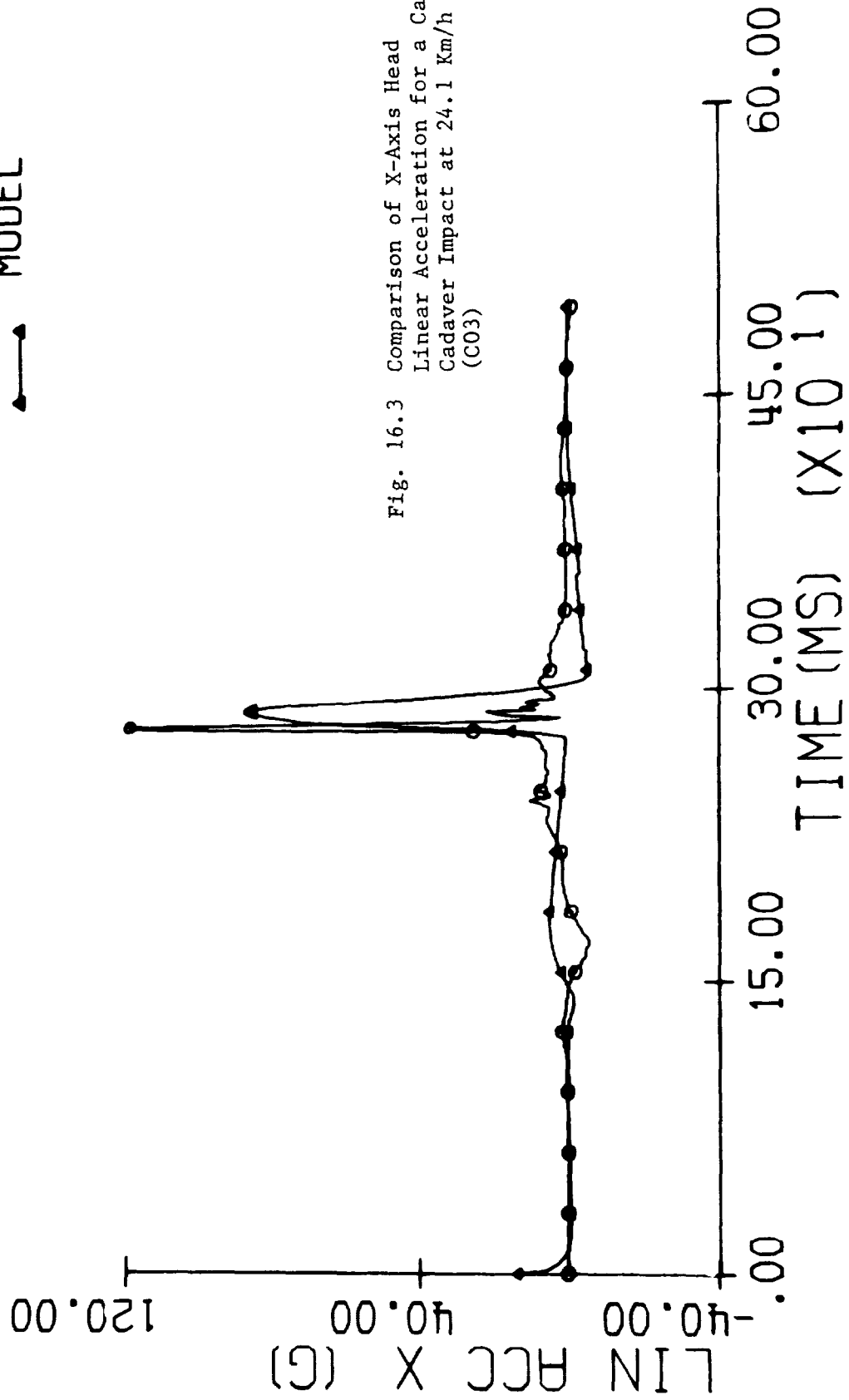


Fig. 16.3 Comparison of X-Axis Head Linear Acceleration for a Car-Cadaver Impact at 24.1 Km/h (C03)

RUN NO.: C03-LT

EXPT.
MODEL

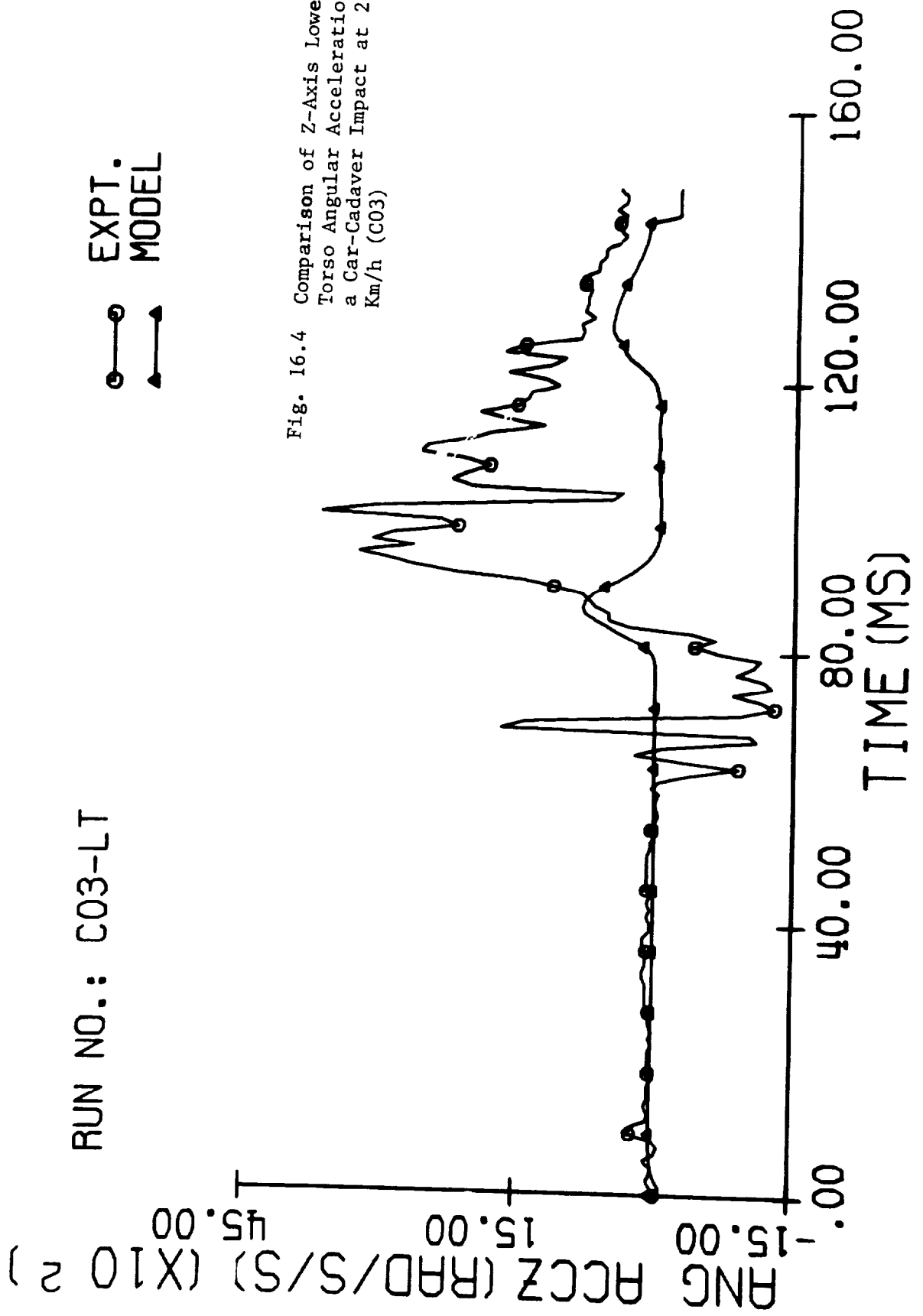


Fig. 16.4 Comparison of Z-Axis Lower Torso Angular Acceleration for a Car-Cadaver Impact at 24.1 Km/h (C03)

RUN NO.: C03-LT

EXPT. MODEL

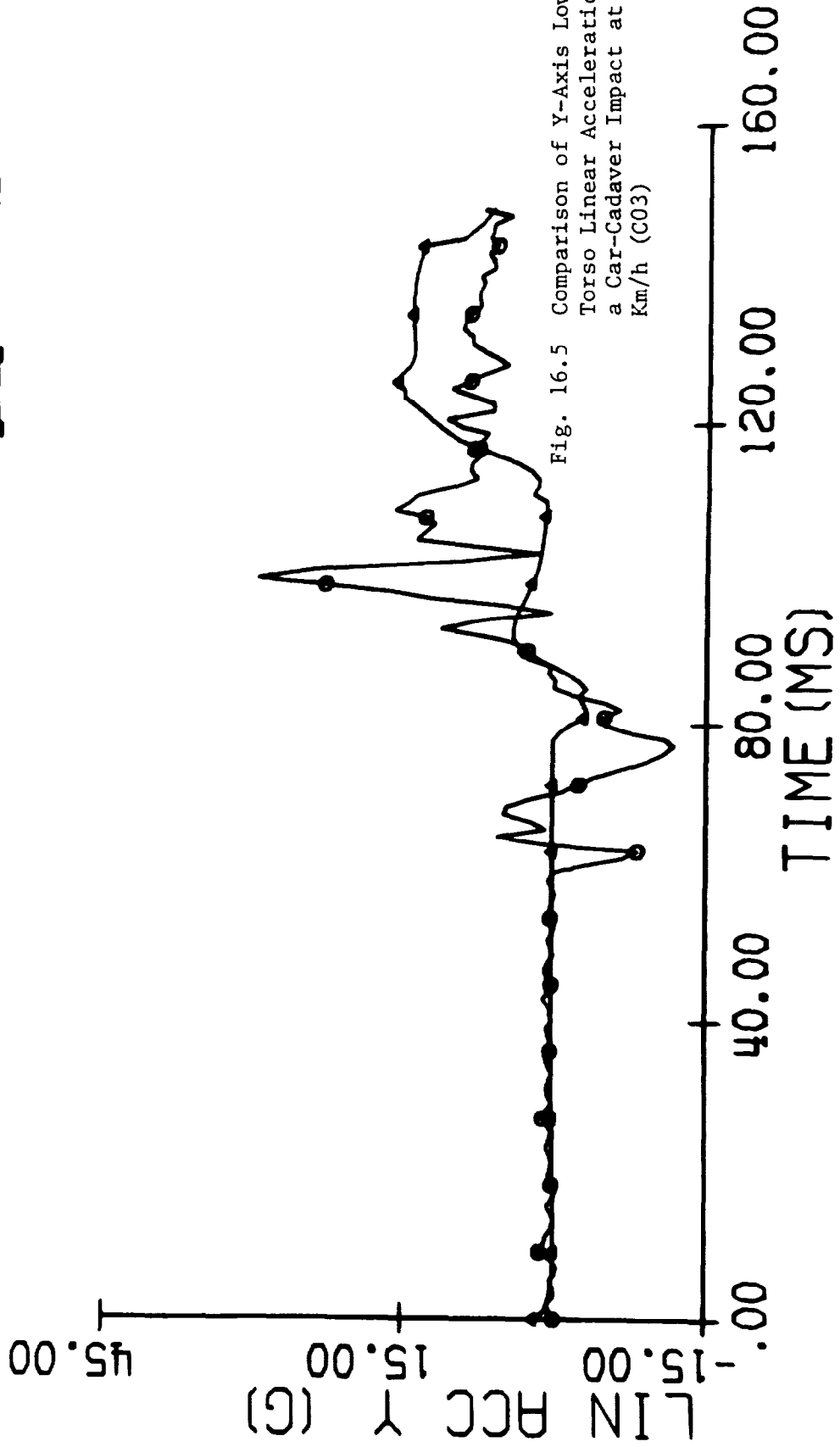
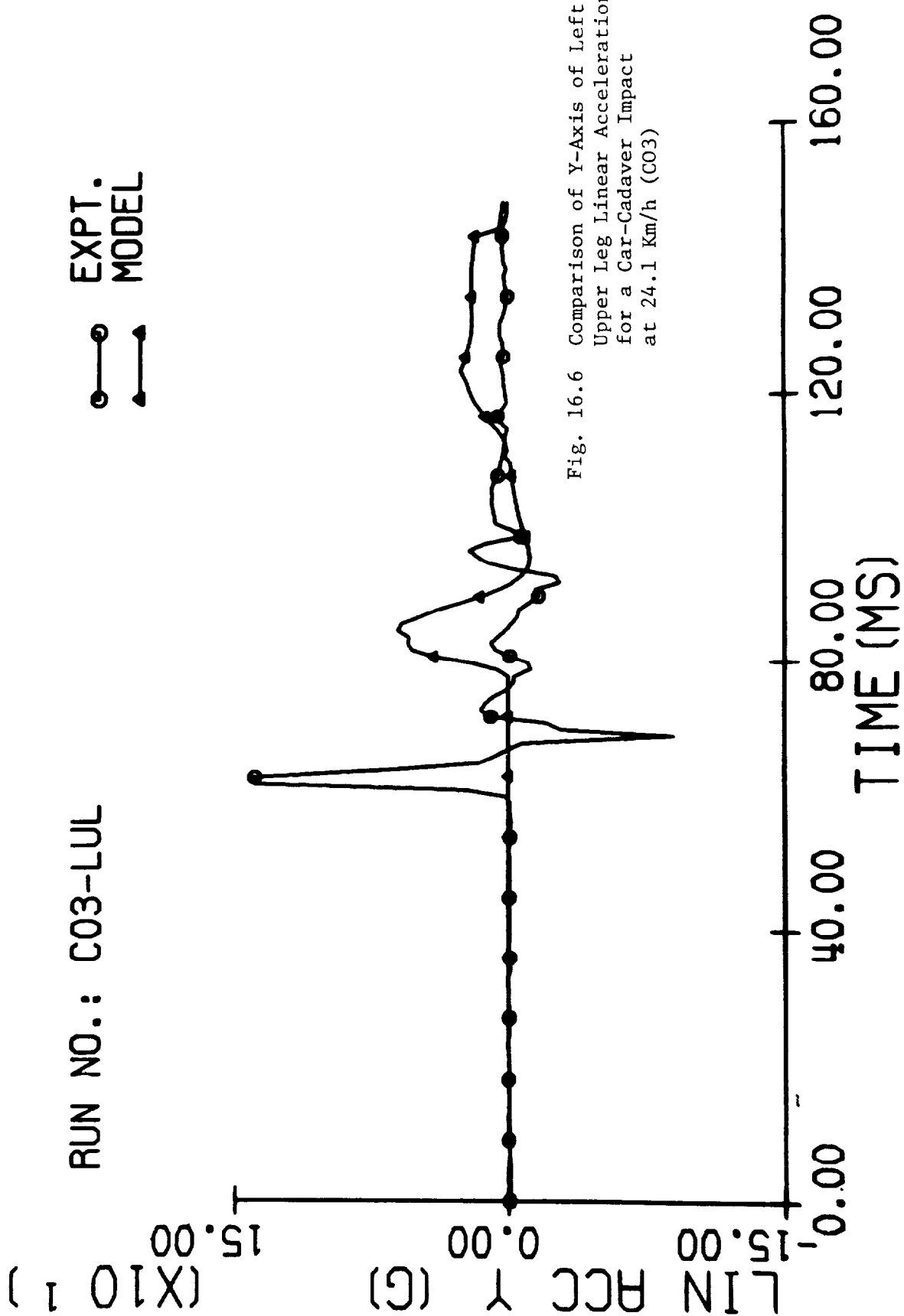


Fig. 16.5 Comparison of Y-Axis Lower Torso Linear Acceleration for a Car-Cadaver Impact at 24.1 Km/h (C03)



RUN NO.: C03-LUL

MODEL X
MODEL Y
MODEL Z

○ — ○
● — ●
+ — +

PNG PCC (R/D/S/S) (X10²)

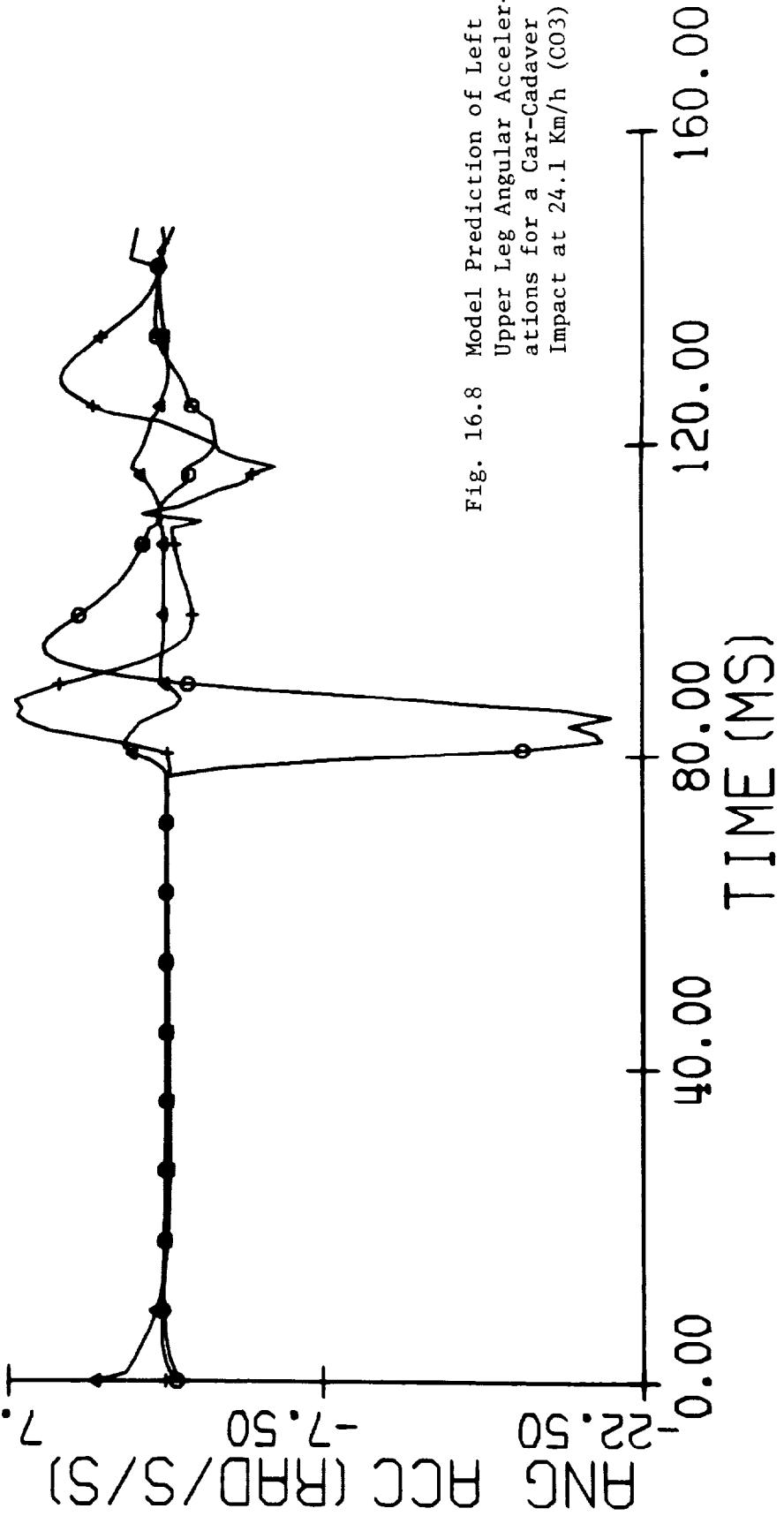
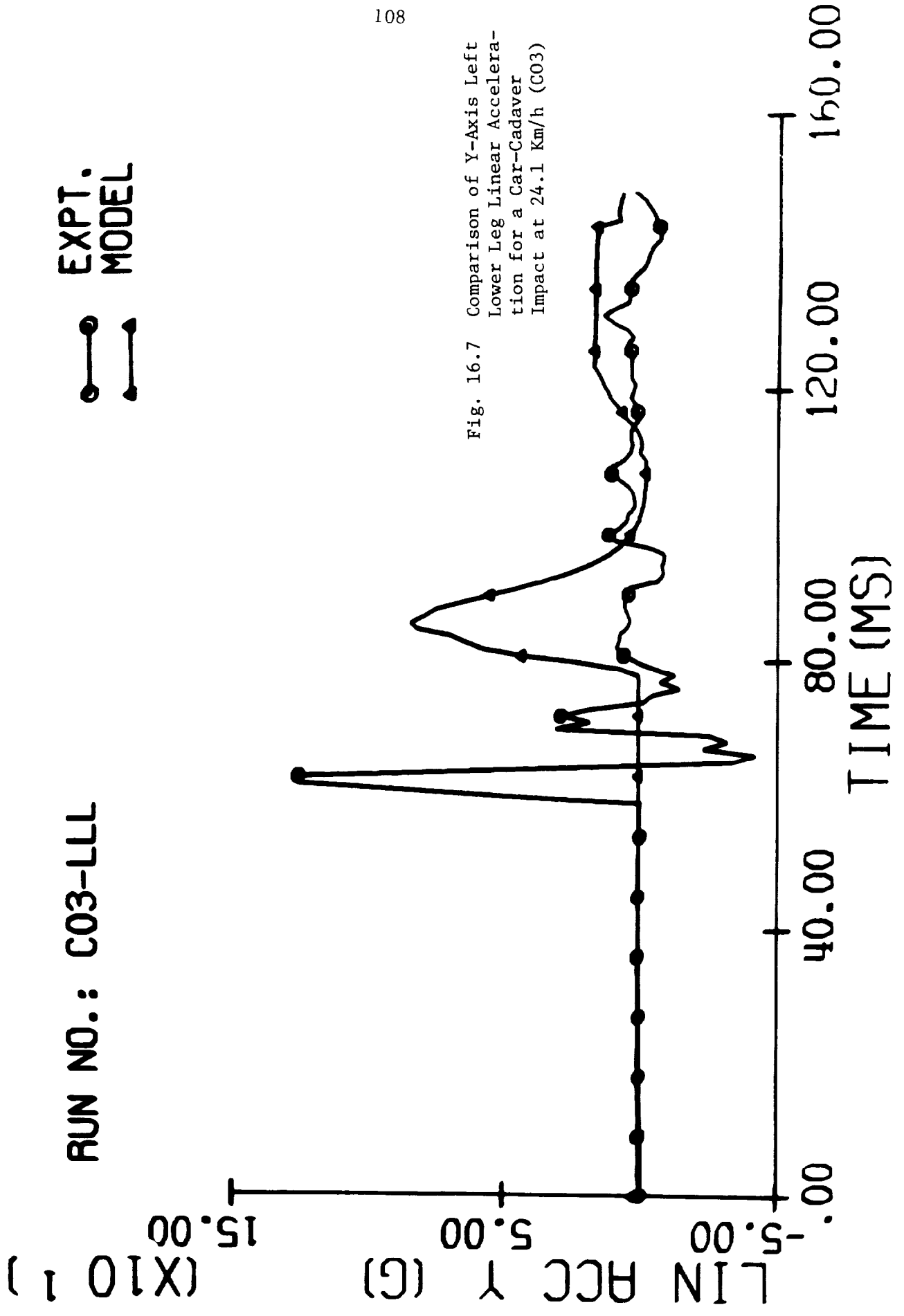
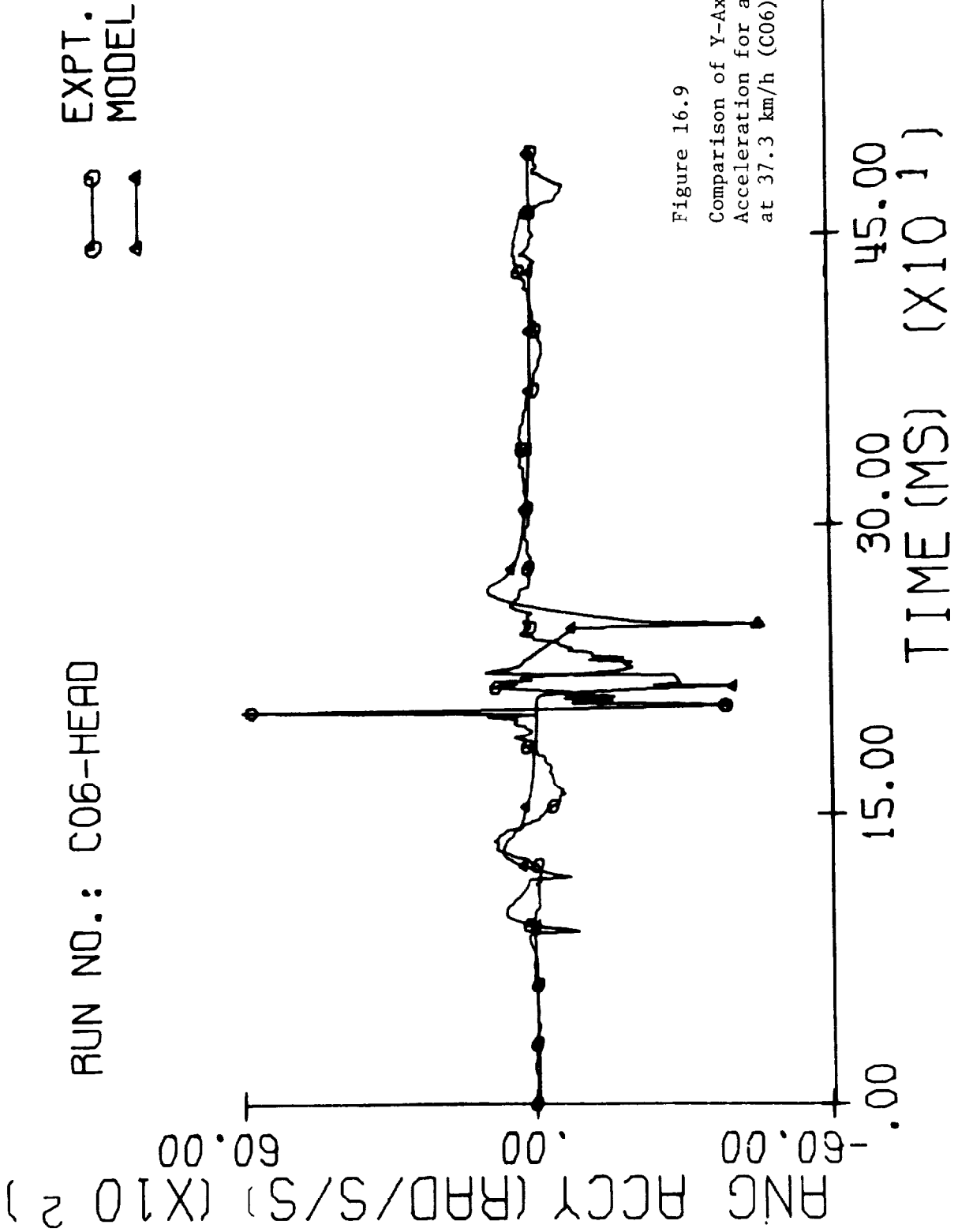


Fig. 16.8 Model Prediction of Left Upper Leg Angular Accelerations for a Car-Cadaver Impact at 24.1 Km/h (C03)





RUN NO.: C06-HEAD

EXPT.
MODEL

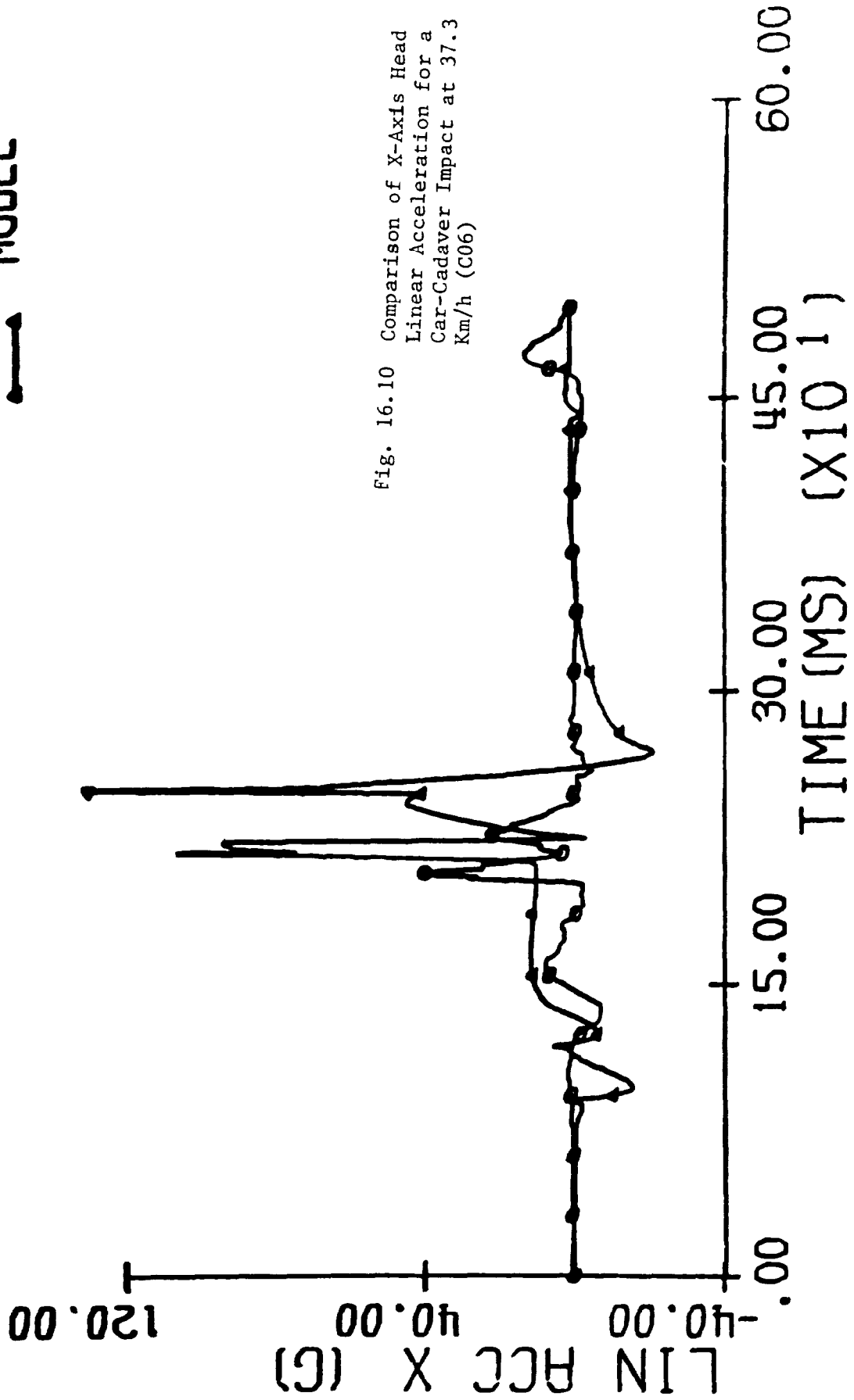


Fig. 16.10 Comparison of X-Axis Head
Linear Acceleration for a
Car-Cadaver Impact at 37.3
Km/h (C06)

RUN NO.: C06-HEAD

EXPT.
MODEL

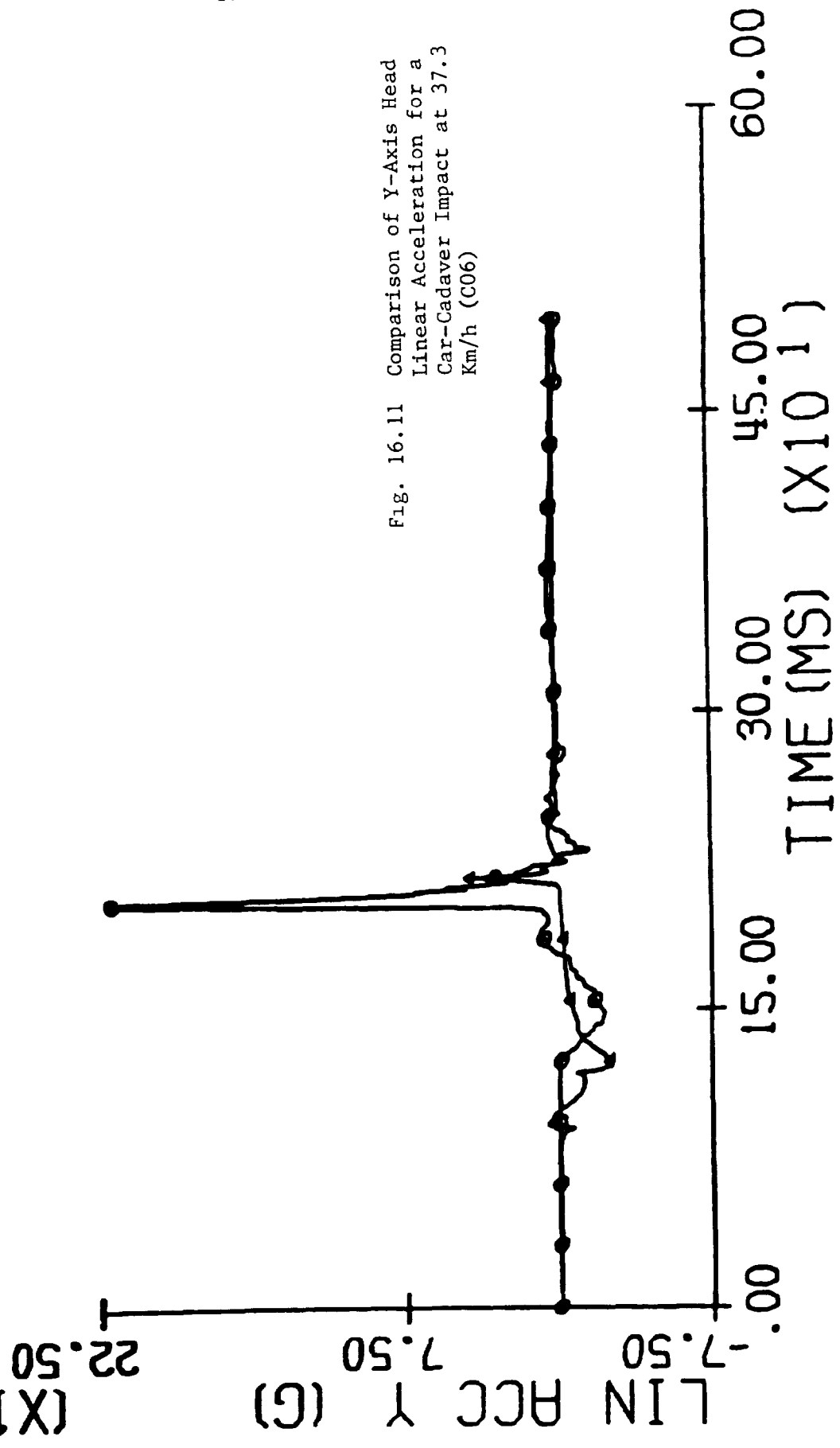


Fig. 16.11 Comparison of Y-Axis Head
Linear Acceleration for a
Car-Cadaver Impact at 37.3
Km/h (C06)

RUN NO.: C06-LT

EXPT.
MODEL

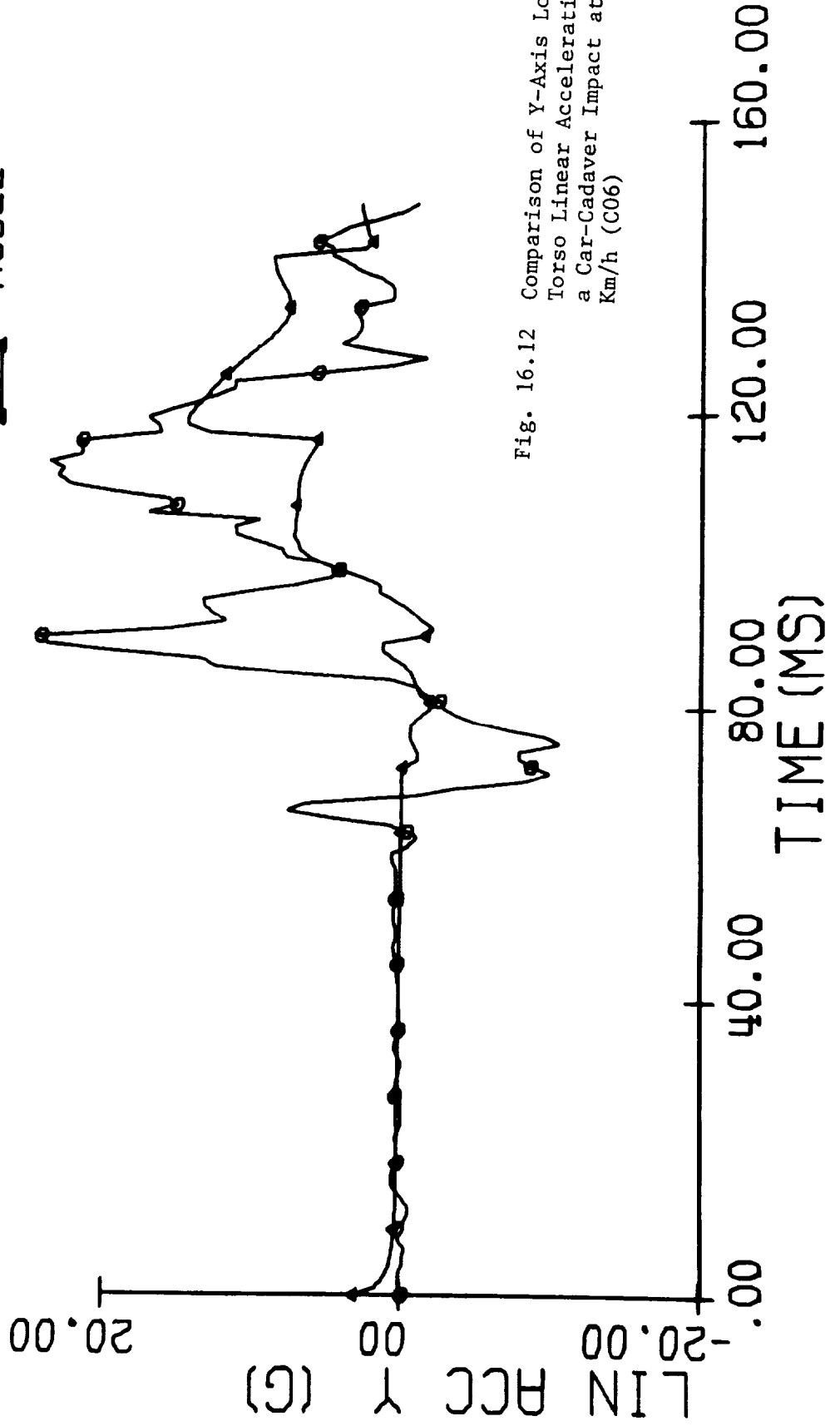


Fig. 16.12 Comparison of Y-Axis Lower Torso Linear Acceleration for a Car-Cadaver Impact at 37.3 Km/h (C06)

RUN NO.: C06-LT

EXPT.
MODEL

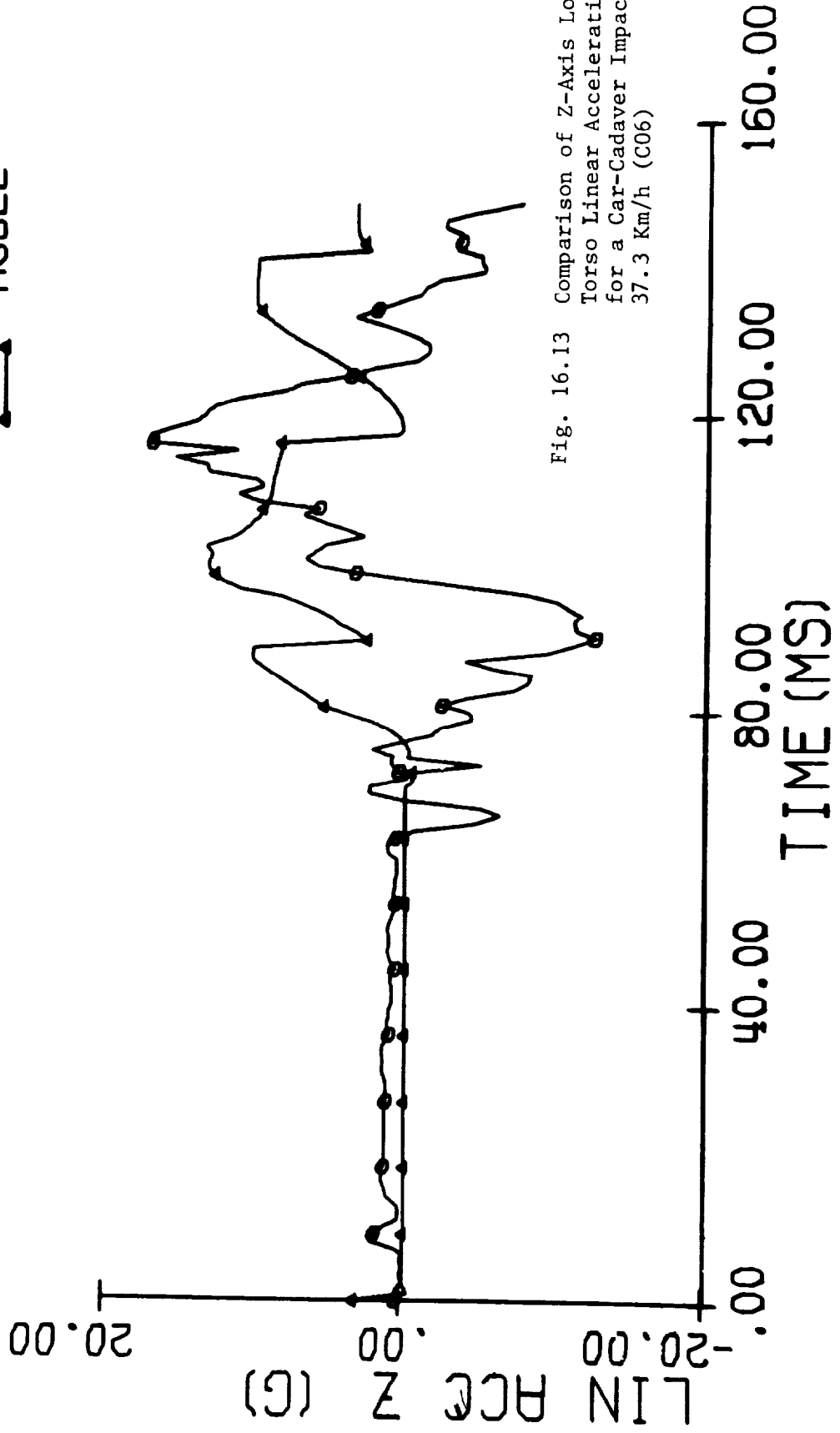
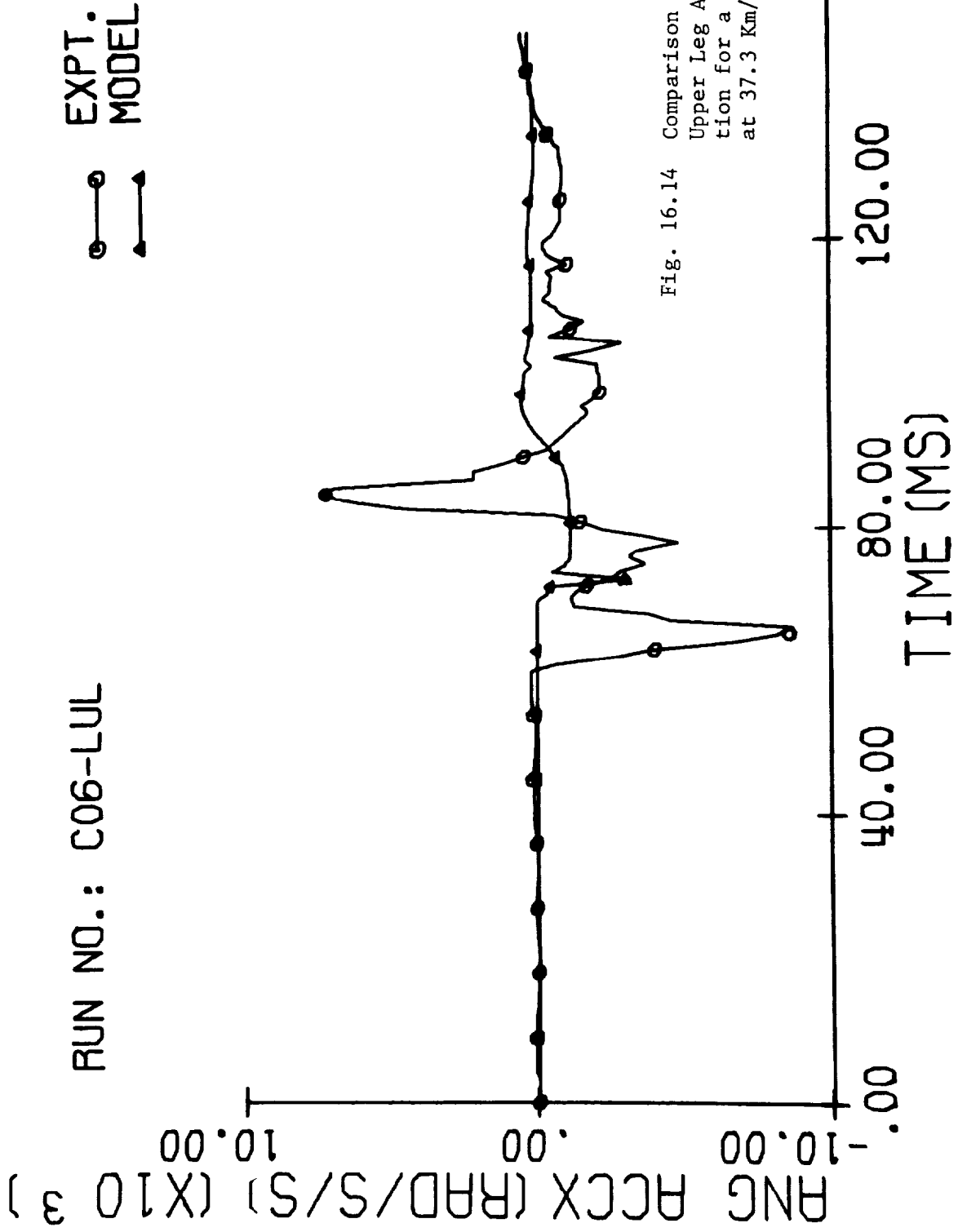
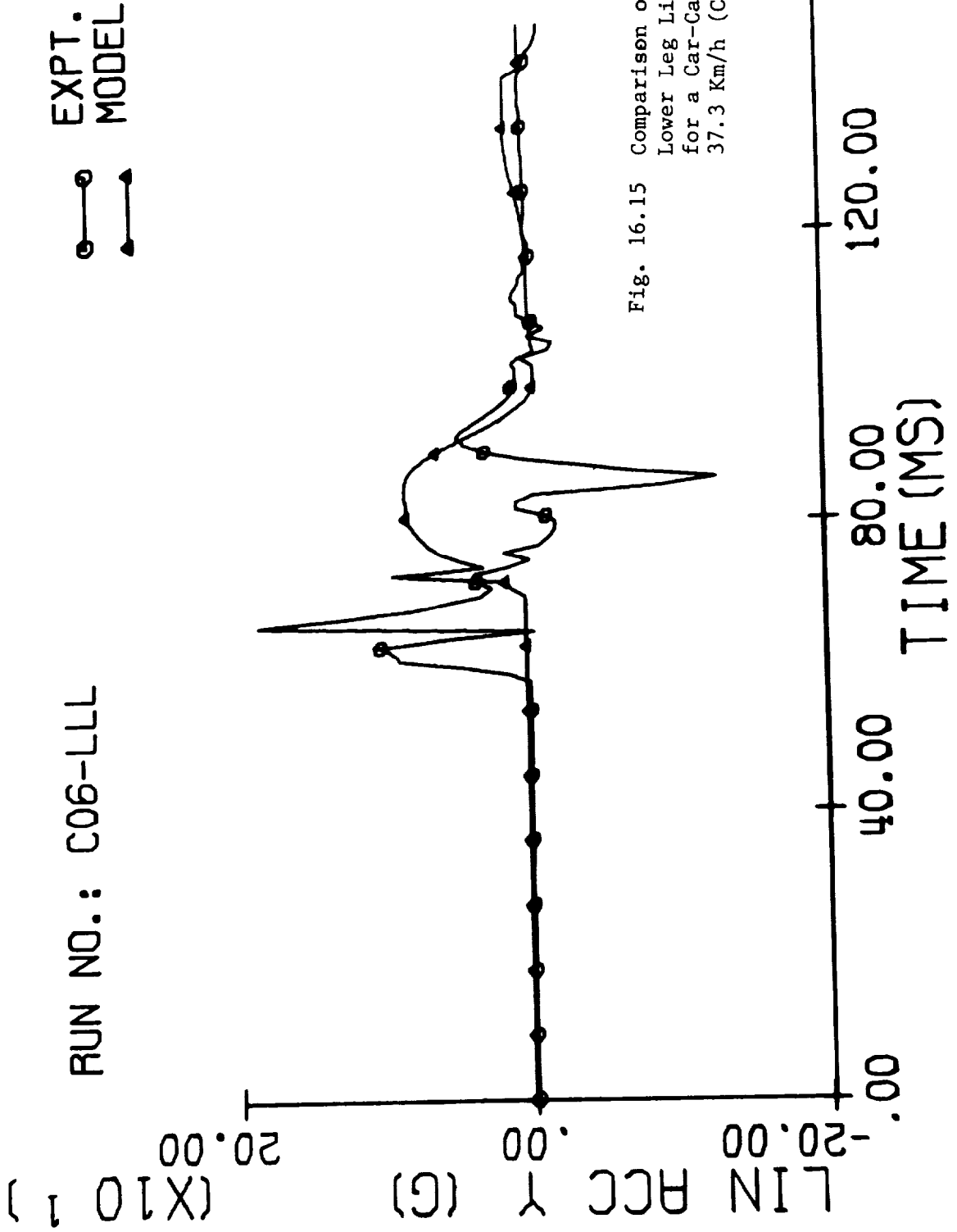


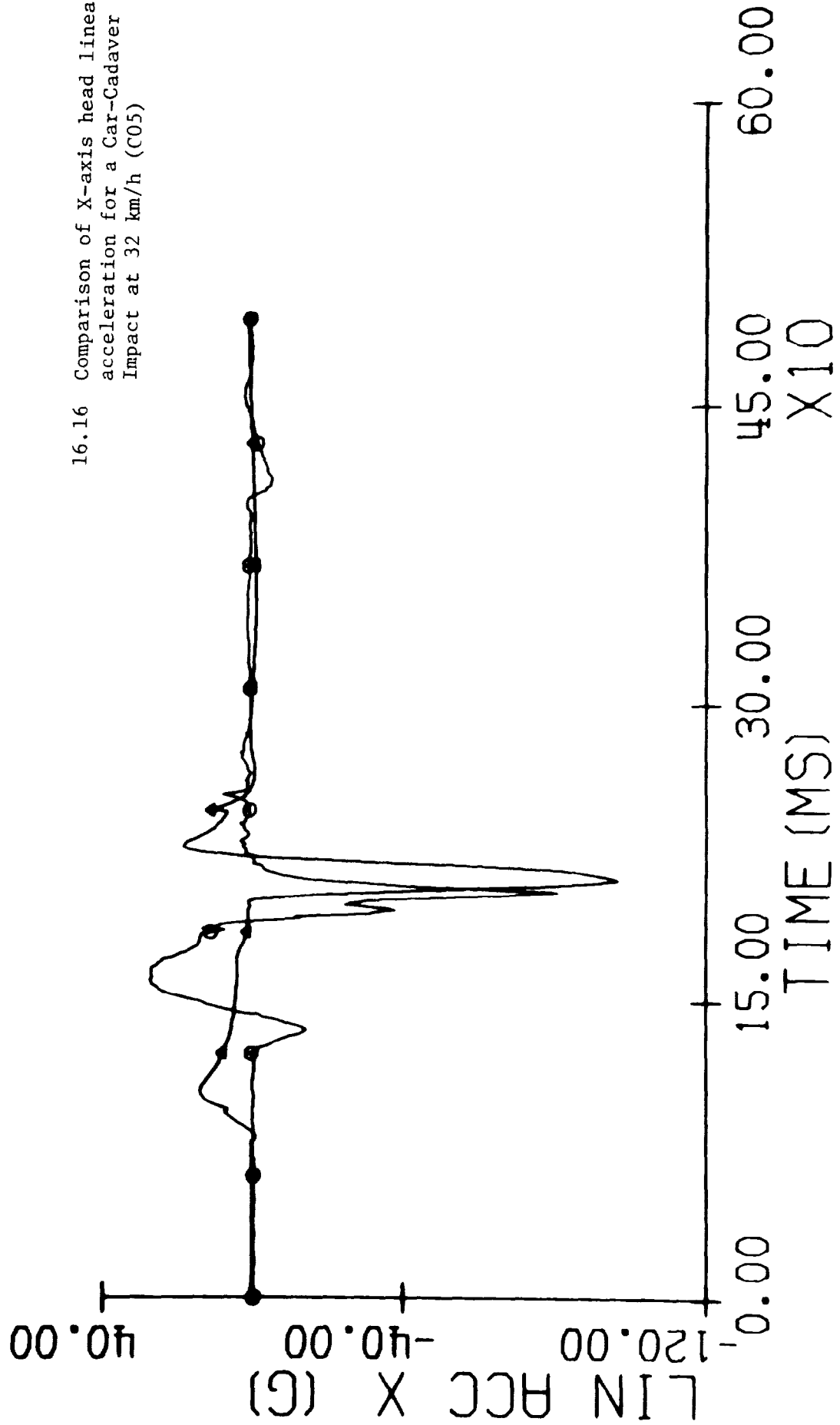
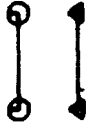
Fig. 16.13 Comparison of Z-Axis Lower Torso Linear Acceleration for a Car-Cadaver Impact at 37.3 Km/h (C06)





RUN NO.: C05-HEAD

EXPT.
MODEL



16.16 Comparison of X-axis head linear acceleration for a Car-Cadaver Impact at 32 km/h (C05)

RUN NO.: C05-HEAD

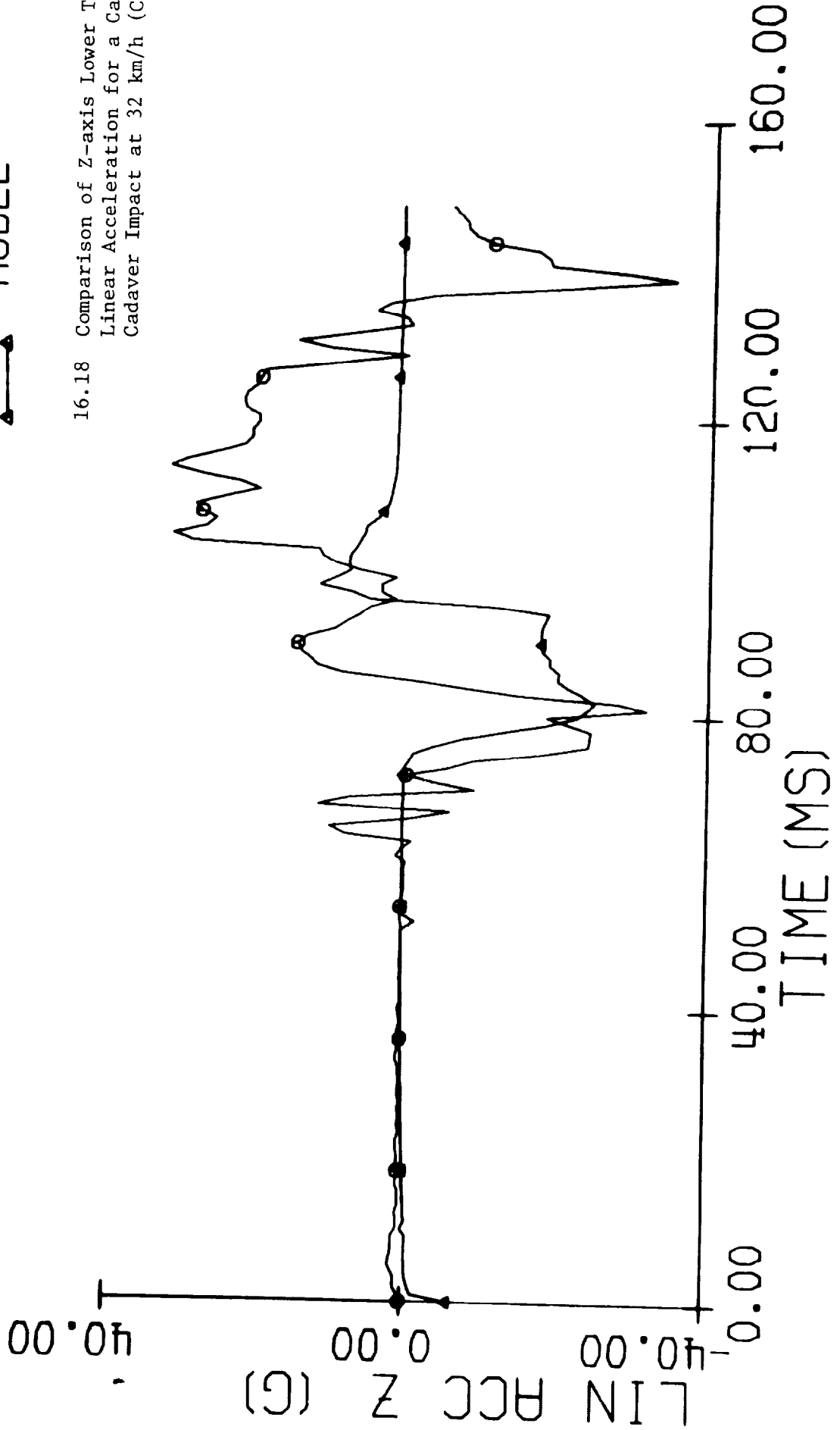
EXPT.
MODEL



16.17 Comparison of Y-axis head angular acceleration for a Car-Cadaver Impact at 32 km/h (C05)

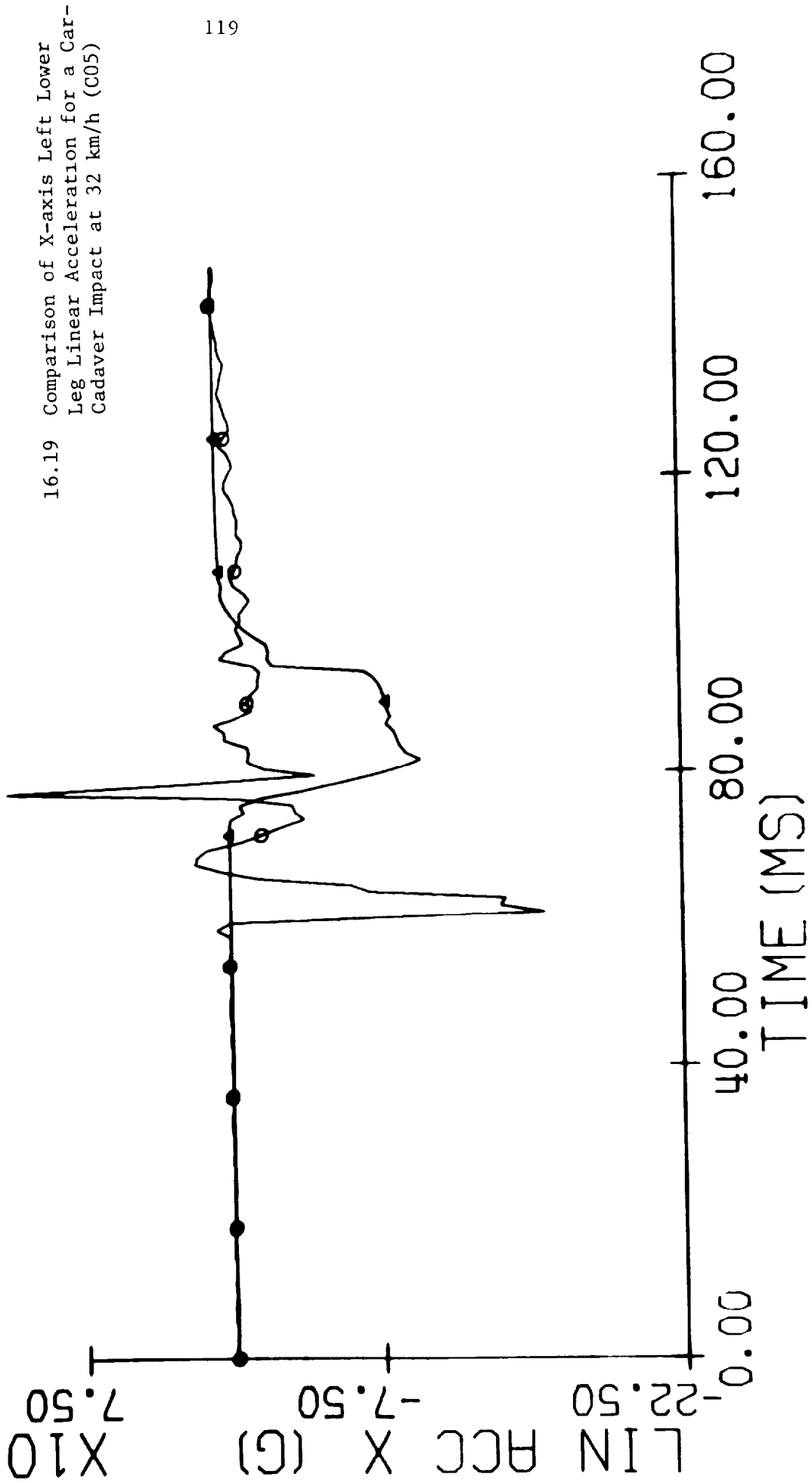
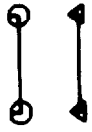
RUN NO.: C05-LT

EXPT.
MODEL



RUN NO.: C05-LLL

EXPT.
MODEL



DISCUSSION OF MODEL RESULTS

17.1 Comparison of Model Results for Different Types of Impacts

The model was used to study the difference in response between a cadaver and a dummy. Figure 17.1 compares model predictions of head angular acceleration about the Y-axis for two 24.1 km/h simulations with different subjects (Runs D10 and C03). The response is quite similar. However, the X-axis linear acceleration amplitudes are markedly different in view of the fact that the dummy head is much stiffer than that of the cadaver, as seen in 17.2. The predominant X-components of angular acceleration of the impacted lower leg in the same runs are plotted in Figure 17.3. An initial positive angular acceleration is observed only for the cadaver impact, otherwise the pattern is the same. This difference is attributable to the difference in the type of knee joint simulated by the model. Moreover, the magnitude of acceleration for the dummy is higher. This was also the case for head linear acceleration. Again, this is due to the difference in stiffness between the metallic skeleton of the dummy and the bony skeleton of the cadaver. Effects of the difference in stiffness is also seen in Figure 17.4, where the Y-component of linear acceleration of the lower leg is compared. This is the impact direction. A similar comparison is made for two cadaver runs, (C06 at 37.3 km/h and C03 at 24.1 km/h) at different impact velocities. It is evident from the Figure 17.5 that the magnitude of the Y-component linear acceleration (impact direction) is approximately the same for both runs. Note that in Run C06, the front-end was padded but the impact speed was higher. The same level of acceleration was generated because of the foam rubber padding but it did not reduce the angular acceleration level, as can be seen in Figure 17.6. The pattern is similar for both runs.

17.2 Frequency Content Analysis

Every pulse contains a combination of pulses of different frequencies. In other words, a pulse can be represented by a Fourier series. The function of frequency in a validation study requires some investigation. To this end, a spectral analysis was performed for both experimental data and model output. Figure 17.7 illustrates that the Z-components of angular acceleration of the head have roughly the same frequency content. Furthermore, Figure 17.8 indicates no significant change in correlation by filtering the results at 150 Hz. (See Figure 15.7). Figure 17.9 indicates that head angular acceleration about the Z-axis exhibited a different frequency content. The experimental data contain higher frequency components. However, the dominant frequency levels are less than 150 Hz. Figure 17.10 illustrates that in the filtered data there was a reduction in the peak value of the experimental data. Correlation for the filtered data appear to better than that observed in Figure 16.2.

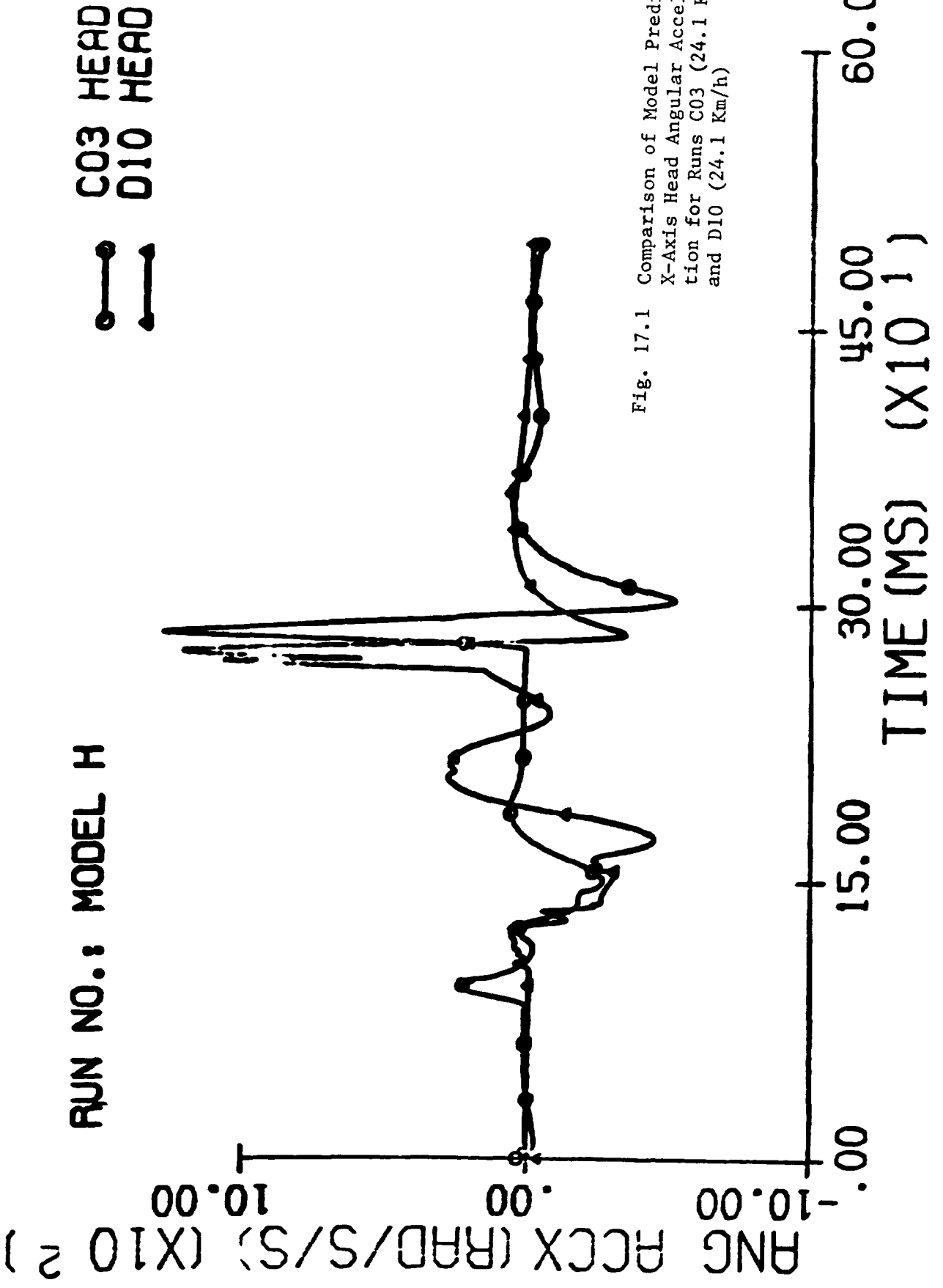


Fig. 17.1 Comparison of Model Prediction X-Axis Head Angular Acceleration for Runs C03 (24.1 Km/h) and D10 (24.1 Km/h)

C03 HEAD
D10 HEAD



RUN NO.: MODEL H

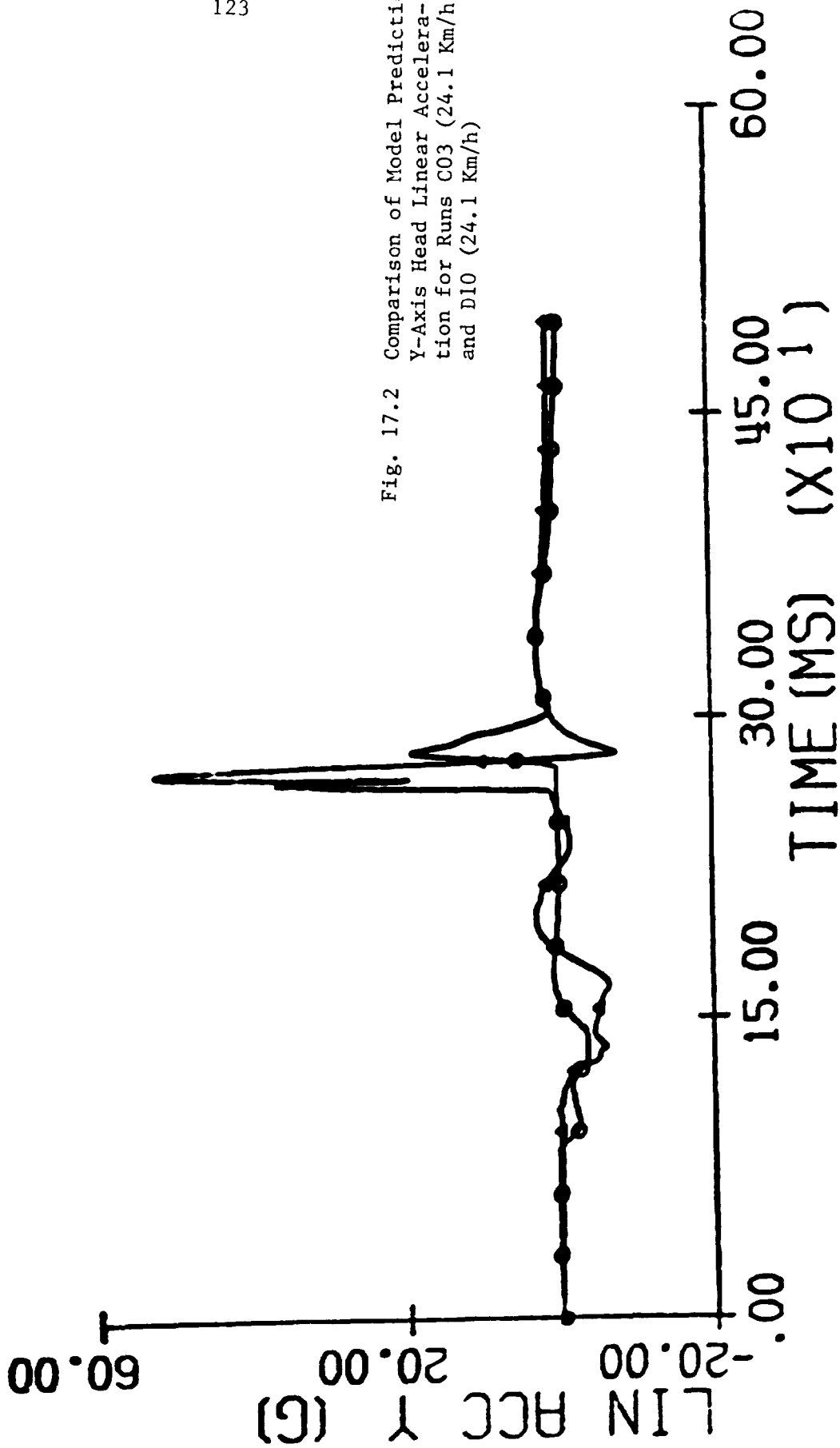


Fig. 17.2 Comparison of Model Prediction Y-Axis Head Linear Acceleration for Runs C03 (24.1 Km/h) and D10 (24.1 Km/h)

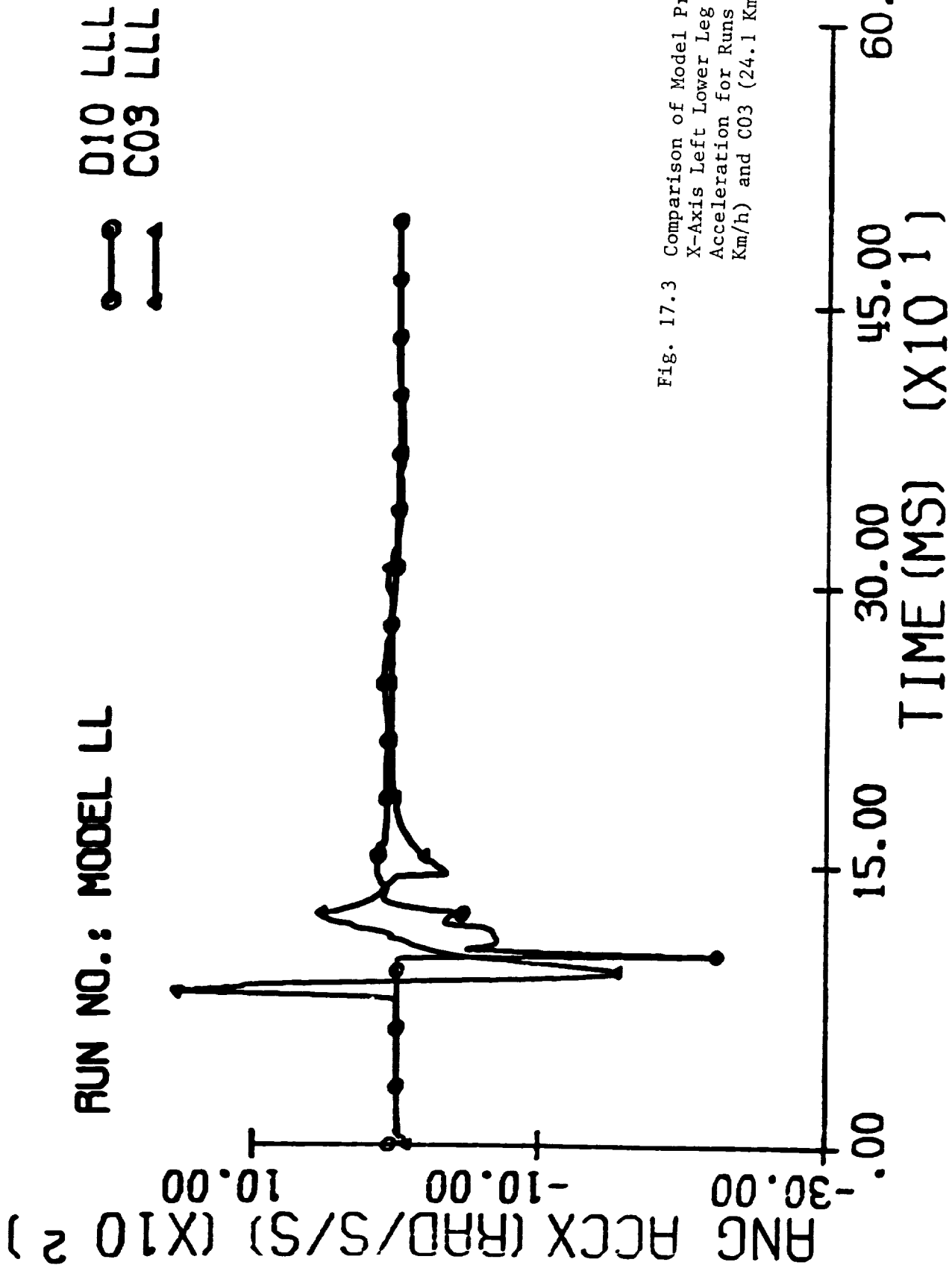
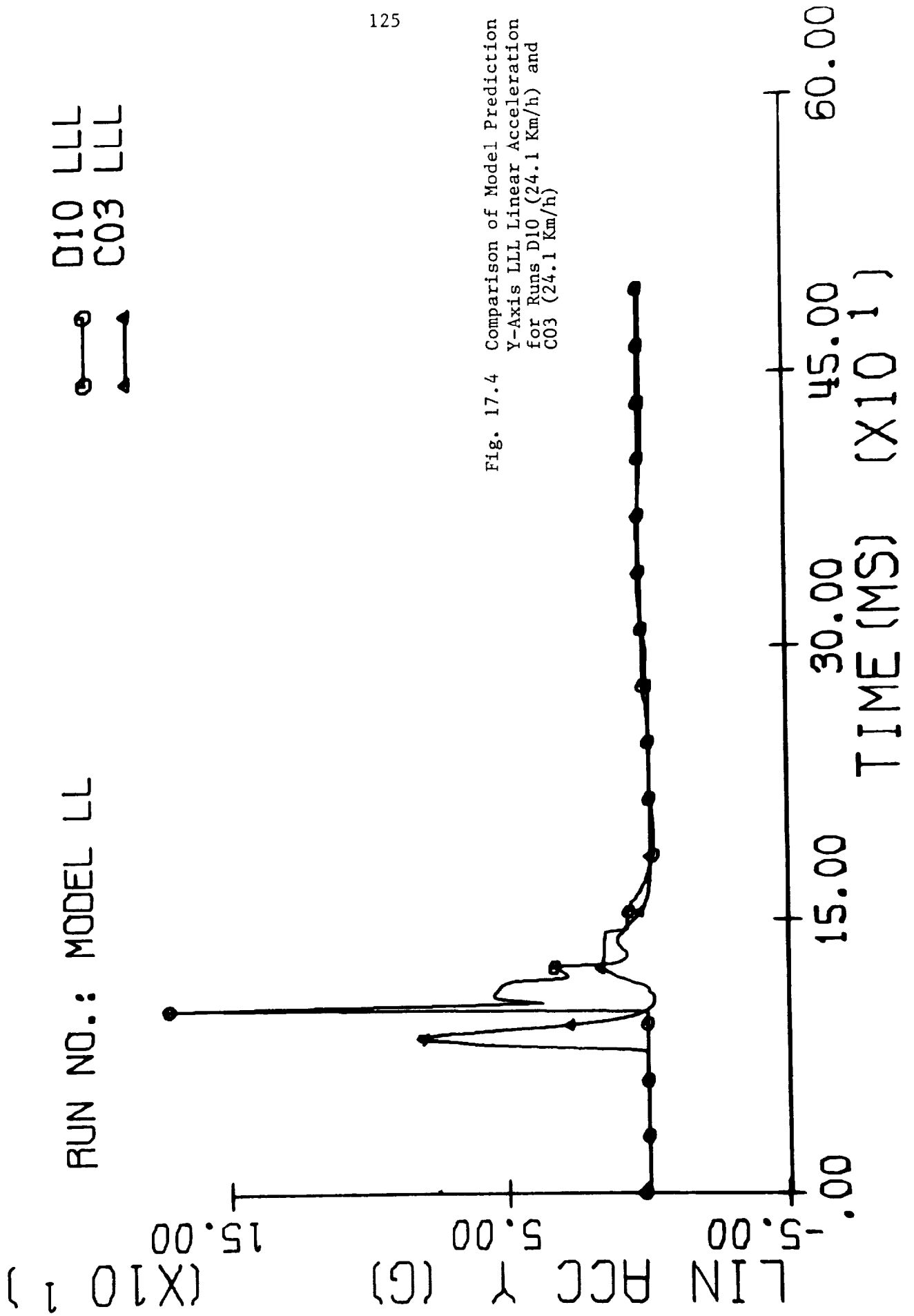


Fig. 17.3 Comparison of Model Prediction
X-Axis Left Lower Leg Angular
Acceleration for Runs D10 (24.1
Km/h) and C03 (24.1 Km/h)



C03 LLL
C06 LLL

RUN NO.: MODEL LL

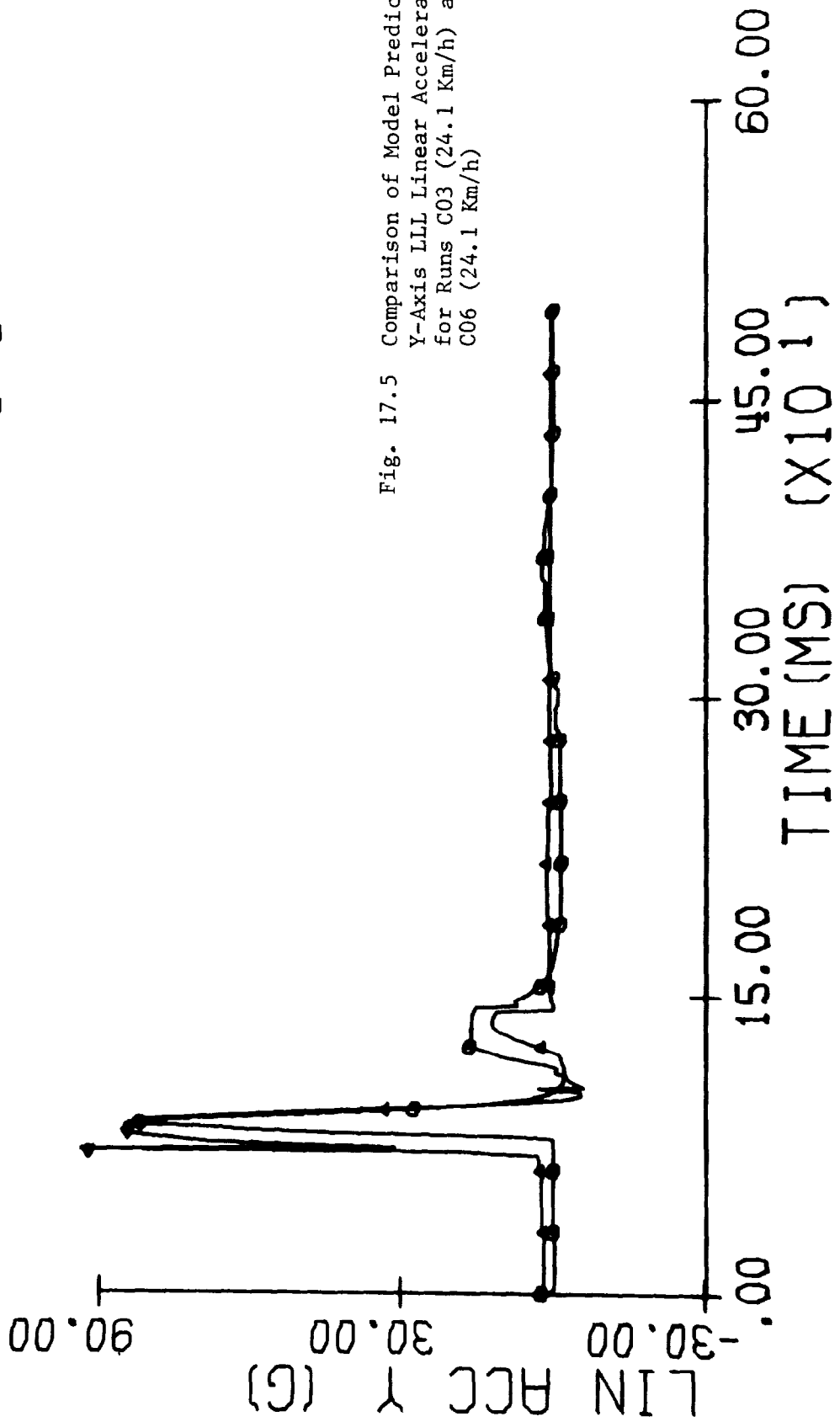


Fig. 17.5 Comparison of Model Prediction Y-Axis LLL Linear Acceleration for Runs C03 (24.1 Km/h) and C06 (24.1 Km/h)

RUN NO.: MODEL LL C03 LLL C06 LLL

○ — ○ —

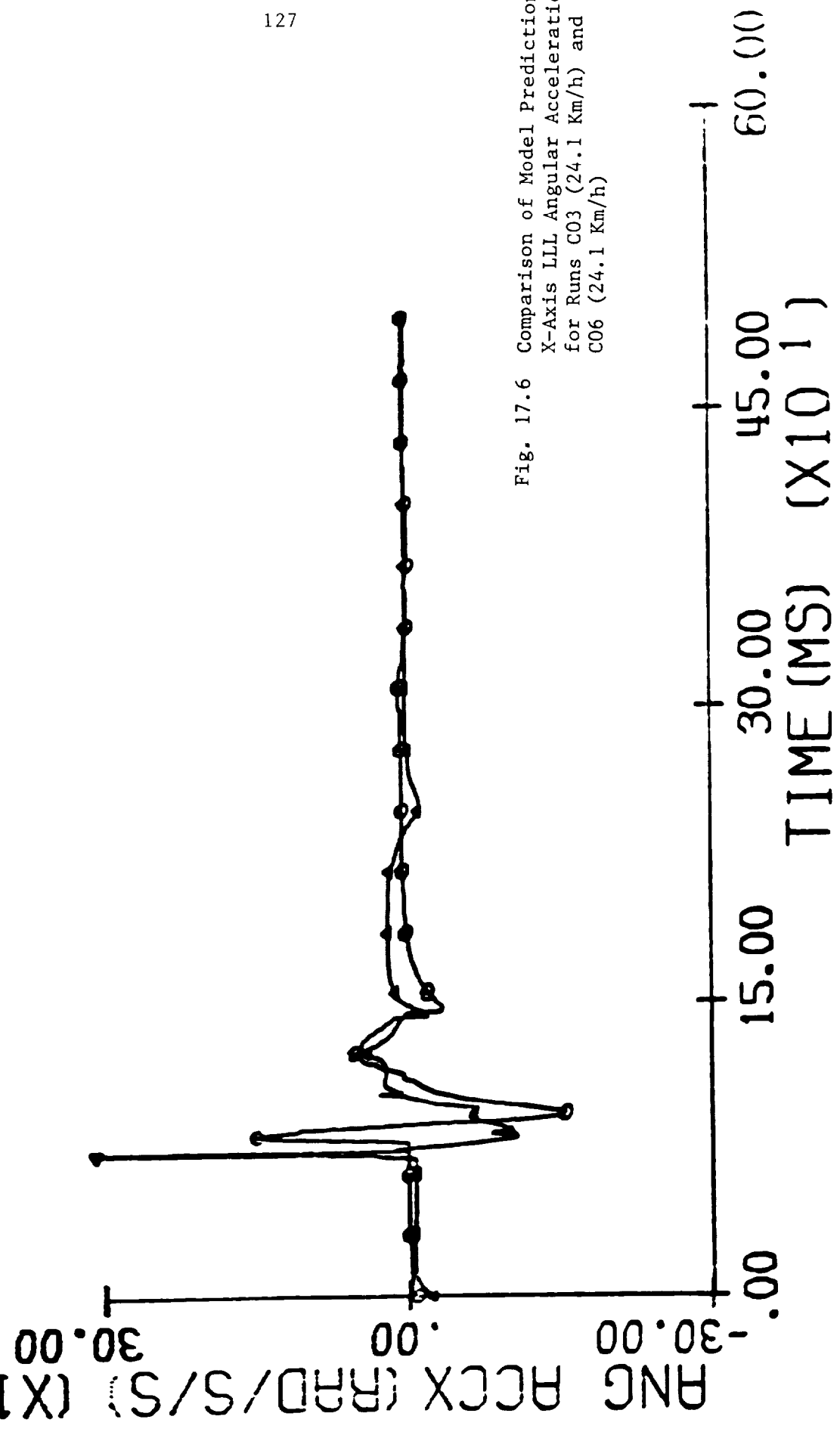


Fig. 17.6 Comparison of Model Prediction X-Axis LLL Angular Acceleration for Runs C03 (24.1 Km/h) and C06 (24.1 Km/h)

RUN NO.: D10-HEAD

EXPT. MODEL

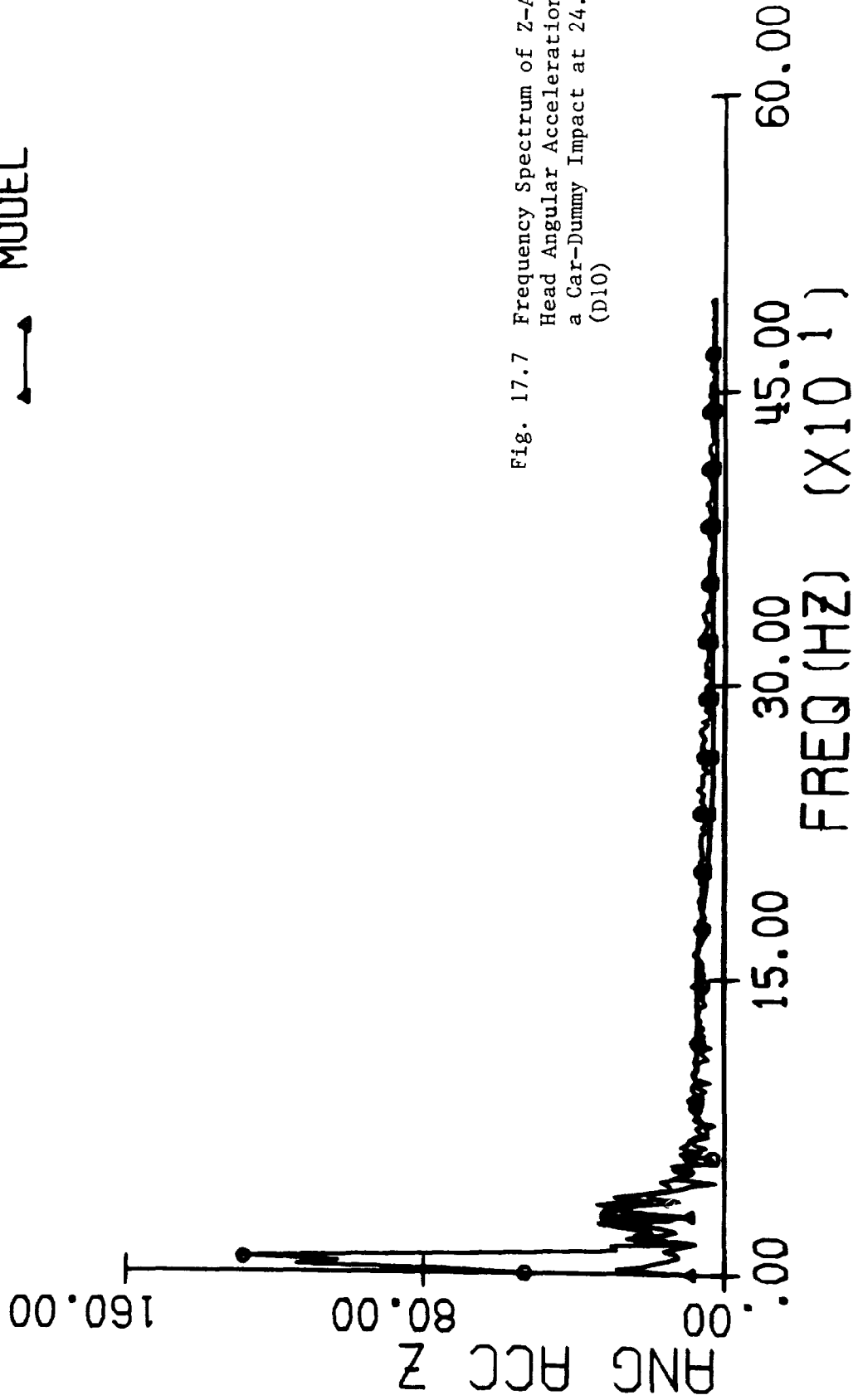


Fig. 17.7 Frequency Spectrum of Z-Axis Head Angular Acceleration for a Car-Dummy Impact at 24.1 Km/h (D10)

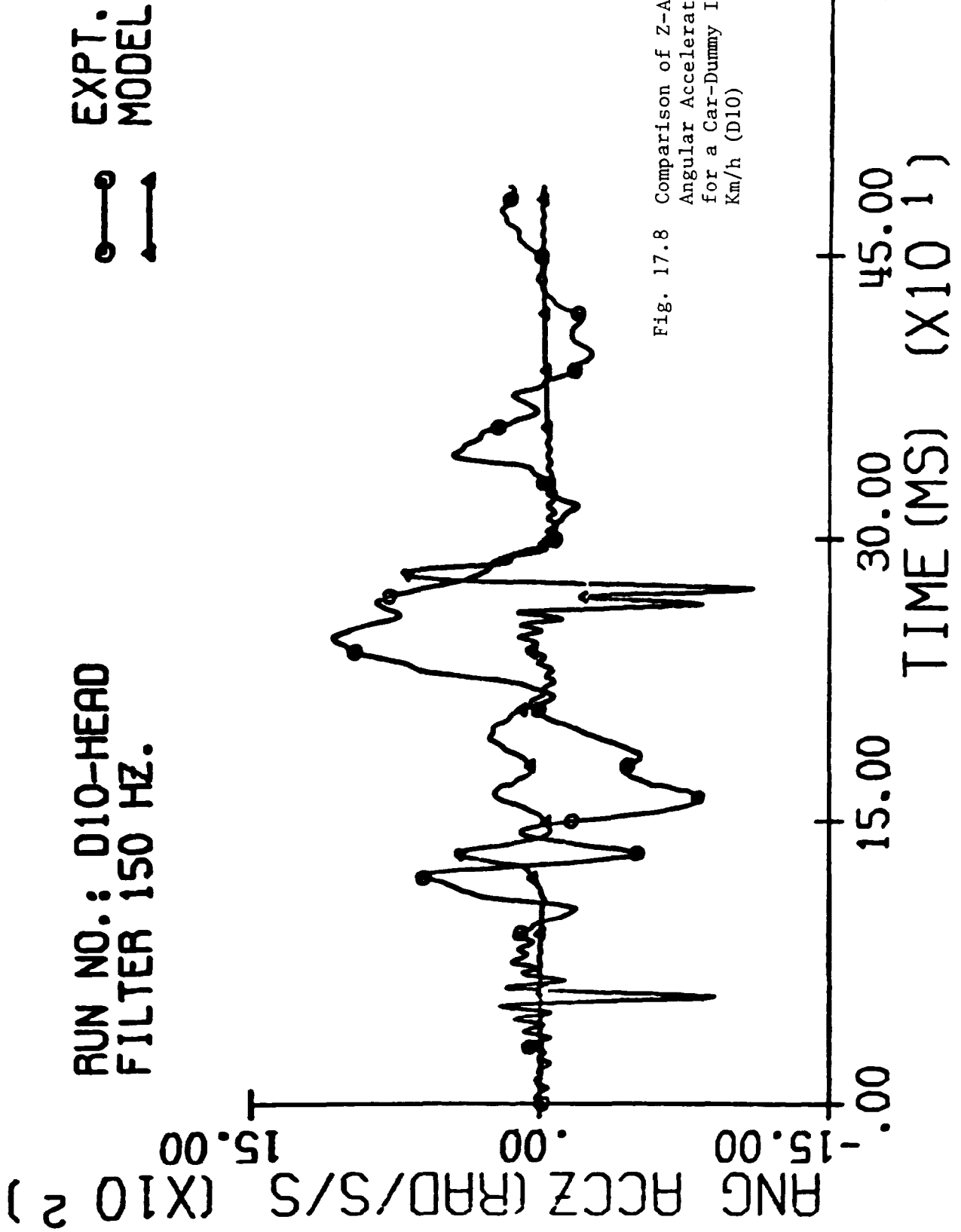


Fig. 17.8 Comparison of Z-Axis Head Angular Acceleration (Filtered) for a Car-Dummy Impact at 24.1 Km/h (D10)

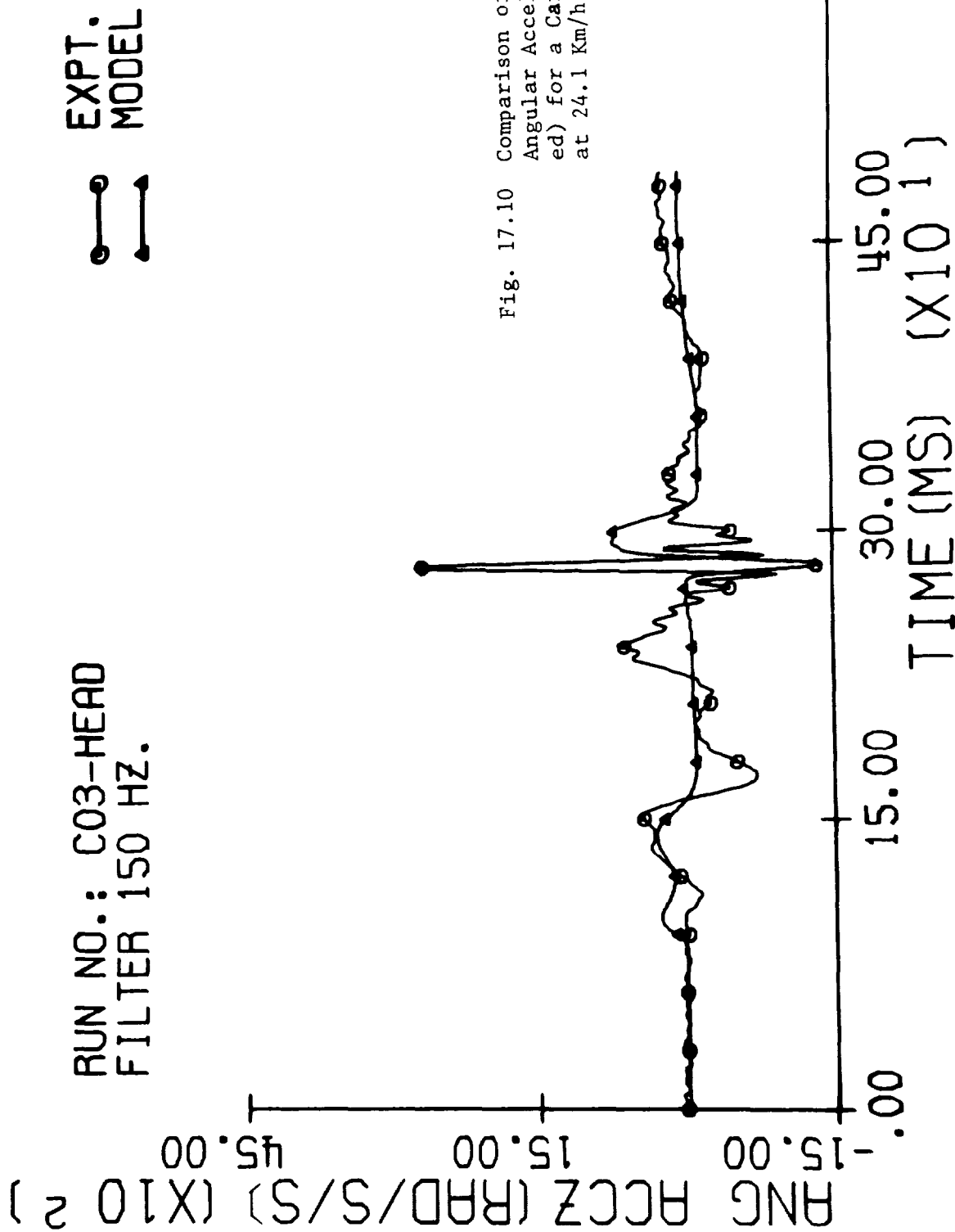


Fig. 17.10 Comparison of Z-Axis Head Angular Acceleration (Filtered) for a Car-Cadaver Impact at 24.1 Km/h (C06)

DISCUSSION AND CONCLUSIONS

18.1 Introduction

A rather extensive experimental and analytical program was carried out to study in detail the kinematics of pedestrian-vehicle impact and to compare these experimental results with those generated by a three-dimensional crash victim simulator (CVS) developed by Calspan Corporation. Although there were only 10 dummy runs and 6 cadaver impacts, the experimental work constituted a major portion of this research effort. One of the primary difficulties was the simultaneous recording of up to 59 channels of transducer data for an impact event, the outcome of which was difficult to predict. There were a maximum of 53 body-mounted accelerometers which were adjusted to provide the optimal signal-to-noise ratio without saturation and were protected from damage during impact. Moreover they were connected to signal conditioning amplifiers via miniature connectors which were prone to short or open circuits. In any event, the number of data channels for a biological impact experiment far exceeded that normally used in previous studies and many new techniques were developed to solve the problems encountered.

The modelling effort was also very demanding. It not only simulated the dummy and cadaver experiments of pedestrian impact but also single segment impacts and dummy drop tests carried out by the Texas Transportation Institute. Data set preparation was a lengthy procedure requiring extreme care and total familiarity with the computer program. In fact, the program was modified to simulate the single segment impact and the modification was adopted by Calspan in one of their later versions as an added feature. The constant issuance of new versions of the CVS by Calspan was rather disconcerting. Each version had to be installed on the computer and debugged before it could be used.

18.2 Experimental Aspects of the Research Program

A reliable method of measuring angular acceleration of a rigid body in three-dimensional motion was developed as a result of this investigation. A special configuration of 9 linear accelerometers was proposed to overcome the difficulty of error accumulation when the minimum number of 6 accelerometers was used. It is felt that this was not only a basic contribution to mechanics but also a pioneering effort to point out the need for accurate acceleration measurements during impact testing. The method provides a means to compute angular acceleration, even though some error in linear acceleration measurement is present. The result, however, is still dependent on the accuracy of the measurement. With the 6-accelerometer method, very small errors are intolerable resulting in failure to obtain reasonable angular accelerations. In retrospect, it is necessary to note that the 9-accelerometer method was developed at a critical juncture during which the 6-accelerometer approach resulted in chaotic values of angular acceleration at many laboratories using the latter configuration. It does not claim to be an accurate angular accelerometer. In fact, it challenges the state-of-the-art in the manufacture of accelerometers with high accuracy and low cross-axis sensitivity. Thus, it would be grossly unfair to criticize the method as being subject to errors shortly after it was developed to solve a problem that was apparently unsolvable.

This research also had many other positive aspects in experimental biomechanics. The feasibility of recording up to 59 data channels in a rather unpredictable impact environment was clearly demonstrated. It took over 36 hours to make the first run but the run was accomplished and the time required for subsequent runs steadily decreased. Much of the delay was caused by electrical problems associated with the use of miniature connectors and long multiconductor cables. The hardware and technology evolved from the need to reduce the weight of the connectors attached to the test subject and to minimize the influence of the data cables on the kinematics of the body segments.

The ability to process and identify all of the data channels was also an art which had to be developed. Good record keeping and organization of data handling techniques were required to produce accurate and usable data. For example, if one of the three accelerometer readings from the triaxial cluster of the 9-accelerometer package failed to come through or was not accompanied by a valid calibration signal, the angular kinematics could not be determined for the segment to which this accelerometer package was attached. Similarly, if any 2 channels were mistakenly identified, it was almost impossible to obtain the correct angular acceleration of the body segment.

Many post-run measurements were made in order to obtain data required by the Calspan CVS for model validation. New methods of locating body segment centers of gravity and their moments of inertia were developed. Contact force characteristics were also determined experimentally. A light-weight trifilar pendulum was used to measure mass moments of inertia of body segments. The wires were suspended from load cells to locate the center of gravity of the segment at the center of the pendulum table. These innovations improved the accuracy of the data since the 2 principal sources of error are large moments of inertia of the pendulum itself and the transfer term made up by the product of the mass and the square of the distance from the center of gravity to the center of oscillation.

Body-fixed coordinate systems based on anatomical landmarks were proposed for every body segment to permit comparability of data among laboratories. The landmarks used were skeletal. They had to be identifiable on x-ray or palpable; preferably, they should satisfy both conditions. It is hoped that the proposed coordinate systems will be accepted by the research community and used consistently to facilitate comparison of data.

18.3 Comments on Model Validation

The evaluation of a mathematical model by investigators who were not involved in its development can be expected to be objective and fair. Every attempt was made to create an input data set which was based on measured values instead of conjectures. Similarly, every precaution was taken to obtain the best experimental data possible. The procedure for validation was to compare experimental acceleration and displacement time histories with those predicted by the model. A qualitative judgment was made regarding the degree of correlation. The model was unable to predict accelerations that matched the experimental curves exactly. However, they were usually of the same order of magnitude and were not very much out of phase, in time. The model was thus considered to be a reasonable accurate simulator of the actual impact event. The deficiency is obviously an objective and quanti-

tative means of evaluating the model. Of course, criteria should have been established prior to making the comparisons. Such criteria should be drawn up by the research community before another major evaluation of a CVS is carried out.

With reference to existing 3-D CVS, one of the major shortcomings is the assumption that all body segments are rigid bodies. The accuracy of the predicted contact force is necessarily comprised and hence the resulting kinematics are not directly comparable. Thus, stringent criteria for validation are not advisable at this time. For instance, if a root mean square error were to be computed, the correlation between model results and experimental data would turn out to be quite poor in cases where there are strong interactions between body segments and deformable vehicular surfaces.

18.4 Conclusions

- a) Extensively instrumented dummies and cadavers were used in the simulation of a pedestrian vehicle impact, up to speeds of 40km/hr (25 mph). The simultaneous recording of over 50 transducers was shown to be feasible.
- b) A reliable method of computing angular acceleration and velocity of rigid bodies in 3-D motion was developed. The accuracy of these parameters, however, is still dependent upon the quality of the linear accelerometers employed.
- c) The Calspan 3-D CVS was used to simulate the controlled pedestrian impacts. It predicted reasonable kinematic results for both the dummy and the cadaver but the correlation is far from a perfect match. In general the correlation can be considered to be quite good, in view of the complexity of the impact event.
- d) The validation study was performed with objectivity. Input data were measured whenever possible and were not adjusted. Those that were assumed were based on previous usage or measurements made by other investigators. Each computer run was made only once.
- e) Improvements to the contact model are required if better correlation is desired. These should include a better formulation of the force-deflection characteristics to account for velocity of impact and the mutual deformability of the body segments and the vehicular surfaces.
- f) The comparison of 3-D angular acceleration of the body segments is made possible by the use of the 9-accelerometer method of measurement.
- g) The fact that all accelerations are body-fixed renders the correlation of angular displacement a prior necessity before the accelerations can be meaningfully compared.
- h) Pedestrian-vehicle impact is a 3-D event during which the body segments execute a wide variety of complex motions. In particular, there is a tendency during lateral impact for the subject to rotate onto its back as it impacts the hood. This was observed in both dummy and cadaver impacts.

- i) Dummy impacts were more repeatable than cadaver impacts. The height of the subjects determined the time of head-hood contact and the impact velocity determined the violence of motion on the head.
- j) A padded front end appeared to lower linear acceleration but not angular acceleration of the impacted leg.
- k) Dummy and cadaver response to almost identical impacts was quite different.
- l) Skeletal fractures occurred in every cadaveric test. However, a large number of screw holes were made in the boney skeleton for the attachment of accelerometers. In many cases, it was not possible to ascertain the exact cause of the fracture.

REFERENCES

VOLUME 3

1. Bartz, J. A., (1972), Development and Validation of a Computer Simulation of a Crash Victim in Three Dimensions, Proceedings of the 16th Stapp Car Crash Conference, pp. 105-127. Published by SAE, N.Y.
2. Boeing Computer Services, Inc., (1973), Progress Report, Aircraft Crash Simulation Project, Contract No. N00014-75-C-0223, Feb. - May, p. 3.
3. Bortz, J. E., (1971), A New Mathematical Formulation For Strapdown Inertial Navigation, IEEE Transactions on Aerospace and Electronic Systems, Vol. AES7, No. 1, pp. 61-66.
4. Fleck, J. T., Butler, F. E., and Vogel, S. L., (1974), An Improved Three Dimensional Computer Simulation of Motor Vehicle Crash Victims, Final Technical Report No. ZQ-5180-L-1, Calspan Corporation, (in 4 Vols. Special reference p. 248, Vol. I and p. 241 Vol. IV).
5. Fleck, J. T., (1975), Calspan Three-Dimensional Crash Victim Simulation Program, in Aircraft Crashworthiness ed. by K. Saczalski, et. al., University of Press of Virginia, Charlottesville, pp. 299-310.
6. Krieger, K. W., (1976), Full-Scale Experimental Simulation of Pedestrian-Vehicle Impacts, Ph.D. Dissertation, Wayne State University.
7. Nyquist, G. W., (1976), Personal Communication About Parallax Problems.
8. Texas Transportation Institute, (May, 1973), Vehicle Exteriors and Pedestrian Injury Prevention, Final Report on Contract DOT-HS-065-1-217, Research Report RF 814-1, Vol. IV.